2019

Center Manifold Dynamics in Randomly Coupled Oscillators and in Cochlea

Dimitrios Moirogiannis

CENTER MANIFOLD DYNAMICS IN RANDOMLY COUPLED OSCILLATORS AND IN COCHLEA

A Thesis Presented to the Faculty of

The Rockefeller University

in Partial Fulfillment of the Requirements for

the degree of Doctor of Philosophy

by

Dimitrios Moirogiannis

June 2019

CENTER MANIFOLD DYNAMICS IN RANDOMLY COUPLED OSCILLATORS AND IN COCHLEA

Dimitrios Moirogiannis, Ph.D.

The Rockefeller University 2019

In dynamical systems theory, a fixed point of the activity is called nonhyperbolic if the linearization of the system around the fixed point has at least one eigenvalue with zero real part. The *center manifold existence theorem* guarantees the local existence of an invariant subspace of the activity, known as a center manifold, around nonhyperbolic fixed points. A growing number of theoretical and experimental studies suggest that neural systems utilize dynamics on center manifolds to display complex, nonlinear behavior and to flexibly adapt to wide-ranging sensory input parameters. In this thesis, I will present two lines of research exploring nonhyperbolicity in neural dynamics.

In the first part of this thesis, I present a technique to study the statistical properties of a high dimensional dynamical system with random connectivity and examine which statistical properties determine both the shape of the center manifold and the corresponding dynamics on it. This is relevant to the field of theoretical neuroscience, which has traditionally employed random connectivity as a first-order "zero information" approach in modeling neural systems. This technique also gives us constraints on the family of center manifold models that could arise from a large-scale random network. I demonstrate this approach on an example network of randomly coupled damped oscillators.

In the second part of this thesis, I focus on nonhyperbolicity in cochlear dynamics. Cochlea displays complex and highly nonlinear behavior in response to wide-ranging auditory stimuli. While there have been many recent advancements in the modeling of cochlear dynamics, most of these models are just empirical, containing large

amounts of biological detail, and thus don't shed much light on what mathematical structures underlie the essential features of the extended cochlea. We construct a dynamical system consisting of a series of strongly coupled critical oscillators to show that high-dimensional nonhyperbolic dynamics can account for high-order compressive nonlinearities, amplification of weak input, frequency selectivity, and traveling waves of activity. As a single Hopf bifurcation generically gives rise to features of cochlea at a local level, the nonhyperbolicity mechanism proposed in this thesis can be seen as a higher-dimensional analogue for the entire extended cochlea.

Table of Contents

List of Figures

Part I

Introduction

Chapter 1

Introduction

1.1 Center Manifolds around nonhyperbolic fixed points

In dynamical systems theory, the classical approach to studying behavior in the neighborhood of an equilibrium point is to examine the eigenvalues of the Jacobian of the system at this point. If all eigenvalues have nonzero real part, then the equilibrium point is called *hyperbolic*. In this case, according to the *Hartman-Grobman theorem*, the dynamics around the point is topologically conjugate to the linearized system determined by the Jacobian [Grobman 1959, Hartman 1960a, Hartman 1960b]. This implies that solutions of the system near the hyperbolic fixed point exponentially decay (or grow) with time constants determined by the real part of the eigenvalues of the linearization. Thus, locally, the nonlinearities in the system do not play an essential role in determining the dynamics.

This behavior around hyperbolic points is in stark contrast to the dynamics around *nonhyperbolic* fixed points, where there exists at least one eigenvalue of the Jacobian with zero real part. The linear space spanned by the eigenvectors of the Jacobian corresponding

to the eigenvalues on the imaginary axis (*critical modes*) is called the *center subspace*. In the case of nonhyperbolicity, the Hartman-Grobman theorem does not apply, the dynamics are not enslaved by the exponent of the Jacobian, and nonlinearities play a crucial role in determining dynamical properties around the fixed point. The classical approach to studying this nonlinear behavior around nonhyperbolic fixed points is to investigate the reduced dynamics on an invariant subspace called a *center manifold*. The *center manifold existence theorem* [Kelley 1967, Carr 2012] guarantees the local existence of this invariant subspace. It is tangent to the *center subspace*, and its dimension is equal to the number of eigenvalues on the imaginary axis. If it is the case that all eigenvalues of the linearization at a nonhyperbolic fixed point have zero or negative real part (no unstable modes), as is often the case in physical systems, then for initial conditions near the fixed point, trajectories exponentially approach solutions on the center manifold [Carr 2012], and instead of studying the full system, we can study the reduced dynamics on the center manifold. Nonhyperbolic equilibrium points are also commonly referred to as *critical* [Izhikevich 2007b, Shnol 2007], and we will follow that terminology in this thesis. (under some conditions we can also define center-stable and center foliations [Pugh 1997, Katok 2005, Burns 2005, Brown 2016] but this won't be discussed or used farther here.)

Dynamics on center manifolds around nonhyperbolic fixed points are complex and can give rise to interesting nonlinear features. In general, the greater the number of eigenvalues on the imaginary axis, the more complex the dynamics could be [Wiggins 2003]. First, since the dynamics are not enslaved by the exponent of the Jacobian, nonlinearities and input parameters play a crucial role in determining dynamical properties such as relaxation timescales and correlations [Yan 2012, Hayton 2018a]. Moreover activity perturbations on the center manifold neither damp out exponentially nor explode, but instead, perturbations depend algebraically on time. If the center manifold is also delocalized, which can occur even with highly local connections between individual units (units not connected on the original

network can be connected on the reduced system on a center manifold), activity perturbations can then also propagate over large distances. This is in stark contrast to the behavior in stable systems where perturbations are damped out exponentially and information transfer can only occur on a timescale shorter than the timescale set by the system's exponential damping constants.

1.2 Bifurcations - Extended System

Whereas hyperbolic fixed points are essentially left unchanged by small changes of the parameters or the input, dynamics around nonhyperbolic fixed points can change radically when perturbed. For instance, small changes in the external input can drastically alter the dynamics around a nonhyperbolic point by creating new fixed points, periodic/quasiperiodic orbits, and even chaotic dynamics. The higher the dimensionality of the center subspace (more eigenvalues with zero real part), the more rich and complex the resulting dynamics can be. The study of the effects of parameter changes on the qualitative dynamics of a system is known as *bifurcation theory* [Adelmeyer 1999, Kuznetsov 2013]. It is essentially a study of how modes crossing the imaginary axis can affect the topological structure of the dynamics. Bifurcations have been found to play key role in both the modeling of neural networks [Hoppensteadt 2012] and the generation of spikes at the level of a single neuron [Izhikevich 2007a].

The classical technique to study bifurcations is to define the *extended system* with the parameters as dependent variables so that the new extended system exhibits essentially the same dynamics as the original one [Wiggins 2003, Kuznetsov 2013]. In this new system, the existence theorem for center manifolds holds and we are locally guaranteed the existence of a foliation of center manifolds not only for eigenvalues with zero real part but also for eigenvalues whose real part lie in a sufficiently small neighborhood of the imaginary axis. The latter result is crucial to the study of center manifolds in noisy physical systems, where

the fine tuning of the system's spectrum to lie exactly on the imaginary axis is impossible. At best, we can only expect the spectrum to lie in a neighborhood of the imaginary axis. As a first approximation, in this thesis we will only assume that critical modes lie exactly on the imaginary axis, so use of extended systems in this thesis will not be necessary.

1.3 Approximating center manifold dynamics

Computing trajectories on center manifolds is not an easy task as one has to deal with the nonlinear embedding of the center manifold in the full dimensional space, which can give rise to reduced nonlinear equations even more complicated than the original full system equations. Fortunately, there exists a theorem, the *center manifold approximation theorem* [Carr 2012] which gives us a method of computing both the embedding of the center manifold and the reduced dynamics on it up to an arbitrarily large degree of accuracy.

The approximation theorem states that if a local graph tangent to the center subspace and given by a polynomial on the center subspace satisfies center manifold invariance equations to a particular degree of accuracy, then the polynomial approximates the center manifold to a residue of the same degree. The projection of the invariance equation on the center space gives us an ordinary differential equation which can be used to approximate the reduced dynamics using an approximation of the center manifold embedding, and the projection of the invariance equation on the stable subspace gives us quasi-linear partial differential equation that can be used to approximate the center manifold by a polynomial of any degree. These equations gives us an algorithm for approximating the reduced dynamics, although the number of parameters and resulting equations between them grow fast as the desired degree of accuracy increases.

1.4 Center Manifold Dynamics in the nervous system

Conceptually, it is hard to imagine how the nervous system could perform input-dependent calculations over a wide range of inputs and exhibit complex, highly nonlinear behavior without utilizing nonhyperbolic fixed points and their associated center manifolds. While the Hartman-Grobman theorem implies that the activity around a hyperbolic point is homeomorphic to a direct product of single neuron dynamics and thus not capable of performing interesting computations, neural activity around nonhyperbolic equilibriums are more complex and can lead to interesting computations [Izhikevich 2007a].

There are numerous studies which indicate the ubiquitousness and importance of non-hyperbolic neural dynamics. The studies range from direct experimental measurements of center subspaces in cortical dynamics to theoretical toy models demonstrating the capability of center manifolds to explain characteristic features present in a variety of neural systems. I will now review these studies.

Solovey *et al.* [Solovey 2015] performed stability analysis of high-density electrocorticography recordings covering an entire cerebral hemisphere in monkeys during reversible loss of consciousness. Performing a moving vector autoregressive analysis of the activity, they observed that the eigenvalues crowd near the imaginary axis. During loss of consciousness, the number of eigenmodes at the edge of instability decrease smoothly but drift back to the imaginary axis during recovery of consciousness. This study suggests that in the awake, conscious brain cortical activity resides on a high dimensional center manifold [Solovey 2012, Alonso 2014].

More evidence of center manifold dynamics in cortex has been provided by multielectrode recordings in arm reaching tasks in monkeys [Churchland 2012, Shenoy 2013]. Churchland *et al.* recorded activity from primary motor cortex (M1) and the adjacent aspect of dorsal

premotor cortex (PMd), while monkeys executed reaches upon a go cue. They found that during the arm reaching portion of the task, the majority of the variance of the population activity can be captured by an interaction matrix which is antisymmetric and thus has a purely imaginary spectrum. These results suggest that the bulk of population activity in arm reaching tasks take place on a center manifold.

Slow manifolds, which are a specific form of center manifolds, have been proposed as a mechanism to explain the dynamics of oculomotor integrator in the brainstem by both theoretical [Seung 1998] and experimental studies [Seung 2000]. Similarly in two-interval discrimination in prefrontal cortex [Machens 2005]. Hopf bifurcation [Poincarè 1893, Hopf 1942, Andronov] has beed used to model active process of the cochlea and the highly nonlinear response in the auditory periphery [Choe 1998, Eguíluz 2000, Camalet 2000, Kern 2003, Nadrowski 2004, Tinevez2007, Kanders 2017b], and olfactory system [Freeman 2005]. High dimensional center manifold dynamics have also been shown to give rise at the same time and thus connect, several input-dependent computations in the primary visual cortex [Yan 2012, Hayton 2018a]. Finally there is theoretical work on regulated criticality [Bienenstock 1998] proposing regulation mechanisms to keep the brain operating near nonhyperbolicity.

1.5 Hypothesis studied in this thesis

We posit that the nervous system utilizes nonhyperbolic equilibrium points and the unique dynamical properties on the corresponding center manifolds to flexibly respond to a wide range of input parameters and exhibit complex nonlinear behavior.

While this nonhyperbolicity hypothesis has also been commonly referred to as *dynamical criticality*, it is distinct from *statistical criticality* [Beggs 2012], which is related to the statistical mechanics of second-order phase transitions. It has been proposed that neural systems [Chialvo 2010], and more generally biological systems [Mora 2011], are statistically

critical in the sense that they are poised near the critical point of a phase transitions [Silva 1998, Fraiman 2009]. Statistical criticality is characterized by power law behavior such as avalanches [Beggs 2003, Levina 2007, Gireesh 2008] and long-range spatiotemporal correlations [Eguíluz 2005, Kitzbichler 2009]. While both dynamical criticality and statistical criticality have had success in neuroscience, their relation is still far from clear [Magnasco 2009, Mora 2011, Kanders 2017a]. In this thesis we will not be concerned with statistical criticality.

We should emphasize that the nonhyperbolicity hypothesis, as stated above and as studied in this thesis, is a hypothesis for local dynamics only. Global bifurcations very likely also play a role in interesting neural dynamics [Wiggins 2013, Kuznetsov 2013] and computations [Hoppensteadt 2012].

1.6 Work overview

We have explored the nonhyperbolicity hypothesis in three lines of research. The first [Hayton 2018a] has focused on showing how center manifold dynamics can explain how the the primary visual cortex is able to integrate information over scales in visual space in an input dependent manner. Studies have shown that the functional connectivity in V1 is strongly modulated by stimulus contrast [Nauhaus 2009]. In the absence of stimulus contrast, spike-triggered traveling waves of activity propagate over large areas of cortex. As contrast is increased, the waves become weaker in amplitude and travel over increasingly small distances. It has also been found that the receptive field size of V1 cells (defined as the length of spatial summation), increase with decreasing stimulus contrast. Moreover, neuronal responses become contrast-independent for large stimulus extents. Unsurprisingly, it has also been observed that the response latencies in V1 decrease with increasing stimulus contrast [Gawne 1996, Kapadia 1999].

Building upon previous work [Yan 2012], we have proposed a simple dynamical mech-

anism, relying on high-dimensional nonhyperbolicity, that captures these input-dependent observations, linking the contrast dependence of functional connectivity, spatial summation (in cortical and visual space), and response latencies [Hayton 2018a]. These properties arise as a consequence of the intrinsic structure of the network and are not explicitly included in an ad hoc fashion. This work [Hayton 2018a] is the focus of the thesis of the first author and will not be discussed in more details in this thesis.

The other two lines of research are separately described in the two parts of this thesis. While the two parts both deal with center manifold dynamics in neural systems, they can be read in any order. In the first part, we explore center manifold dynamics arising on a network having random connectivity as it's base. This is inspired by the Sompolinsky family of neural network models [Sompolinsky 1998], which assume an interaction structure given by a Gaussian random matrix scaled to have a spectrum in the unit disk. This family of neural networks has led to a number of useful results, including a flurry of recent publications [Stern 2014, Lalazar 2016, Rajan 2016, Ostojic 2014, Kadmon 2015, Landau 2016, Sompolinsky 2014, Engelken 2016, Harish 2015]. Unlike the usual approach in the theory of coupled oscillators where changes in global coupling parameters moves the whole cloud of eigenvalues, in our model each mode can be moved separately using the Brauer shift formula [Brauer 1952] as will be discussed in more detailed later (Fig. 2.3).

We study which statistical properties of the random connectivity are essential in determining both the shape of the center manifold and the corresponding reduced dynamics on it. We have previously [Moirogiannis 2017] presented a naive linear approach of this calculation in another paper, but here we will include the nonlinearities of the center manifolds as well. Using the center manifold reduction algorithm, we find that the resulting equations depend crucially on the structure and the statistics of the eigenvectors of the connectivity matrix. Even though the statistical distribution of eigenvalues of a broad class of random matrices

has been extensively characterized [Tao 2008], the statistical distribution of the eigenvectors is not well understood [Chalker 1998, Tao 2012, O'Rourke 2016]. Our analysis shows that the reduced dynamics on the center manifold, and thus the collective dynamics of the full system, can be drastically different from the dynamics of the individual subunits that are randomly coupled. We also find interesting constraints on the family of center manifold models that could arise from a large-scale random network.

In the second part of the thesis, we show that center manifold dynamics can explain several essential nonlinear features of cochlear dynamics [Hayton 2018b]. Studies have shown that the cochlea does not operate as a passive Fourier transformer, but instead, as an active nonlinear process which gives rise to three key characteristic properties: high gain amplification, sharp frequency tuning, and nonlinear compression of the dynamic range [Ruggero 1992, Ruggero 1997]. At the level of a single hair cell in the cochlea, a single Hopf bifurcation has been suggested as the underlying mathematical description of this nonlinear behavior [Choe 1998, Eguíluz 2000, Camalet 2000, Nadrowski 2004, Tinevez2007]. A single Hopf bifurcation alone, however, fails to describe the rich nonlinear behavior at the level of the full extended cochlea. Several models relying on multiple Hopf bifurcations, [Kern 2003, Duke 2003, Magnasco 2003, Dierkes 2008] have had success in capturing properties of the active process at the level of the extended cochlea; however, these models are comprehensive models [Hoppensteadt 1997], containing large amounts of biophysical details of basilar membrane mechanics, and surrounding fluid hydrodyanmics, and thus fail to answer the question: what is the mathematical structure underlying the nonlinear features of cochlear dynamics?

Here we propose a minimalist toy model poised at a nonhyperbolic equilibrium point as a proof of existence that higher dimensional center manifold dynamics could be the underlying mathematical mechanism for the dynamic response features of cochlea. Our toy model is similar to the one used in the theoretical model of V1, except with the linear part now being

a series of coupled critical oscillators, and we use similar analytical and integration methods. Our results suggest that as a single Hopf bifurcation generically gives rise to features of cochlea at a local level, the nonhyperbolicity mechanism proposed in this part of the thesis can be seen as a higher-dimensional analogue for the entire extended cochlea.

1.7 Toy models

Ordinary language models, comprehensive models, and empirical models have been used extensively in the field of neuroscience [Hoppensteadt 2012]. These three classes of models, however, are centered around the inclusion of a number of neurophysiological details and are often difficult to study with classical mathematical or computational techniques; furthermore, they are typically not useful in elucidating which mathematical structures give rise to particular dynamical properties and which structures could be eliminated to simplify the original system of equations. For example, normal form transformations [Dulac 1903, Poincarè, Arnold 1982, Kuznetsov 2013] can simplify the equations without reducing the dimension while center manifold reduction reduces the dimensionality without simplifying the reduced equations. The later technique will be discussed in details in the first part of this thesis.

To avoid the disadvantages of ordinary language, comprehensive models, and empirical models, one can instead construct canonical models [Hoppensteadt 1997, Hoppensteadt 2001, Hoppensteadt 2012, Izhikevich 2007a, Wiggins 2003] which are used to study universal properties of families of models. Roughly speaking, a canonical model, for a family of models exhibiting a particular desired set of properties, is a model such that any model in the family can be transformed into it with an appropriate change of variables [Dulac 1903, Poincarè, Arnold 1982, Kuznetsov 2013]. They have the huge advantage of switching the focus from studying the specific details of the "cherry picked" model to studying the dynamical regime itself giving rise to the desired property.

Inspired by this approach, our aim in this thesis is not to provide detailed anatomical and biophysical models of the cortex or cochlea but rather follow a minimalist approach by removing as many biological details as we can in hopes of elucidating the underlining mathematical structure describing the phenomena. We also do not claim that our models are canonical or make any attempt to reduce other models to our models, but hopefully by maintaining a minimalist approach, we can inform future research in constructing canonical models for these particular systems.

In the first part of this thesis, we study the simplest form of coupling between simple active units, while in the second part, we construct a minimalist *toy model* which provides an *existence proof* that center manifold dynamics can account for and connect key characteristic properties of cochlea: high-order compressive nonlinearities, amplification of weak input, frequency selectivity and traveling waves of activity. The same approach was followed in [Yan 2012, Hayton 2018a]. This approach of constructing a minimalist toy model to explain how a given mechanism can lead to a particular set of properties is common practice in theoretical physics and is the underlying philosophical approach of several well known theoretical neuroscience models, e.g. Wilson-Cowan equations, Hopfield networks, and Kuramoto models [Ermentrout 2012, Hoppensteadt 2012].

It is hard to explain what a toy model is better than Jack Cowan did: "...there is a way in which physicists approach the world, theoretical physicists, that I think really, really works and is really interesting. They don't try to put in every detail of what the phenomenon is like. They, if they have good taste, they select only those details that are really important for the questions they want to answer. And they construct what are sometimes called toy models, which aren't facing reality, to quote the title of a book by a friend of mine, Sir John Eccles, but they abstract from reality just what is needed to understand something. And I think that's what I've been trying to do with respect to brain mechanisms: try to make toy

models that contain enough details to answer questions about and give you ways to think about what's going on in the brain. Its not, I mean, it's not something that's commonly done. A lot of the time people do computational neuroscience where they put in a lot of details and make simulations and study what goes on. I don't do that. I tend to put in as few details as possible and say things that are interesting with few details rather than put in a lot of details. "

As our system of equations is a toy model of center manifold dynamics, we do not suggest that such simple equations describe actual anatomical structures in the cortex or that a simple 1-D line topology is necessarily present in cochlear anatomy; although, if the cochlea does indeed utilize center manifolds in the processing of sound, it might be the case that the full high dimensional phase space of cochlear dynamics could be reduced to simple, low dimensional structures on the center manifold.

Part II

Center Manifold Dynamics in Random Networks

Chapter 2

Center Manifold Dynamics in Random Networks

We consider a large number $N \to \infty$ of arbitrary, identical oscillators, coupled through random connectivity, in such a way that a few modes are critical. Our purpose is to determine the relationship of the arising dynamics to the individual units and the connectivity between them, in the same way that statistical mechanics determines macroscopic properties from microscopic. In contrast to classical statistical mechanics theory, in our model, each active unit is going to be described by dissipative and rotational dynamics. The bulk of studies of coupled oscillators use, as is appropriate in physics, a global coupling constant that confines strength of coupling with the effective dimensionality of the resulting dynamics. We propose a coupling more appropriate to neural circuitry where the coupling strength and the dimensionality can be controlled separately. Our setting highlights the statistical structure of the eigenvectors of the connectivity matrix as the fundamental determinant of collective behavior and gives rise to some interesting constrains on the family of center manifold models that could arise from a large-scale random network.

2.1 Introduction

Equilibrium statistical mechanics is static in nature, its program being the reduction of a thermodynamically large system to a handful of relevant variables and their equations of state. A major subprogram of nonequilibrium statistical mechanics similarly consists of reducing a thermodynamically large system to a handful of relevant variables and their dynamical laws.

We can describe this schematically as understanding under which conditions the diagram in Fig. 2.1 commutes, i.e. when taking either branch leads to the same result.

At the top left we have our thermodynamically large system, which lives in dimension N_H, ruled by a high-dimensional dynamical law. At the bottom right we have a low-dimensional space, the reduced variables, which live in dimension N_L. On the left branch, we first perform a detailed, costly and precise simulation of every variable in the system, and then we project this high-dimensional solution down into the lower-dimensional space. On the right branch, instead, we first project down the equations of motion themselves, to obtain an effective dynamics on the lower-dimensional subspace. Then we evolve the effective dynamics in its low-dimensional space. If we get the same low-D trajectories (or equivalent trajectories in some appropriately-defined sense) as a result of both branches, then we can say we have reduced our system.

We shall carry out this program for a particular setting inspired by the theory of neural networks. A number of studies have highlighted the recurrent intracortical connections as a major determinant of the patterns of global activity within the cerebral cortex. For example, the spontaneous activity of individual units in primary visual cortex is strongly coupled to global patterns evincing the underlying functional architecture [Tsodyks 1999, Kenet 2003]: during spontaneous activity in the absence of input, global modes are transiently activated that are extremely similar to modes engaged when inputs are presented (Fig. 2.2). Similarly

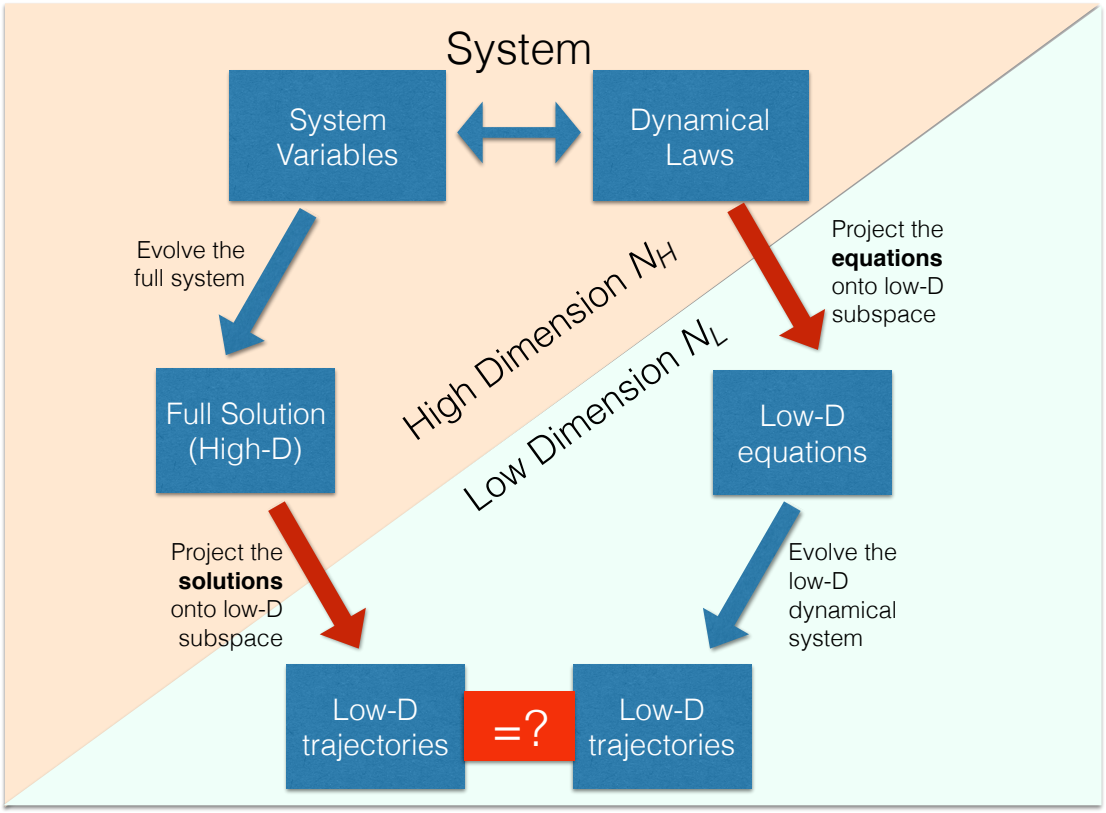

Figure 2.1: An abstract view of the effective description program in statistical mechanics

in motor control it has been shown both in motor reach actions [Churchland 2012] as well as in songbirds [Amador 2013] that motor gestures result in the transient activation of extended patterns of coherent activity. It has been previously argued that homeostatic mechanisms, such as those seeking to balance excitation and inhibition, will result in many dynamical modes of the system posing themselves close to the boundary between stability and instability [Magnasco 2009]. Near the onset of instability, the spatial layout of such dynamical modes is determined as eigenvectors of a connectivity matrix [Yan 2012, Hayton 2018a]; their transient activation is then consistent with the eigenvalue of such an eigenvector being driven through the instability line, and back [Amador 2013, Gardner 2001].

We will therefore try to take a point of view in which we have as our two ingredients, a cortical circuit, and a pattern of intracortical connections between copies of the same circuit [Silberberg 2002, Casanova 2015]. Cortical microcolumns have been hypothesized to be the fundamental processing subunits of the neocortex [Jones 2000]. Neurons within the same microcolumn are tightly interconnected with interlayer vertical connections [Casanova 2015] and the neocortex is made up of these repeating vertical structures bound together by mostly horizontal connections [Casanova 2015]. Inspired by this we first consider dynamical systems in which we have modules (thought of, generally, as the vertical direction) with a prescribed identical dynamics laid out on a surface (thought of, generally, as horizontal) coupled through homologous elements across modules i.e. only horizontal or vertical connections no diagonal. In keeping with a long tradition in computational neuroscience, we shall model the intermodule connectivity as being random [Sompolinsky 1998]. Therefore our model will be on one side highly structured (the given cortical circuit) and on the other side entirely structureless (the random connectivity across columns). Our aim is not to provide an anatomical model of neocortex but we rather use this example to demonstrate an approach that can be used in more general cases of randomly coupled dynamical systems.

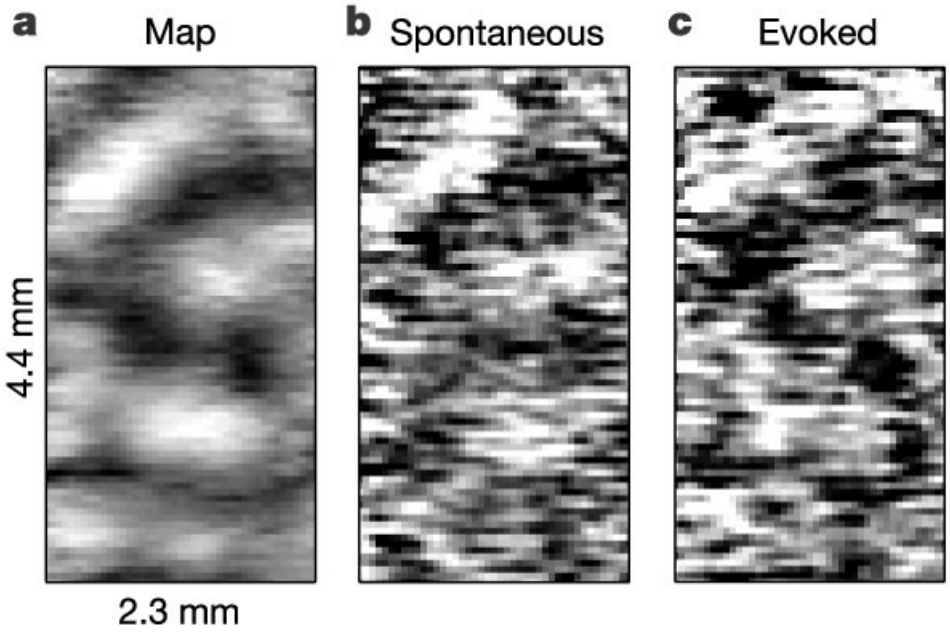

Figure 2.2: Reprinted by permission from [the RightsLink Permissions Springer Nature Customer Service Centre GmbH]: [Springer Nature] [Nature] [[Kenet 2003](Spontaneously emerging cortical representations of visual attributes, Tal Kenet, Dmitri Bibitchkov, Misha Tsodyks, Amiram Grinvald, Amos Arieli), Copyright (2003) .Activity corresponding closely to orientation maps spontaneously arises in the absence of input in an area with orientation selectivity. a) An orientation map of vertical orientation from cat area 18, where most cells are selective for stimulus orientation, obtained by using voltage sensitive dye imaging. b) A map obtained in a single frame from a spontaneous recording session. c) A single frame from an evoked session using the same orientation as for the map.

When pitted against the seemingly unfathomable depth of complexity within living beings, it is a natural zero information approach to modeling to assume the structure of interactions is, for all practical purposes of the modeler, structureless, a jumble of random numbers and noise. A classical embodiment of this line of thought are Kauffman nets [Kauffman 1967, Kauffman 1969], a modelization of transcriptional regulation networks as random boolean nets that was instrumental in highlighting the intrinsically dynamical nature of cell differentiation. In this family of models, the complex web of transcriptional regulation is described as a random boolean network, its fixed point attractors representing steady, self-consistent states of transcriptional activation that Kauffman equates to stable cell fate types; differentiation then being a process of climbing over metastable barriers separating basins of adjacent fixed points.

In neuroscience, a fruitful line of inquiry started with the Sompolinsky family of neural net models, which assume as a basis an interaction structure given by a Gaussian random matrix scaled to have a spectrum in the unit disk, and the overall excitatory/inhibitory balance set so the unit disk is displaced to the left until it osculates the imaginary axis [Sompolinsky 1998]. These results have been particularly instrumental as a beachhead in the study of recurrent neural networks, which have otherwise proved to be resilient to analysis.

Using this connectivity as their basis, a long series of works shows that by careful tampering with such a structure one may achieve a number of useful ends, with a notable flurry of recent activity [Stern 2014, Lalazar 2016, Rajan 2016, Ostojic 2014, Kadmon 2015, Landau 2016, Sompolinsky 2014, Engelken 2016, Harish 2015].

In [Magnasco 2009] it was shown that certain slow dynamics to evolve the connectivity structure itself, such as anti-Hebbian evolution, could result in drastic re-shaping of the eigenvalue distribution, where eigenvalues were flattened onto the imaginary axis, the edge of stability for the model.

In this part we shall work with a network that is not structureless as in the previous paragraphs, but rather has a cross product structure between a rigidly-defined object (the column) and a random-structure connectivity (across columns). This structure, though simplistic, can be viewed as a useful approximation to the structure of cortex, where the intracolumnar dynamics is largely defined by anatomy, while the recurrent intercolumnar dynamics may be usefully modeled as mostly random, within various degrees of geometrical restriction. The eigenspectrum of our system is therefore determined in equal measure by the rigid intracolumnar connectivity as well as the random intercolumnar interactions. As the aim of the thesis is to derive the coarse-grained dynamics (the eigencolumn) from the microscopic dynamics, we assumed a level of control over the spectrum which is bound to be somewhat unrealistic for biological structures. In further work, this restriction will be relieved gradually, as the setting allows for evaluating the interactions between multiple active eigencolumns. See Fig. 2.3 for a summary.

The structure of this part is as follows. We shall first introduce some general definitions and general framework as seen in Fig. 2.4. Moreover we introduce the nature of the random connectivity matrix and the type of control on its spectrum as seen in Fig. 2.5. Then we introduce a specific simple example that we are going to use in this thesis to describe the proposed techniques. Then we introduce some basic linear algebra notations that we will be using and the important random variables Γ's associated with the interaction matrix. Those random variables will be crucial in describing both the reduced dynamics and the dynamics of individual units as a function of the reduced dynamics. Following, we will show the linear projection of the dynamics on the center space and use this projection for a naive approximation and show results in the simplest case of a normal interaction matrix and a single real eigenvalue as our bifurcation parameter. Then we will show how this naive approximation may fail and proceed in introducing the basic center manifold reduction theorems which can be thought as a nonlinear generalization of the linear projection on the

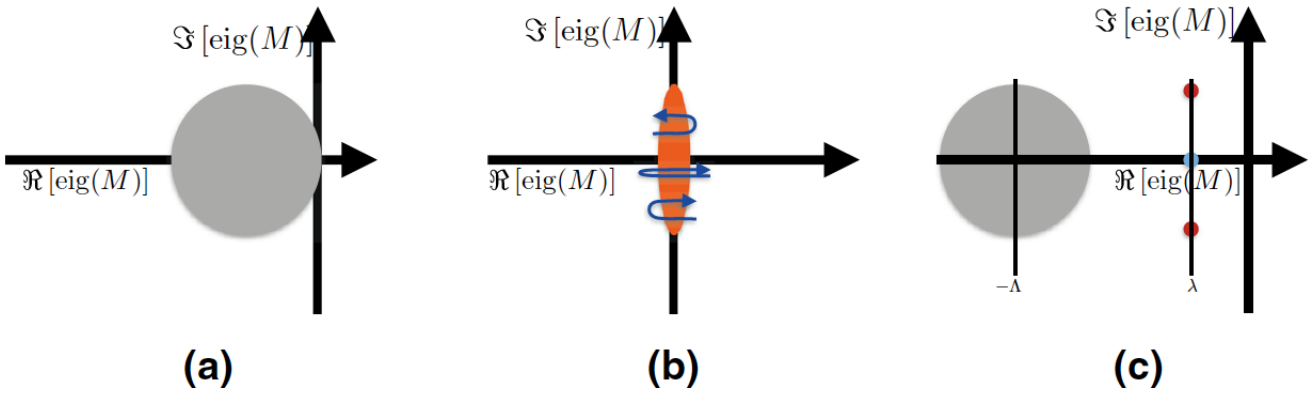

Figure 2.3: The eigenspectra of the interaction matrix in three models. a The SompolinskyAbbott family of models assumes as its basic state a matrix of i.i.d. Gaussians of variance 1/N (thus the spectrum is the unit disk) displaced to the left by 1 so that the spectrum osculates the imaginary axis. Various strategies for modifying the underlying connectivity allow this model to display a remarkably large variety of behaviors. b The self-tuned-critical model [Magnasco 2009] allows a matrix as in a to be modified by anti-Hebbian interactions; the result of such a dynamics is to stably flatten the entire cloud of eigenvalues onto the imaginary axis. The price to pay for this stabilization is that the eigenvalue dynamics never stops evolving, as all eigenvalues ceaselessly flutter around the imaginary axis. c The model considered here, starts by pushing most of the eigenvalue cloud to the stable region in the left, leaving only a few modes active. The aim of such a procedure is not to model a specific brain process, but rather to be able to derive the laws of motion of each collective mode from the microscopic dynamics, and subsequently to derive the interactions between multiple modes. Please carefully note that what is displayed is the spectrum of the interaction matrix; the spectrum of the system as a whole is determined both by this interaction matrix as well as by the Hessian of the internal dynamics of each column.

center space. Although the center manifold reduction algorithm is highly complicated we proceed by showing the first order approximation which takes a very simple form. Then we follow by using the resulting approximations as numerical Ansatz to correct both the reduced dynamics equations in the case where the naive approximation fails as well as to describe the dynamics of individual units using the reduced dynamics. Finally we take a very quick glimpse on preliminary results in the case of a finite number of real eigenvalues or a pair of compex conjugate eigenvalues crossing the real line. We close with a quick discussion on the case of non-normal matrices.

2.2 Definitions

Let us now establish the notation to be used in further detail, shown schematically in Fig. 2.4:

Again, at the top left we have our thermodynamically large system: many variables $x \in \mathbb{R}^{N_H}$ ruled by a high-dimensional dynamical law $\dot{x} = f(x)$ given by a vector field f in $\mathbb{R}^{N_H}$, stated as $f \in \mathcal{T}(\mathbb{R}^{N_H})$. At the bottom right we have a low-dimensional space, the reduced variables, which live in $\mathbb{R}^{N_L}$. On the left branch we first evolve in N_H and then we use a projection operator Π to project the high-dimensional solution down into the lower-dimensional space On the right branch, instead, we first project down the equations of motion, to obtain an effective dynamics F on the lower-dimensional subspace: $F \in \mathcal{T}(\mathbb{R}^{N_L})$. We call the projector operator for the equations Φ; then $F = \Phi\{f\}$. Then we evolve this simpler dynamics $\dot{X} = F(X)$. If we get the same trajectories (or equivalent trajectories in some well-defined sense) as a result of both branches, then we can say we have reduced our system.

In addition to this projection, we may want to lift back those low-dimensional solutions onto the original space, to obtain a high-dimensional solution of the original equations. We

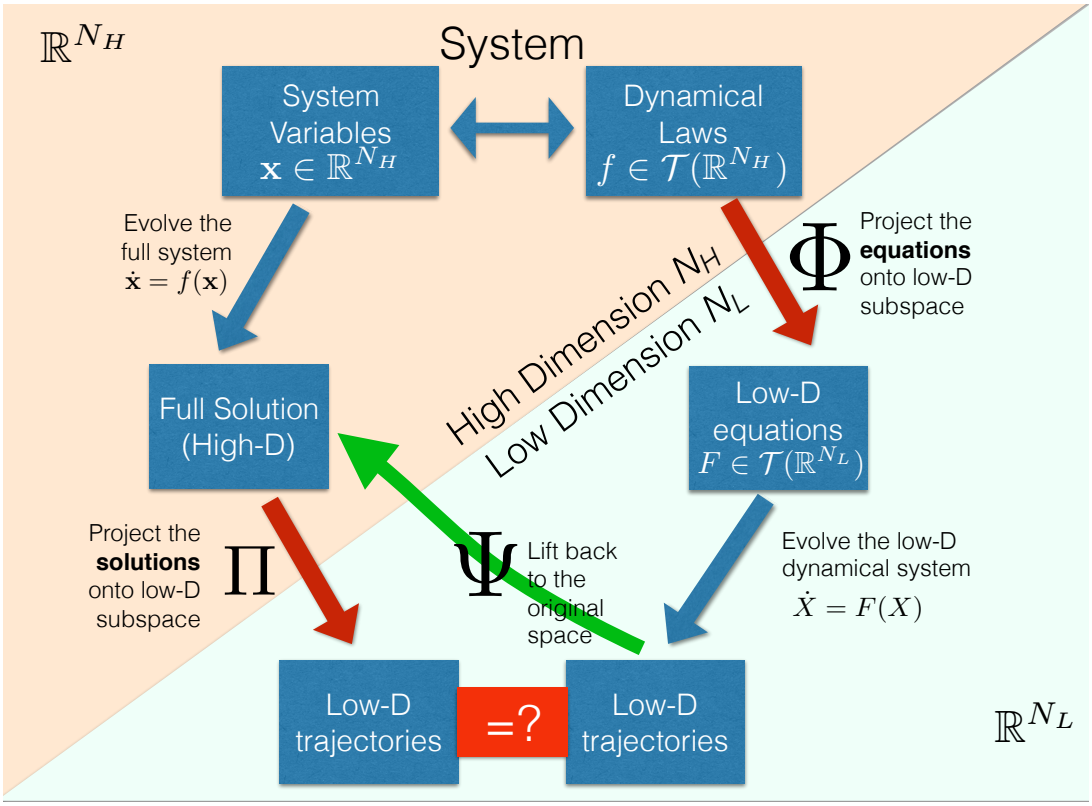

Figure 2.4: An abstract view of the effective description program in statistical mechanics

call the lift operator Ψ.

We have explored these questions in different examples in the setting of randomly coupled identical dynamical systems

The simplest such case is that of 1-D dynamical systems $\dot{x} = f(x)$, $x \in \mathbb{R}$ randomly coupled by a matrix M:

$$\dot{x}_i = f(x_i) + \sum_j M_{ij} x_j \tag{2.1}$$

We will try to demonstrate the above described methods using more interesting 2-D examples. Individual modules dynamics are described by equations of the form:

$$\begin{aligned} \dot{x} &= w_{xx}x + w_{xy}y + f(x) \\ \dot{y} &= w_{yx}x + w_{yy}y + g(y) \end{aligned} \tag{2.2}$$

The nonlinearities are captured by the analytic functions f and g with $f(0) = g(0) = Df(0) = Dg(0) = 0$.

Let $i \in \{1, 2, \ldots, N\}$ be a parametrization of cortical modules. We replicate the intramodule dynamics (2.2) for each of the N modules and couple all modules through variable x with a linear synaptic matrix M (and through layer y with a linear synaptic matrix L, but we will later consider $L = 0$):

$$\begin{aligned} \dot{x}_i &= w_{xx}x_i + w_{xy}y_i + f(x_i) + \sum_j M_{ij}x_j \\ \dot{y}_i &= w_{yx}x_i + w_{yy}y_i + g(x_i) + \sum_j L_{ij}y_j \end{aligned} \tag{2.3}$$

A common way to study such systems is to define $M_{ij} = \lambda G_{ij}$, where λ is a global coupling constant and G_{ij} a graph connectivity matrix, whose elements are either 0 or 1, which can be used to describe the connections as occurring only along an underlying lattice. This is a standard setting in Physics, where the interaction strength is controlled by a physical constant and therefore affects all extant interactions in parallel. This approach leads to a changing effective dimensionality of the dynamical system, because as λ is varied, all dynamical eigenvalues of the system move in unison, and hence the number of modes which can potentially enter the dynamics increases with increasing λ. We will take a different approach.

We shall assume the matrix M_{ij} is under control from slow homeostatic processes, and that the stability of different eigenmodes is under biological control. To approach this goal in a graded fashion we shall begin by assuming that most of the eigensystem $(\lambda^i, e^i) \ni Me = \lambda e$ has strongly negative eigenvalues. In addition we shall place the more specific hypothesis on the vector field (f, g) that when all eigenvalues λ of M are sufficiently negative there exists a single, stable fixed point of the dynamics.

Then we shall allow either one single real eigenvalue or a couple of complex-conjugate eigenvalues to increase and approach the stability limits from the left (Fig. 2.5). At the end we consider a finite number of eigenvalues approaching the stability limit too.

A simple form of doing this is by first generating a base matrix M_0 with a given controlled spectrum. Following a long history of modeling studies, one can assume M_0 to be given by

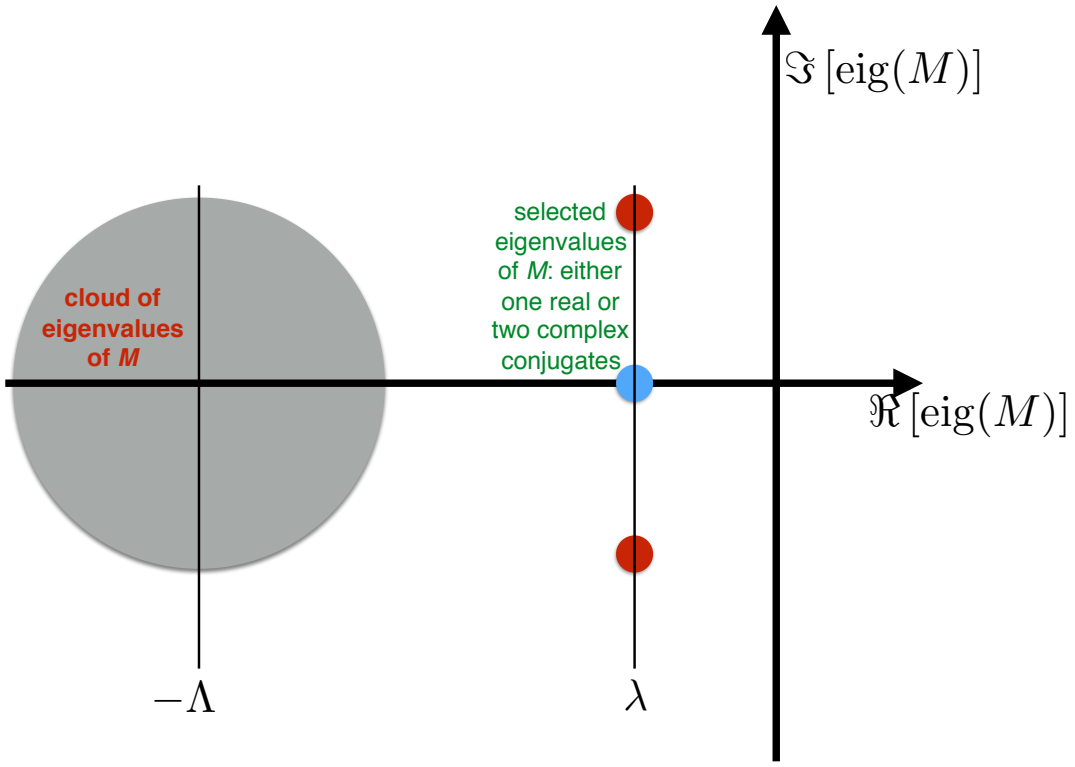

Figure 2.5: The eigenvalues of M in the complex plane. We shall construct M so that most eigenvalues have strongly negative real parts, around $-\Lambda$, while either one real or two complex-conjugate eigenvalues with real part λ will be allowed to approach the imaginary axis.

suitably-scaled i.i.d. Gaussian random variables [Sompolinsky 1998]. Following this line of thought, in this work we shall either use M_0 as an $N \times N$ array of i.i.d Gaussians of variance $1/N$ (spectrum in the unit disk in the complex plane, matrix almost surely non-normal) or the antisymmetric component of said M_0, $M_a = (M_0 - M_0^t)/\sqrt{2}$ (purely imaginary spectrum, matrix is normal).

For large enough $d \in \mathbb{R}^+$, $M = M_{0/a} - d\mathbf{I}$ has the effect of moving the cloud of eigenvalues from a disk centered at zero to a disk centered at $-d$. We can then move a single real eigenvalue $\lambda \in \mathbb{R}$ (with v and w the corresponding right and left eigenvectors) at $\mu \in \mathbb{R}$ using the Brauer shift formula [Brauer 1952]:

$$M_\mu = M_{0/a} - d\mathbf{I} + (d + \mu - \lambda)(\mathbf{vw}) \tag{2.4}$$

or a pair of complex conjugate eigenvalues λ, $\bar{\lambda}$ at $\mu \pm im(\lambda)\, i$:

$$M_\mu = M_{0/a} - d\mathbf{I} + (d + \mu - Re(\lambda))(\mathbf{vw}) + (d + \mu - Re(\bar{\lambda}))(\bar{\mathbf{v}}\bar{\mathbf{w}}) \tag{2.5}$$

Antisymmetric matrices are normal. Thus consider M to be given by eqn 2.4 with M_a, the antisymmetric component of a matrix of $N \times N$ i.i.d. Gausian variables of std $1/\sqrt{N}$; its eigenvalues are purely imaginary $\lambda = i\omega$ with imaginary component distributed like $p(\omega) \approx \sqrt{1 - \omega^2/4}$. Consider one of its null eigenvalues (one is guaranteed to exist if N is odd) and the corresponding eigenvector v. Then define as per Eq (2.4)

$$M_\lambda = M_a - \Lambda I + (\Lambda + \lambda)(\mathbf{vv}^\intercal) \tag{2.6}$$

where the left (dual) eigenvector $\mathbf{w}$ of $v\mathbf{v}$ is just it's transpose $\mathbf{v}^\intercal$. All eigenvalues of M, except for the null one we chose, get moved to $-\Lambda$, while the null one now has value λ.

The Jacobian matrix at the fixed point 0 is $J = \left[\begin{array}{c|c} M + w_{xx}I & w_{xy}I \\ \hline w_{yx}I & L + w_{yy}I \end{array}\right]$.

Both intermodule and intramodule connectivity and their interplay is essential in evaluating the eigenvalues - eigenvectors pairs of the Jacobian. A useful tool for this evaluation is the following lemma:

Lemma 1: Let $W = \left[\begin{array}{c|c} M & w_{xy}I \\ \hline w_{yx}I & L \end{array}\right]$ with $ML = LM$. Then :

(a) $Wv = \lambda v \iff \lambda^2 - (\lambda_M + \lambda_L)\,\lambda + (\lambda_M\lambda_L - w_{xy}w_{yx}) = 0$ & $v = \begin{pmatrix} u \\ \phi u \end{pmatrix}$, where $Mu = \lambda_M u$, $Nu = \lambda_L u$ and $\phi = \dfrac{\lambda - \lambda_M}{w_{xy}} = \dfrac{w_{yx}}{\lambda - \lambda_L}$.

Proof: Trivial using that 2 matrices commute iff they are simultaneously diagonalizable. ■

The system as a whole, then, has a stability structure given by $2N$ eigenvalues that is a complex interplay of the structured column and the unstructured connections.

2.3 Example used in this thesis

We now consider a particular case which we can solve in pretty good detail, so as to concentrate on what are the central figures and concepts in this approachh. Since each individual unit is 2-D obviously it cannot do much more than have a number of fixed points

and limit cycles. In what follows we will deal exclusively with the following N coupled identical damped oscillators $\left(\ddot{x}_i + F(x_i)\,\dot{x}_i + x_i = \sum_j M_{ij}\dot{x}_j\right)$, i.e. for $i \in \{1, \ldots N\}$:

$$\begin{aligned} \dot{x}_i &= y_i + f(x_i) + \sum_j M_{ij} x_j \\ \dot{y}_i &= -x_i \end{aligned} \tag{2.7}$$

where $f(x) = \sum_{n\geq 2} c_n x^n$ is analytic.

For example, in the special case $f(x) = -x^3$ we have N coupled identical van der Pol oscillators:

$$\ddot{x}_i = -3\dot{x}_i x_i^2 - x_i + \sum_j M_{ij}\dot{x}_j$$

We will show below we can evaluate the reduced dynamics for a Taylor series of f order-by-order, so some of what follows concentrates on $f(x) = x^\alpha$. But the main issue is the structure of M, whether it's normal or non-normal; and whether we control a single real or two complex-conjugate eigenvalues.

As we shall see shortly, our procedure for obtaining the global dynamics from the microscopic dynamics involves both the right and the left eigenvectors of M. In general the matrix of left eigenvectors is the inverse of the matrix of right eigenvectors. However if M is normal, then the inverse reduces to the complex conjugate making their relationship much simpler. Therefore we shall explore first normal matrices and then examine the additional issues raised by non-normality. Within normal matrices we shall, as anticipated in Fig. 2.5, either control a single real eigenvalue or two complex-conjugate ones.

We can evaluate the eigenvalue-eigenvector pairs of the Jacobian of the system from the corresponding eigenvalue-eigenvector pairs of M using the following corollary:

Corollary 2: Let $W = \left[\begin{array}{c|c} M & w_{xy}I \\ \hline w_{yx}I & 0I \end{array}\right]$ with $w_{xy}w_{yx} < 0$. Then:

(a) $Wv = \lambda v \iff \lambda + \frac{-w_{xy}w_{yx}}{\lambda} = \lambda_M \ \& \ v = \begin{pmatrix} \lambda u \\ w_{yx}u \end{pmatrix}$, where $Mu = \lambda_M u$

(b)$sign\left(Re\left(\lambda\right)\right) = sign\left(Re\left(\lambda_M\right)\right)$

(c)If M has a zero eigenvalue , then W has a pair of complex conjugate eigenvalues $\pm i\sqrt{-w_{xy}w_{yx}}$

(d)If M has a pair of complex conjugate eigenvalues $\pm\alpha i$ then W has 2 pair of complex conjugate eigenvalues with 2 frequencies $\frac{\alpha \pm \sqrt{\alpha^2 - 4w_{xy}w_{yx}}}{2}$.

Proof: Trivia corollary of lemma 1 or see [Hoppensteadt 2012] Theorem 12.1 for a similar statement. ■

2.4 Connectivity matrix M

Let us assume that the elements of $M = (m_{i,j})$ are independent randomly distributed gaussians of variance $\frac{1}{N}$ eg: $m_{i,j}$ *i.i.d.* $\sim \mathcal{N}\left(0, \frac{1}{N}\right)$ with spectrum in the unit disk in the complex plane[Tao 2008]. Let $\{V_{,1}, \ldots, V_{,N}\}$ be the basis in $\mathbb{C}^{N\times 1} \cong C^{\mathrm{N}}$ of normalized right eigenvectors of $M \in \mathbb{R}^{N\times N}$ i.e. $MV = V \begin{pmatrix} \lambda_1 & & 0 \\ & \ddots & \\ 0 & & \lambda_N \end{pmatrix}$, where $V = \begin{bmatrix} V_{,1}, & \cdots & , V_{,N} \end{bmatrix} \in \mathbb{C}^{N\times N}$. Let $\left\{W_{i,} = V^*_{,i}\right\}_{i\in\{1,\ldots N\}}$ be the dual basis of left eigenvectors of M in $\mathbb{R}^{1\times N} \cong \left(\mathbb{R}^{\mathrm{N}}\right)^*$

(where $* : \mathbb{R}^{\mathrm{N}} \to \left(\mathbb{R}^{\mathrm{N}}\right)^*$ is the dual map induced by the bilinear form $< V_{,i}, V_{,j} >= \delta_{i,j}$) i.e. $W = \begin{bmatrix} W_{1,} \\ \vdots \\ W_{N,} \end{bmatrix} = V^{-1}$.

For any $k \in \{1, \ldots, N\}$ and for any sequence of natural numbers of finite length N : $p : \{1, \ldots, N\} \to \mathbb{N}$, and for a given ordered basis (in this case the right eigenvectors with a chosen ordering) let's define:

$$\Gamma_k^p \coloneqq \sum_{\varphi} \left(V_{\varphi,k}\right)^* V_{\varphi,1}^{p(1)} \ldots V_{\varphi,N}^{p(N)} = \sum_{\varphi} W_{k,\varphi} V_{\varphi,1}^{p(1)} \ldots V_{\varphi,N}^{p(N)} = W_{k,} \times \circledast_i V_{,i}^{p(i)} \tag{2.8}$$

where $\times$ is matrix multiplication and $\circledast$ is element-wise multiplication (and the powers $V_{,i}^{p(i)}$ are elementwise).

In particular for the sequence $\delta_{i,\bullet}$ defined by $j \mapsto \delta_{i,j}$ (2.8) defines for $k = i$:

$$\Gamma_i^{k\delta_{i,\bullet}} \coloneqq \sum_{\varphi} \left(V_{\varphi,i}\right)^* V_{\varphi,i}^k = \sum_{\varphi} W_{i,\varphi} V_{\varphi,i}^k \tag{2.9}$$

As we will see these random variables play crucial role in describing the essential dynamics of the system. All the results in this part depend on M only through the distribution of the Γ_k^ps and therefore can be extended to any connectivity type (for instance sparse matrices or only close neighbors connections) as long as we know the statistical properties of the Γ_k^ps. As we will see the limits:

$$\lim_{N\to\infty} \left(N^{\frac{n-1}{2}} \frac{n!}{k_1! \cdots k_N!} \Gamma_{\mu}^{(k_1,\ldots,k_N)} \right)$$

where $n = k_1 + \ldots + k_N$ are crucial, and in particular the limits: $\lim_{N\to\infty} \left(N^{\frac{k-1}{2}} \Gamma_i^{k\delta_{i,\bullet}} \right)$.

2.5 Calculate Γ's for normal matrix with antisymmetric gaussian i.i.d. entries

In the case of normal matrices (2.9) can be written us:

$$\Gamma_i^{k\delta_i,\bullet} = \sum_{\varphi} V_{\varphi,i}^{k+1} \tag{2.10}$$

In the case of antisymmetric matrices we numerically observe that the elements of the eigenvectors approximate Gaussians of variance $\frac{1}{N}$ as $N \to \infty$ with:

$$\lim_{N\to\infty} \left(N^{\frac{k-1}{2}} \Gamma_i^{k\delta_i,\bullet} \right) = \begin{cases} k!! & k \text{ odd}, \\ 0 & k \text{ even}. \end{cases} \tag{2.11}$$

given by the moments of Gaussian, where $k!!$ is the double factorial $k!! = 1 \cdot 3 \cdots (k-2) \cdot k$. Similarly :

$$\lim_{N\to\infty} \left(N^{\frac{n-1}{2}} \frac{n!}{k_1! \cdots k_N!} \Gamma_i^{(k_1,\ldots,k_N)} \right) = \frac{n!}{k_1! \cdots k_N!} (k_1-1)!! \cdots k_i!! \cdots (k_N-1)!! = n!! \binom{\frac{n-1}{2}}{\frac{k_1}{2} \cdots \frac{k_i-1}{2} \cdots \frac{k_N}{2}} \tag{2.12}$$

if k_i and n are odd and k_j for $j \neq i$ are even. Else $= 0$. So the Γ's are given by co-moments of independent Gaussians.

Let us notice that it is known that for random symmetric matrices (Gaussian orthogonal ensemble) eigenvectors are uniformly distributed in the sphere and independent of the

eigenvalues (Corollary 2.5.4 in [Anderson 2010]). This is implied by the invariance of the law of X under arbitrary orthogonal transformations as in our case. From [O'Rourke 2016] we know that if v is uniformly distributed on the sphere then $\|v_i\|^2 \sim Beta\left(\frac{1}{2}, \frac{N-1}{2}\right)$ and $\lim_{N\to\infty} \|N^{\frac{p}{2}-1}\|v\|_{l_p}^p - E|N(0,1)|^p\| = 0$ almost surely.

2.6 Linear projection onto the stable and the center spaces - Definitions

Let $X_{\lambda_k} = \frac{1}{\sqrt{N}} W_{k,} \times \begin{pmatrix} x_1 \\ \vdots \\ x_n \end{pmatrix} = \frac{1}{\sqrt{N}} \sum_i W_{k,i} x_i$ be the normalized (so that X_{λ_k} is of order 1, because $x \cdot x \approx N$ while if M is normal $W_{k,} \cdot W_{k,} = 1$ so that $W_{k,} \cdot x \approx \sqrt{N}$ generically.) coordinates of activity in the basis of right eigenvalues, so :

$$x = \begin{pmatrix} x_1 \\ \vdots \\ x_N \end{pmatrix} = \sqrt{N} V \begin{pmatrix} X_{\lambda_1} \\ \vdots \\ X_{\lambda_N} \end{pmatrix} = \sqrt{N} \sum_i X_{\lambda_i} V_{,i} \tag{2.13}$$

where $V_{,i}$, for $i = 1, ..., N$ are the right eigenvectors, columns of the matrix V.

Applying $\frac{1}{\sqrt{N}} W$ to equations (2.7) we have, for an eigenvalue $\mu \in spec(M)$:

$$\begin{aligned} \dot{X}_\mu &= \frac{1}{\sqrt{N}} \sum_i W_{\mu,i} f(x_i) + Y_\mu + \mu X \\ \dot{Y}_\mu &= -X_\mu \end{aligned} \tag{2.14}$$

Equation (2.14) will be essential in defining the operator Φ as seen in Fig. 2.4. Equation (2.13) will be essential in defining the operator Ψ.

The Hartman–Grobman theorem only holds for hyperbolic equilibriums, so as eigenvalues move close to the critical boundary, the nonlinearities:

$$F_\mu \coloneqq \frac{1}{\sqrt{N}}\sum_i W_{\mu,i} f\left(x_i\right) = \frac{1}{\sqrt{N}}\sum_i W_{\mu,i} f\left(\sqrt{N}\sum_k V_{i,k} X_{\lambda_k}\right) \tag{2.15}$$

became essential in describing the dynamics.

Equations (2.7) (similarly for the general equations (2.3)) can be written in the basis of right eigenvectors corresponding to the eigenvalues, for $\mu \in spec\left(M\right)$:

$$\begin{aligned} \dot{X}_\mu &= F_\mu\left(X_{\lambda_1}, \ldots, X_{\lambda_N}\right) + Y_\mu + \mu X_\mu \\ \dot{Y}_\mu &= -X_\mu \end{aligned} \tag{2.16}$$

where

$$F_{\mu_i}\left(X_{\lambda_1}, \ldots, X_{\lambda_N}\right) = \sum_{n\geq 2} c_n \sum_{k_1+\ldots+k_N=n} \left(\frac{n!}{k_1!\cdots k_N!}\sqrt{N}^{(n-1)}\Gamma_\mu^{(k_1,\ldots,k_N)}\right) X_{\lambda_1}^{k_1}\cdots X_{\lambda_N}^{k_N} \tag{2.17}$$

2.7 Naive approach - Single real eigenvalue, normal matrix

Let us consider the system (2.7) as a single real eigenvalue of M, $\lambda = \lambda_1 \in \mathbb{R}$, crosses the imaginary axis (2.4) (the critical boundary for this case, look at corollary 2) becoming

slightly positive, while the rest of the eigenvalues $\mu \in \{\lambda_2, \ldots, \lambda_N\}$ have negative real part. The naive approximation would be to consider $X_\mu \approx 0$ for $\mu \in spec\,(M) \setminus \{\lambda\}$ and we can reduce the $2N$-dimensional system (2.7) into the 2-dimensional system :

$$\begin{aligned} \dot{X} &= F(x) + Y + \mu X \\ \dot{Y} &= -X \end{aligned} \tag{2.18}$$

Where $X \coloneqq X_\lambda$, $Y \coloneqq Y_\lambda$ and $F(x)$ is given by (2.15):

$$F(x) \coloneqq F_\lambda(x) = \frac{1}{\sqrt{N}} \sum_i W_{\lambda,i} f\,(x_i) = \frac{1}{\sqrt{N}} \sum_i W_{\lambda,i} f\left(\sqrt{N} V_{i,1} X + \sqrt{N} \sum_{\mu \in spec(M) \setminus \{\lambda\}} V_{i,\mu} X_\mu \right) \tag{2.19}$$

Evaluation of the $\sum_i W_{\lambda,i} f\,(x_i)$ term is the key; assuming conversely that the projection of x_i onto the complement of $V_{,1}$ (space perpendicular to $V_{,1}$ in the normal case) is small (an assumption we shall revisit in detail below) we'd get an ansatz which is our first, naive approximation of the lift operator Ψ which gives the microscopic variables as a function of the macroscopic ones $x = \Psi[X]$:

$$\begin{aligned} x_i &\approx \sqrt{N} X V_{i,1} \\ y_i &\approx \sqrt{N} Y V_{i,1} \end{aligned} \tag{2.20}$$

Then (2.18) can be written us :

$$\begin{aligned} \dot{X} &= F(X) + Y + \mu X \\ \dot{Y} &= -X \end{aligned} \tag{2.21}$$

Where :

$$F(X) = \frac{1}{\sqrt{N}} \sum_i W_{\lambda,i} f\left(\sqrt{N} V_{i,1} X\right) \tag{2.22}$$

The coarse-graining operator Φ, which transforms the microscopic dynamics to the coarsened dynamics is defined by

$$F \equiv \Phi[f]$$

In other words the $2N$ dimensional equation (2.14) is reduced to the 2 dimensional equation:

$$\begin{aligned} \dot{X}_\lambda &= \sum_{k\geq 2} \left(c_k \sqrt{N}^{(k-1)} \Gamma_\lambda^{k\delta_{1,\bullet}}\right) X_\lambda^k + Y_\lambda + \lambda X_\lambda \\ \dot{Y}_\lambda &= -X_\lambda \end{aligned} \tag{2.23}$$

We see that the dynamics of X_λ is determined by the random variables: $\sqrt{N}^{(k-1)} \Gamma_\lambda^{k\delta_{1,\bullet}} = \sqrt{N}^{(k-1)} \sum_{\varphi=1}^{N} W_{1,\varphi} V_{\varphi,1}^k$ where $V_{\cdot,1}$ is normalized so that $\sum_\varphi V_{\varphi,1}^2 = 1$:

In the case of normal matrices and $f(x) = \sum_{n\geq 2} c_n x^n$ analytic we have:

$$F(X) = \frac{1}{\sqrt{N}} \sum_{\varphi=1}^{N} W_{1,\varphi} f\left(V_{\varphi,1} \sqrt{N} X\right) = \sum_{k\geq 1} \left(c_{2k+1} (2k+1)!!\right) X^{2k+1} \tag{2.24}$$

.

The first thing to notice is that Φ is linear in f, meaning we can try to apply it order-by-order in a Taylor expansion of f. Applying Eq (2.22) to individual integer powers yields, in the large N limit, an evaluation of the moments of a Gaussian distribution:

$$\Phi[x^\alpha] = X^\alpha N^{\frac{\alpha-1}{2}} \sum_i e_i^{\alpha+1} = \begin{cases} \alpha!!\ X^\alpha & \alpha \text{ odd}, \\ 0 & \alpha \text{ even}. \end{cases} \tag{2.25}$$

The most important property to note is that the result is independent of which eigenvector v we chose, because under these circumstances the operator is self-averaging. Then, the power-law is unchanged except for a prefactor: the cubic X^3 nonlinearity gets renormalized by a factor of 3, X^5 by 15, X^7 by 105. Curiously this operator *destroys all even nonlinearities*. As we shall see later the even nonlinearities get absorbed in the overall shape of the center manifold, which we have assumed in the ansatz Eq (2.20) to be linear in x_i. However the naive reduced equations Eq (2.18) are not affected.

We first simulate randomly coupled Van der Pol oscillators given by Eq (2.7) with $f(x) = -x^3$ and for random matrix M defined using Eq (2.6) with $N = 351$ and $\Lambda = -30$. We let $\lambda = 0.1$ cross the real line by a small value. We numerically integrate the whole system for random initial values and let it settle after a transient on the limit cycle. In movie: `https://drive.google.com/open?id=14ku9fZlCUAW_mzEHIvezkRw4G6fbAAix` we plot at each time frame t the values $\{(x_i(t), y_i(t))|i \in \{1, \ldots, N\}$ as black dots. Moreover for each i we plot as a thin black line the orbit of (x_i, y_i) for a short time past interval $(t - \Delta t, t)$ to visualize the orbits. We plot with a green cycle (X_λ, Y_λ) the linear projection of x and y in the critical eigenvector and with a red cross the simulation of Eq (2.21) with $F(X) = -3X^3$ (and initial condition the linear projections on the critical mode of the initial conditions used for the high dimensional Eq (2.7)). Snapshots of the simulation movie are shown in Fig 2.6. As in the case of individual orbits we also plot part of the past orbits for visualization with

green and red colors respectable. As we can see in this case diagram Fig. 2.4 using our naive definition of our Φ operator Eq (2.25). Moreover we see that the cubic nonlinearity doesn't survive in the lift Ψ a statement that we shall see theoretically shortly.

In movie: `https://drive.google.com/open?id=1Ldn_YvlXaCSRc9L3dS_5smrh_39OqzOP` we can see the corresponding simulation for $f(x) = x^2 - x^3$. Snapshots of the simulation movie are shown in Fig. 2.7. As we can see the added even nonlinearity doesn't survive in the Φ operator and our approximation is still accurate (as we will see later a more accurate statement would be that the even nonlinearity doesn't survive as an even nonlinearity but can have small "leak" into higher order odd nonlinearities). But in this case it becomes apparent that the naive linear approximation of Ψ Eq (2.20) fails and the even nonlinearity survives in the operator. We will see that theoretically shortly.

2.8 Failure of above

The above approximation is studied in [Moirogiannis 2017] and assumes that the center space $E^c = \mathbb{R}\begin{pmatrix} v_1 \\ 0 \end{pmatrix} \oplus \mathbb{R}\begin{pmatrix} 0 \\ v_1 \end{pmatrix}$ is invariant which is only true up to linear approximation. In fact the nonlinearities of the invariant center manifolds tangent to E_c can change the qualitative behavior of the reduced to the manifold dynamics and there are examples that show that the above naive linear projection fails to capture the reduced dynamics [Guckenheimer 2013]. In our model particularly equations (2.23) predict that the Hopf bifurcation is supercritical iff $c_3 < 0$ independently of the value of c_2 but as numeric simulations show and as we will prove later the bifurcation is supercritical for large enough $|c_2|$.

We can see the failure of our naive Φ approximation Eq (2.25) by simulating a system as in the last movie with a higher order of even nonlinearity $f(x) = 4.1 * x^2 - x^3$. We can see this in movie: `https://drive.google.com/open?id=1FpkxPm5kRCjHi_TSl_`

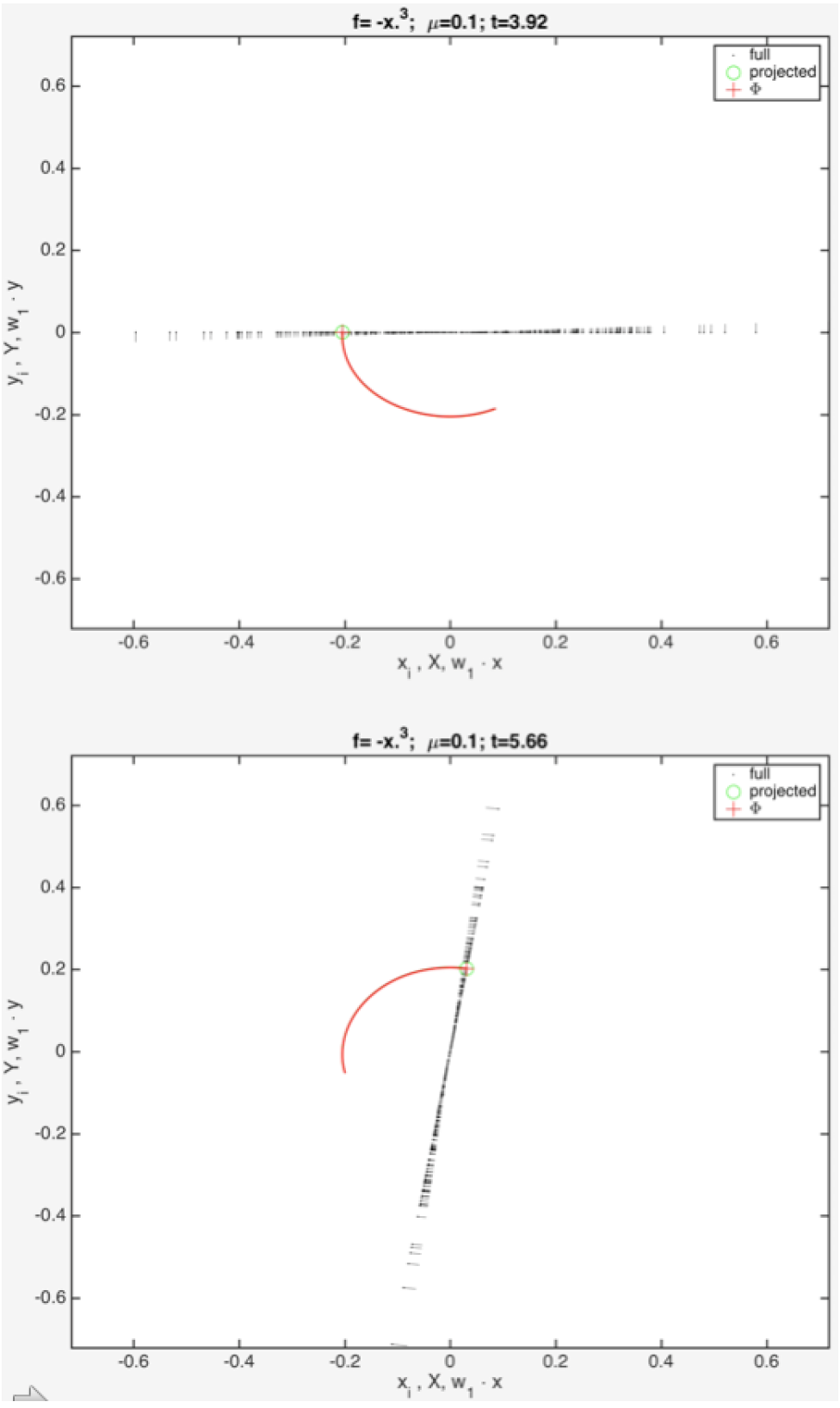

Figure 2.6: Randomly coupled Van der Pol oscillators given by Eq (2.7) with $f(x) = -x^3$ and for random matrix M defined using Eq (2.6) with $N = 351$ and $\Lambda = -30$. We let $\lambda = 0.1$ cross the real line by a small value.

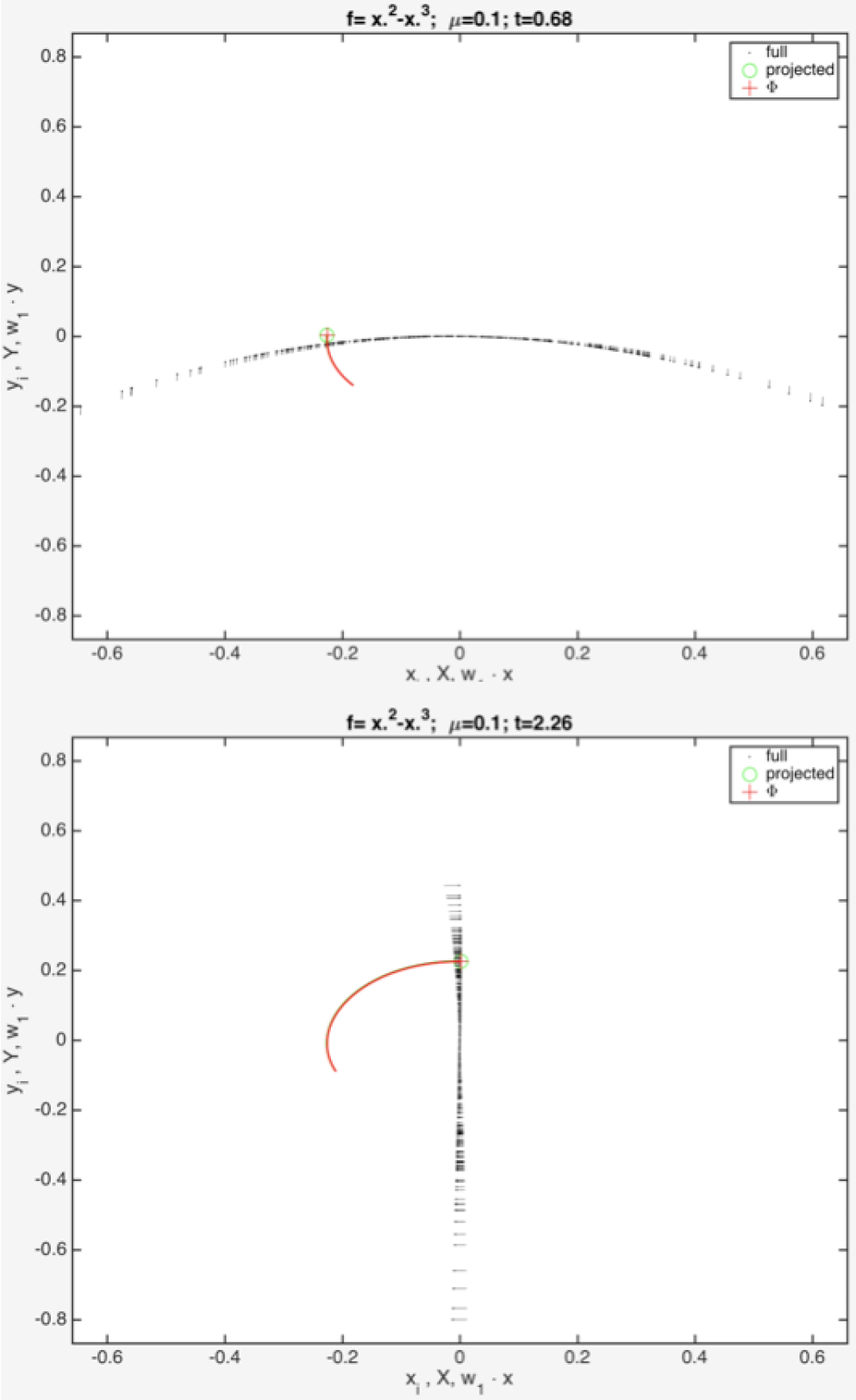

Figure 2.7: Randomly coupled Van der Pol oscillators given by Eq (2.7) with $f(x) = x^2 - x^3$ and for random matrix M defined using Eq (2.6) with $N = 351$ and $\Lambda = -30$. We let $\lambda = 0.1$ cross the real line by a small value.

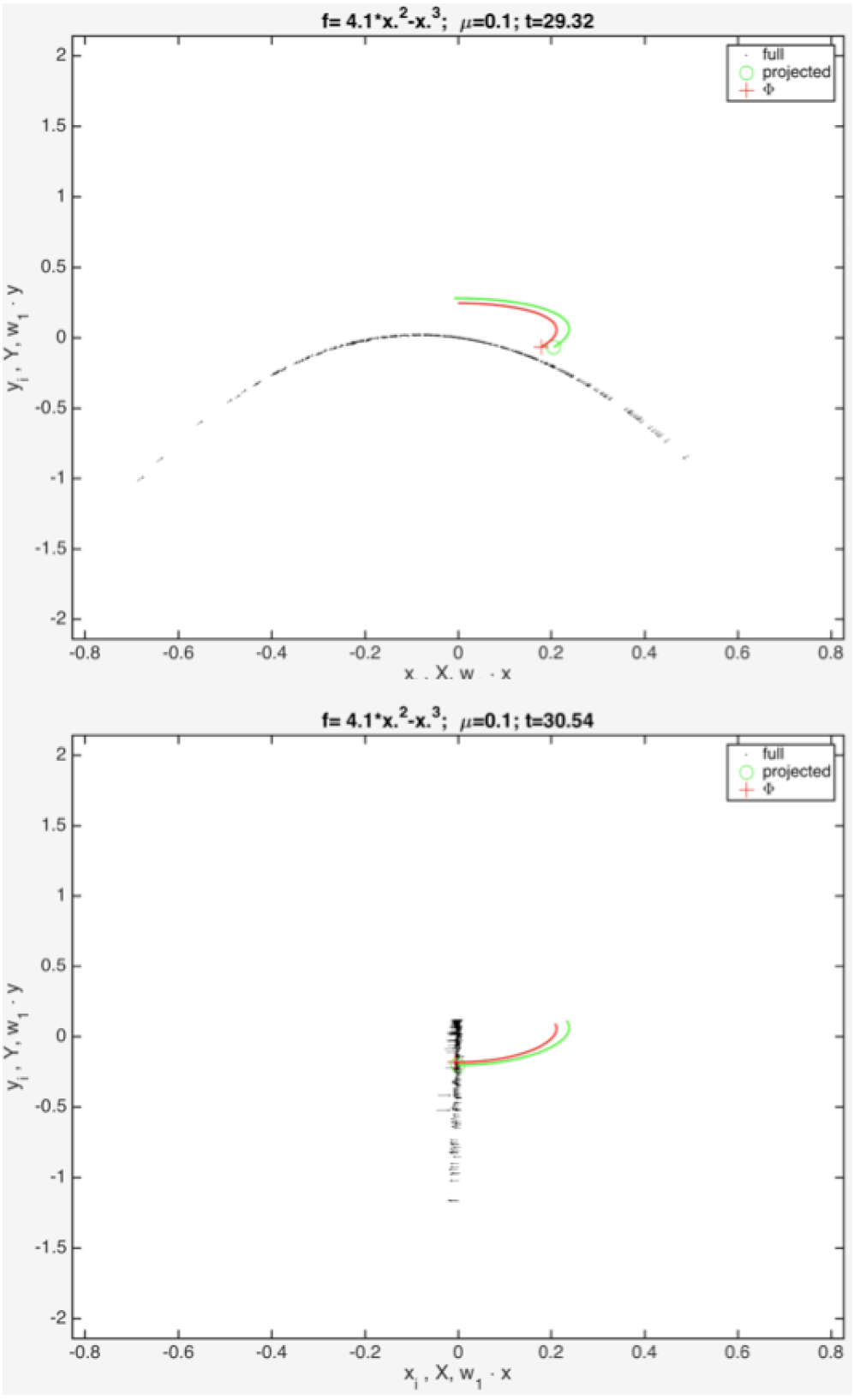

Figure 2.8: Randomly coupled Van der Pol oscillators given by Eq (2.7) with $f(x) = 4.1 * x^2 - x^3$ and for random matrix M defined using Eq (2.6) with $N = 351$ and $\Lambda = -30$. We let $\lambda = 0.1$ cross the real line by a small value.

`5Mrk3Jn6HQgAlr`. Snapshots of the simulation movie are shown in Fig. 2.8.

2.9 Center manifold reduction

We will follow similar notation and approach as in [Hoppensteadt 2001] , in particular look at section 12.7 for the 3nd order approximation of ψ for $f(x) = x^2$ and 2nd order approximation of ψ for $f(x) = \pm x^3$ in the case of symmetric interaction matrix. Here we care about more general forms of matrices and for any abstract nonlinearity. For more details on center manifolds look at [Ioos 1999] or for formal proofs at [Carr 2012].

We can rewrite equation (2.7) as:

$$(2.7) \Leftrightarrow \quad : \dot{Z} = G(Z) = WZ + F(Z)$$

$$\text{where } Z = \begin{pmatrix} x_1 \\ \vdots \\ x_N \\ y_1 \\ \vdots \\ y_N \end{pmatrix} \in \mathbb{R}^{2N}, \quad W = \left(\begin{array}{c|c} M & I \\ \hline -I & 0 \end{array}\right), \quad F(Z) = \begin{pmatrix} f(x_1) \\ \vdots \\ f(x_N) \\ 0 \\ \vdots \\ 0 \end{pmatrix}.$$

Let us assume that a single real eigenvalue of M, $\lambda = \lambda_1 \in \mathbb{R}$ (with corresponding right eigenvector v_1) crosses the imaginary axis. Corollary 2 implies that the corresponding eigenvalues of the whole system are $\pm i$ with corresponding eigenvectors $\begin{pmatrix} \pm i v_1 \\ -v_1 \end{pmatrix}$. Let $E^c = \mathbb{R}\begin{pmatrix} v_1 \\ 0 \end{pmatrix} \oplus \mathbb{R}\begin{pmatrix} 0 \\ v_1 \end{pmatrix} = \left\{ x\begin{pmatrix} v_1 \\ 0 \end{pmatrix} + y\begin{pmatrix} 0 \\ v_1 \end{pmatrix} \mid x, y \in \mathbb{R} \right\}$ be the center space, $E^s =$

$E^{\lambda_2} \oplus \ldots \oplus E^{\lambda_N} = \mathbb{R} \begin{pmatrix} v_2 \\ 0 \end{pmatrix} \oplus \mathbb{R} \begin{pmatrix} 0 \\ v_2 \end{pmatrix} \oplus \ldots \oplus \mathbb{R} \begin{pmatrix} v_N \\ 0 \end{pmatrix} \oplus \mathbb{R} \begin{pmatrix} 0 \\ v_N \end{pmatrix}$ be the stable space, $\Pi_c = \begin{pmatrix} v_1 w_1 & 0 \\ 0 & v_1 w_1 \end{pmatrix} : \mathbb{R}^{2N} = E^c \oplus E^s \to E^c$, $\Pi_{\lambda_k} = \begin{pmatrix} v_k w_k & 0 \\ 0 & v_k w_k \end{pmatrix} : \mathbb{R}^{2N} \to E^{\lambda_k}$ and $\Pi_s = \Pi_{\lambda_2} + \ldots + \Pi_{\lambda_k} : \mathbb{R}^{2N} = E^c \oplus E^s \to E^s$ the defined by the basis projections. The above projections commute with W since they have the same eigenspaces.

The center manifold theorem ensures that there is a local mapping $\psi : E^c \to E^s$ with

$$\psi(0) = 0 \quad and \quad D\psi(0) = 0$$

such that the manifold $\mathcal{M}$ defined by:

$$\mathcal{M} = \{u + \psi(u) \mid u \in E_c\} = \left\{ x \begin{pmatrix} v_1 \\ 0 \end{pmatrix} + y \begin{pmatrix} 0 \\ v_1 \end{pmatrix} + \psi(x, y) \mid x, y \in \mathbb{R} \right\}$$

is invariant and locally attractive (emergence theorem). The dynamics reduced on $\mathcal{M}$ are locally:

$$\dot{u} = \Pi_c G(u + \psi(u)) = Wu + \Pi_c F(u + \psi(u)) \tag{2.26}$$

A schematic of a center manifold and the invariance equations can be seen in Fig. 2.9. Using the approximation theorem, we can approximate ψ to any order from the equation:

$$D\psi(u)(Wu + \Pi_c F(u + \psi(u))) = D\psi(u)\dot{u} = \Pi_s G(u + \psi(u)) = W\psi(u) + \Pi_s F(u + \psi(u)) \tag{2.27}$$

More precisely, if $Dh(u)(Wu + \Pi_c F(u + h(u))) - Wh(u) + \Pi_s F(u + h(u)) = O\left(|u|^k\right)$ then $\psi(u) = h(u) + O\left(|u|^k\right)$.

ψ approximated by (2.27) is used to define the lift operator Ψ_f and equation (2.26) defines the reduction operator Φ.

This gives us an algorithm of calculating orders of increasingly degree in the Taylor expansions of both reduced dynamics and the center manifold embedding by iteratively interchanging equations (2.26) : $\dot{u} = Wu + \Pi_c F(u + \psi(u))$ and (2.27) : $D\psi(u)\dot{u} = W\psi(u) + \Pi_s F(u + \psi(u))$ correspondingly. However this algorithm can be complicated. As the dimension of the center manifold increases (or order of desired approximation increases) the calculations become intractable (the number of unknown parameters and resulting equations grows like $\begin{pmatrix} dimention + order - 1 \\ order \end{pmatrix}$, the number of parameters to keep track of $\sim \sum_{r<order} \begin{pmatrix} dimention + r - 1 \\ r \end{pmatrix}$ + all combinations with repetitions of those up to the specified $order$). So using symbolic algorithms is essential [Freire 1988] .

2.10 n th order approximation of Ψ for $f(x) = c_n x^n + O\left(x^{n+1}\right)$

Even though those questions are in general complicated, when estimating the first nonlinear order of approximation for the center manifold embedding and reduced dynamics on it of (2.7) with $f(x) = c_n x^n + O(x^{n+1})$ the corresponding equations are very simple.

Let $\psi\left(\begin{pmatrix} v_1 \\ 0 \end{pmatrix} x + \begin{pmatrix} 0 \\ v_1 \end{pmatrix} y\right) = \sum_{k=2}^{N} \begin{pmatrix} \left(\sum_{i=0}^{n} \alpha_i^k x^{n-i} y^i\right) V_{,k} \\ \left(\sum_{i=0}^{n} \beta_i^k x^{n-i} y^i\right) V_{,k} \end{pmatrix} + O\left(\left(\sqrt{x^2 + y^2}\right)^n\right)$, and for

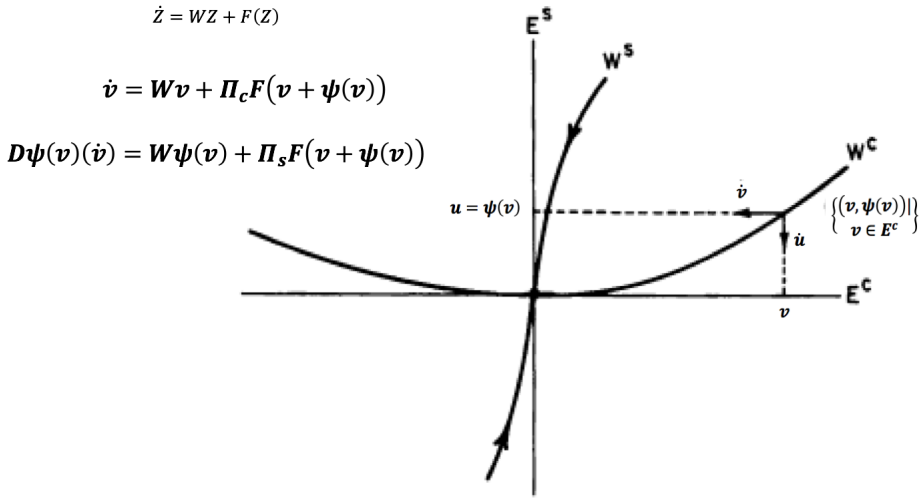

Figure 2.9: A schematic of center manifold and the invariance equations.

convenience let $\alpha_{-1} = \alpha_{n+1} = \beta_{-1} = \beta_{n+1} = 0$.

$$\text{Then } D\psi(u)\,\dot{u} = \sum_{k=2}^{N} \begin{pmatrix} \left(\sum_{i=0}^{n} \left((n-i+1)\,\alpha_{i-1}^k - (i+1)\,\alpha_{i+1}^k\right) x^{n-i}y^i\right) V_{,k} \\ \left(\sum_{i=0}^{n} \left((n-i+1)\,\beta_{i-1}^k - (i+1)\,\beta_{i+1}^k\right) x^{n-i}y^i\right) V_{,k} \end{pmatrix} + O\left(\left(\sqrt{x^2+y^2}\right)^n\right)$$

,

$$W\psi(u) = \sum_{k=2}^{N} \begin{pmatrix} \left(\sum_{i=0}^{n} \left(\lambda_k \alpha_i^k + \beta_i^k\right) x^{n-i}y^i\right) V_{,k} \\ \left(\sum_{i=0}^{n} -\alpha_i^k x^{n-i}y^i\right) V_{,k} \end{pmatrix} + O\left(\left(\sqrt{x^2+y^2}\right)^n\right),$$

$$\Pi_s F(u + \Psi(u)) = c_n \Pi_s \begin{pmatrix} (V_{1,1}x + O(n+1))^n \\ \vdots \\ (V_{N,1}x + O(n+1))^n \\ 0 \\ \vdots \\ 0 \end{pmatrix} = c_n \Pi_s \begin{pmatrix} (V_{1,1}x)^n \\ \vdots \\ (V_{N,1}x)^n \\ 0 \\ \vdots \\ 0 \end{pmatrix} + O(n+1) =$$

$c_n x^n \sum_{k=2}^{N} V_{,k} \Gamma_k^{n\delta_1,\bullet} + O(n+1)$.

Projecting equation (2.27) onto the stable modes using Π_{λ_k} for $k \geq 2$ gives us the equations:

$$\begin{pmatrix} \alpha_0^k \\ \vdots \\ \alpha_n^k \end{pmatrix} = A \begin{pmatrix} \beta_0^k \\ \vdots \\ \beta_n^k \end{pmatrix} \tag{2.28}$$

$$(-\lambda_k id_n - A) \begin{pmatrix} \alpha_0^k \\ \vdots \\ \alpha_n^k \end{pmatrix} - \begin{pmatrix} \beta_0^k \\ \vdots \\ \beta_n^k \end{pmatrix} = \begin{pmatrix} c_n \Gamma_k^{n\delta_1,\bullet} \\ \vdots \\ 0 \end{pmatrix}$$

where $A = \begin{pmatrix} 0 & 1 & & & & & \\ -n & 0 & 2 & & & & \\ & -(n-1) & 0 & \ddots & & & \\ & & \ddots & \ddots & \ddots & & \\ & & & \ddots & 0 & n-1 & \\ & & & & -2 & 0 & n \\ & & & & & -1 & 0 \end{pmatrix}$.

If $f(x) = c_2 x^2 + O(x^3)$ then

$$\Psi\left(\begin{pmatrix} v_1 \\ 0 \end{pmatrix} x + \begin{pmatrix} 0 \\ v_1 \end{pmatrix} y\right) = \tag{2.29}$$

$$= \sum_{k=2}^{N} c_2 \Gamma_k^{2\delta_{1,\bullet}} \begin{pmatrix} \left(\frac{-2\lambda_k}{4\lambda_k^2+9} x^2 + \frac{-6}{4\lambda_k^2+9} xy + \frac{2\lambda_k}{4\lambda_k^2+9} y^2 + O(3)\right) V_{,k} \\ \left(\frac{-(2\lambda_k^2+3)}{4\lambda_k^2+9} x^2 + \frac{-2\lambda_k}{4\lambda_k^2+9} xy + \frac{-(2\lambda_k^2+6)}{4\lambda_k^2+9} y^2 + O(3)\right) V_{,k} \end{pmatrix} \tag{2.30}$$

If $f(x) = c_3 x^3 + O(x^4)$ then

$$\Psi\left(\begin{pmatrix} v_1 \\ 0 \end{pmatrix} x + \begin{pmatrix} 0 \\ v_1 \end{pmatrix} y\right) = \tag{2.31}$$

$$= \sum_{k=2}^{N} c_3 \Gamma_k^{3\delta_{1,\bullet}} \begin{pmatrix} \left(\frac{-9\lambda_k^2-48}{9\lambda_k^3+64\lambda_k} x^3 - \frac{18\lambda_k}{9\lambda_k^3+64\lambda_k} x^2 y + \frac{-48}{9\lambda_k^3+64\lambda_k} xy^2 - \frac{-6\lambda_k}{9\lambda_k^3+64\lambda_k} y^3 + O(4)\right) V_{,k} \\ \left(\frac{2\lambda_k}{9\lambda_k^3+64\lambda_k} x^3 + \frac{-9\lambda_k^2-48}{9\lambda_k^3+64\lambda_k} x^2 y + \frac{-6\lambda_k}{9\lambda_k^3+64\lambda_k} xy^2 + \frac{-6\lambda_k^2-48}{9\lambda_k^3+64\lambda_k} y^3 + O(4)\right) V_{,k} \end{pmatrix} \tag{2.32}$$

Let us notice that for the matrix M generated as in (2.6) we have that for $\Lambda \to \infty$ the 3rd order nonlinearity (odd) doesn't survive on the shape of the center manifold while the 2nd order nonlinearity (even) survives only on the second "layer" and only as even in both x and

y. This is not a general result but comes from the interplay between the vertical (module) and horizontal (M) connectivity. For instance the same calculations for (2.1) gives as a center manifold where even the even nonlinearities go to 0 when $\Lambda \to \infty$.

2.11 Symmetries of α's and β's

The above observation for the first order of approximation of Psi is more general. In particular we can show that: $\alpha_i^k = \dfrac{P_{a,k,i}}{P}$, and $\beta_i^k = \dfrac{P_{\beta,k,i}}{P}$, where P is a polynomial of λ_k of order k and $P_{\alpha,k,i}$, $P_{\beta,k,i}$ polynomials of order $\leq k$. The inequality is strict except for $P_{\beta,k,i}$ when k and i are even. That would imply that for large Λ only even nonlinearities survive by the operate Ψ as even nonlinearities on the y layer (the layer in which the original equations don't include nonlinearities). We will talk about this in details elsewhere but let us just notice that the coefficients are just determined by determinants of submatrices of the pentadiagonal $A^2 + \lambda_k A + id_n$ where:

$$A^2 =$$

$$\begin{pmatrix}
-n & 0 & 1\cdot 2 & 0 & & & & & & & & & \\
0 & -n\cdot 1-2\cdot(n-1) & 0 & 2\cdot 3 & & & & & & & & & \\
n\cdot(n-1) & 0 & -(n-1)\cdot 2-3\cdot(n-2) & 0 & \ddots & & & & & & & & \\
0 & (n-1)\cdot(n-2) & 0 & \ddots & & & & & & & & & \\
 & & \ddots & & \ddots & & (k-1)\cdot k & & & & & & \\
 & & & & & \ddots & 0 & k\cdot(k+1) & & & & & \\
 & & & & (n+2-k)\cdot(n+1-k) & 0 & -(n+1-k)\cdot k-(k+1)\cdot(n-k) & 0 & (k+1)\cdot(k+2) & & & & \\
 & & & & & (n+1-k)\cdot(n-k) & 0 & & & & & & \\
 & & & & & & (n-k)\cdot(n-k-1) & & & & \ddots & & \\
 & & & & & & & & & \ddots & 0 & (n-2)\cdot(n-1) & 0 \\
 & & & & & & & & \ddots & 0 & -3\cdot(n-2)-(n-1)\cdot 2 & 0 & (n-1)\cdot n \\
 & & & & & & & & & 3\cdot 2 & 0 & -2\cdot(n-1)-n\cdot 1 & 0 \\
 & & & & & & & & 0 & 2\cdot 1 & 0 & -n &
\end{pmatrix} 1$$

2.12 Reduced dynamics 3rd order approximation

Let $f(x) = c_2x^2 + c_3x^3 + O(x^4)$, then:

The reduced equations (2.26) are then up to order 3 :

$$\begin{pmatrix} v_1 \\ 0 \end{pmatrix} \dot{x} + \begin{pmatrix} 0 \\ v_1 \end{pmatrix} \dot{y} = W \begin{pmatrix} v_1 \\ 0 \end{pmatrix} x + W \begin{pmatrix} 0 \\ v_1 \end{pmatrix} y +$$

$$+c_2\Pi_c \begin{pmatrix} \begin{pmatrix} \left(V_{1,1}x + \sum_{k=2}^{N} V_{1,k}\left(\alpha_0^k x^2 + \alpha_1^k xy + \alpha_2^k y^2\right)\right)^2 \\ \vdots \\ \left(V_{N,1}x + \sum_{k=2}^{N} V_{N,k}\left(\beta_0^k x^2 + \beta_1^k xy + \beta_2^k y^2\right)\right)^2 \\ 0 \\ \vdots \\ 0 \end{pmatrix} \end{pmatrix} + c_3\Pi_c \begin{pmatrix} \begin{pmatrix} (V_{1,1}x)^3 \\ \vdots \\ (V_{N,1}x)^3 \\ 0 \\ \vdots \\ 0 \end{pmatrix} \end{pmatrix} + O(4)$$

So:

$$\begin{aligned} \dot{x} &= y + c_2\Gamma_1^{2\delta_{1,\bullet}} x^2 + \left(c_3 \Gamma_1^{3\delta_{1,\bullet}} + 2c_2 \sum_{k=2}^{N} \Gamma_1^{\delta_{1,\bullet}+\delta_{k,\bullet}} \alpha_0^k\right) x^3 + \left(2c_2 \sum_{k=2}^{N} \Gamma_1^{\delta_{1,\bullet}+\delta_{k,\bullet}} \alpha_1^k\right) x^2 y + \\ &\quad + \left(2c_2 \sum_{k=2}^{N} \Gamma_1^{\delta_{1,\bullet}+\delta_{k,\bullet}} \alpha_2^k\right) xy^2 + O(4) \\ \dot{y} &= -x \end{aligned}$$

Proposition 3: Let M_0 with $\lambda_1 = 0$, $Re(\lambda_i) < 0$ for $i > 1$ and $M(\mu) = M_0 + \mu V_{,1} W_{1,}$. The system (2.7) undergoes an Andronov-Hopf bifurcation at $\mu = 0$ if $a = c_3 \frac{3}{8} \Gamma_1^{3\delta_{1,\bullet}} - c_2^2 \sum_{k=2}^{N} \Gamma_1^{\delta_{1,\bullet}+\delta_{k,\bullet}} \Gamma_k^{2\delta_{1,\bullet}} \frac{\lambda_k}{4\lambda_k^2 + 9} \neq 0$.

The bifurcation is subcritical (supercritical) iff $a > 0$ ($a < 0$).

Proof sketch: Proposition 2b $\Rightarrow$ non-hyperbolicity and transversality condition. For the

system:

$$\begin{aligned} \dot{x} &= y + \tilde{f}(x,y) \\ \dot{y} &= -x + \tilde{g}(x,y) \end{aligned}$$

the genericity condition parameter is :

$$a = \frac{1}{16}\left(\tilde{f}_{xxx} + \tilde{f}_{xyy} + \tilde{g}_{xxy} + \tilde{g}_{yyy}\right) + \frac{1}{16\omega}\left(\tilde{f}_{xy}\left(\tilde{f}_{xx} + \tilde{f}_{yy}\right) - \tilde{g}_{xy}\left(\tilde{g}_{xx} + \tilde{g}_{yy}\right) - \tilde{f}_{xx}\tilde{g}_{xx} + \tilde{f}_{yy}\tilde{g}_{yy}\right) =$$
$$\frac{1}{16}\left(\tilde{f}_{xxx} + \tilde{f}_{xyy}\right) = c_3\frac{3}{8}\Gamma_1^{3\delta_1,\bullet} - c_2^2\sum_{k=2}^{N}\Gamma_1^{\delta_1,\bullet+\delta_k,\bullet}\Gamma_k^{2\delta_1,\bullet}\frac{\lambda_k}{4\lambda_k^2+9}\blacksquare$$

In particular let us notice that this operator can drastically change the whole dynamics and create a subcritical bifurcation from subunits of supercritical bifurcation if the interaction connectivity is not normal.

Notice: if M is normal then $-\sqrt{N}^{(3-1)}c_2^2\sum_{k=2}^{N}\Gamma_1^{\delta_1,\bullet+\delta_k,\bullet}\Gamma_k^{2\delta_1,\bullet}\frac{\lambda_k}{4\lambda_k^2+9} > 0. \xrightarrow{N\to\infty} 3c_2^2\frac{\lambda_k}{4\lambda_k^2+9}$, and the naive approximation of defining Φ should be appropriate for $c_2 \ll \sqrt{\Lambda}$.

Now we can use the nonlinearities of the newly defined reduced dynamics to define our new Φ. Which is shown as a blue cross in movie `https://drive.google.com/open?id=1NN0wju5Dl_VBD0JkL-PBHvfmJkWKdh8F`. Snapshots of the simulation movie are shown in Fig. 2.10.

2.13 Numerical Ansatz for approximating Ψ when $f(x) = c_2x^2 + c_3x^3$ and M is normal and $\lambda_k \approx -d$ for $k \geq 2$.

Let's use the 2nd order nonlinearities of the center manifold (at the bifurcation point) as a guess of the residuals of individual units for small $\lambda_1 > 0$.

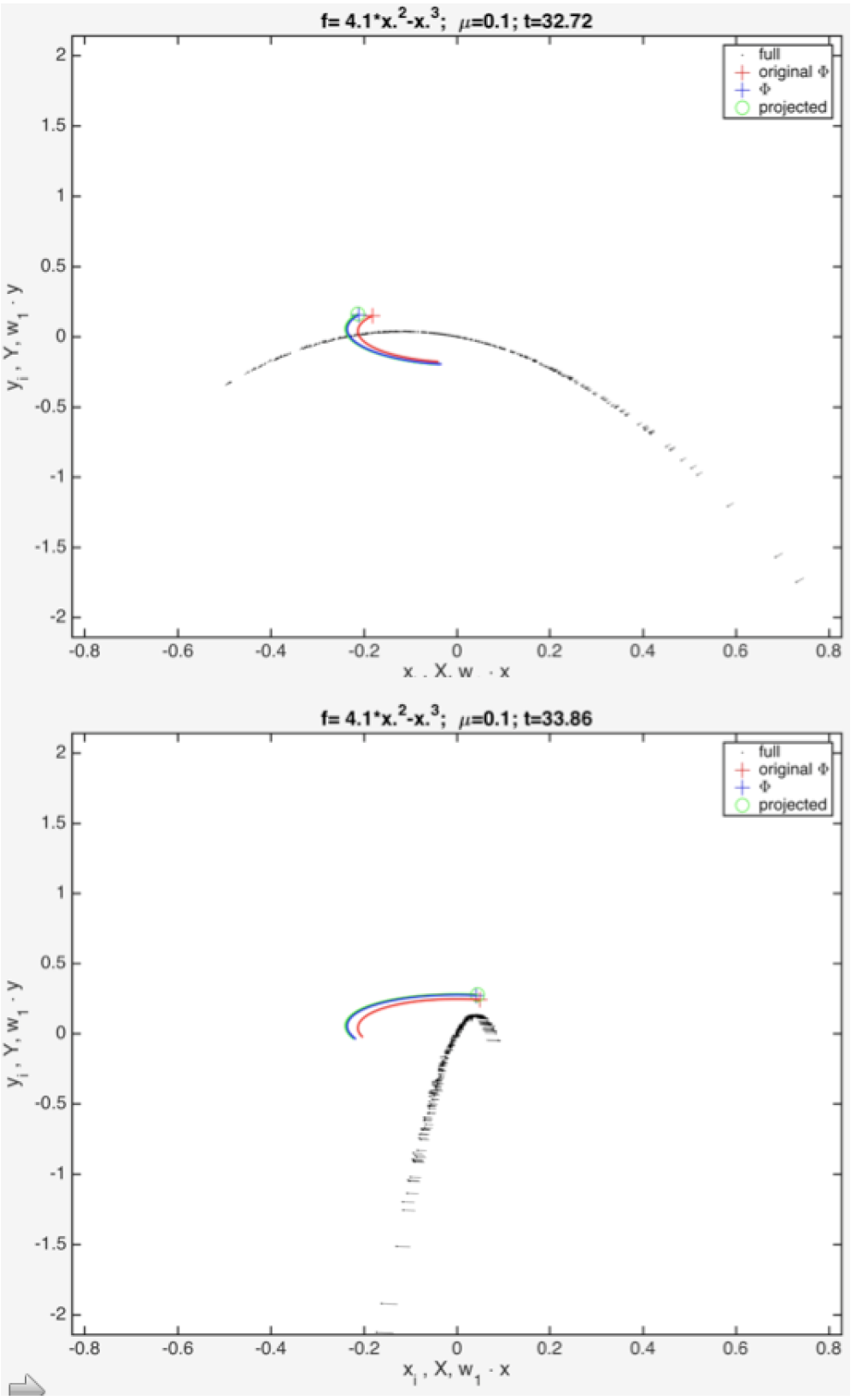

Figure 2.10: As in Fig. 2.8 adding in blue color the correction using the second order terms in the approximation of Φ to capture the reduced dynamics.

$$x_i = V_{i,1}X_{\lambda_1} + \sum_{k=2}^{N} V_{i,k}X_{\lambda_k} \approx V_{i,1}X_{\lambda_1} + \sum_{k=2}^{N} V_{i,k}c_2\Gamma_k^{2\delta_1,\bullet}\left(\frac{-2\lambda_k}{4\lambda_k^2+9}X_{\lambda_1}^2 + \frac{-6}{4\lambda_k^2+9}X_{\lambda_1}Y_{\lambda_1} + \frac{2\lambda_k}{4\lambda_k^2+9}Y_{\lambda_1}^2\right)$$

If for $k \geq 2$,$\lambda_k \approx -d$ then:

$$x_i \approx V_{i,1}X_{\lambda_1} + c_2\sum_{k=2}^{N} V_{i,k}\Gamma_k^{2\delta_1,\bullet}\left(\frac{2d}{4d^2+9}X_{\lambda_1}^2 + \frac{-6}{4d^2+9}X_{\lambda_1}Y_{\lambda_1} + \frac{-2d}{4d^2+9}Y_{\lambda_1}^2\right)$$

If M is normal then : $\sum_{k=2}^{N} V_{i,k}\Gamma_k^{2\delta_1,\bullet} = \sum_{k=2}^{N} V_{i,k}\sum_{\varphi=1}^{N} V_{\varphi,k}V_{\varphi,1}^2 = \sum_{\varphi=1}^{N} V_{\varphi,1}^2\left(\delta_{i,\varphi} - V_{i,1}V_{\varphi,1}\right) = V_{i,1}^2 - V_{i,1}\Gamma_1^{2\delta_1,\bullet}$.

Since $\left(\sqrt{N}\right)^2 V_{i,1}\Gamma_1^{2\delta_1,\bullet} \xrightarrow{N\to\infty} 0$. We get:

$$\begin{aligned} x_i &\approx V_{i,1}X_{\lambda_1} + c_2V_{i,1}^2\left(\frac{2d}{4d^2+9}X_{\lambda_1}^2 + \frac{-6}{4d^2+9}X_{\lambda_1}Y_{\lambda_1} + \frac{-2d}{4d^2+9}Y_{\lambda_1}^2\right) \\ y_i &\approx V_{i,1}Y_{\lambda_1} + c_2V_{i,1}^2\left(\frac{-\left(2d^2+3\right)}{4d^2+9}X_{\lambda_1}^2 + \frac{2d}{4d^2+9}X_{\lambda_1}Y_{\lambda_1} + \frac{-\left(2d^2+6\right)}{4d^2+9}Y_{\lambda_1}^2\right) \end{aligned}$$

The corrected Ψ is shown in green color in the movie: `https://drive.google.com/open?id=1GAUPMhUs04eMjNSbMxjPw8MK2kIGlTZG` . Simulation is in red color. Snapshots of the simulation movie are shown in Fig. 2.11.

We see that higher order even nonlinearities also survive on Ψ . `https://drive.google.com/open?id=1mb3QK2JGSVxShdKyUA_0bNDhOgSAk_tA`. Snapshots of the simulation movie are shown in Fig. 2.12.

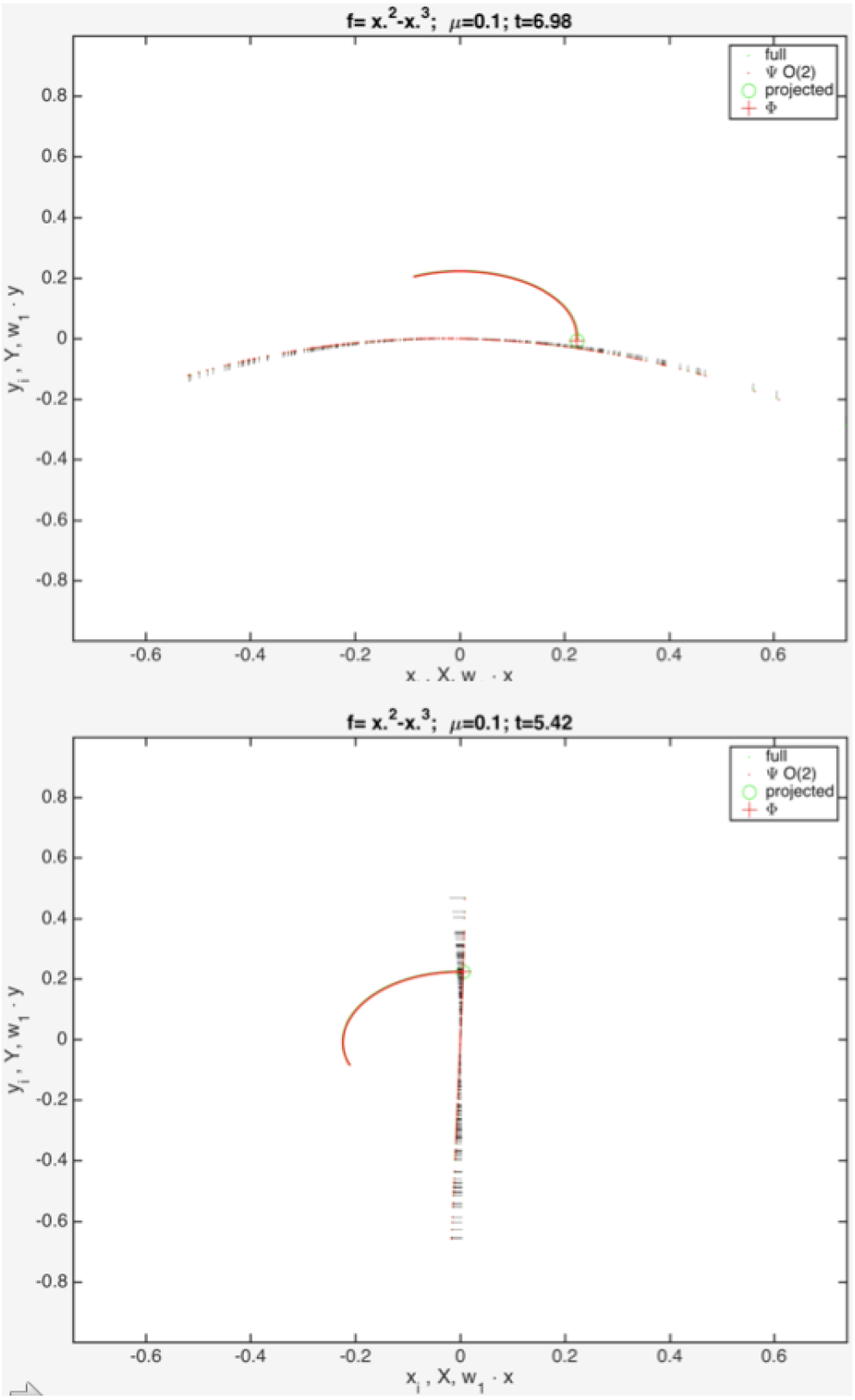

Figure 2.11: As in Fig. 2.7 adding in red color the second order terms in the of approximation Ψ to capture the dynamics of individual units from the reduced dynamics.

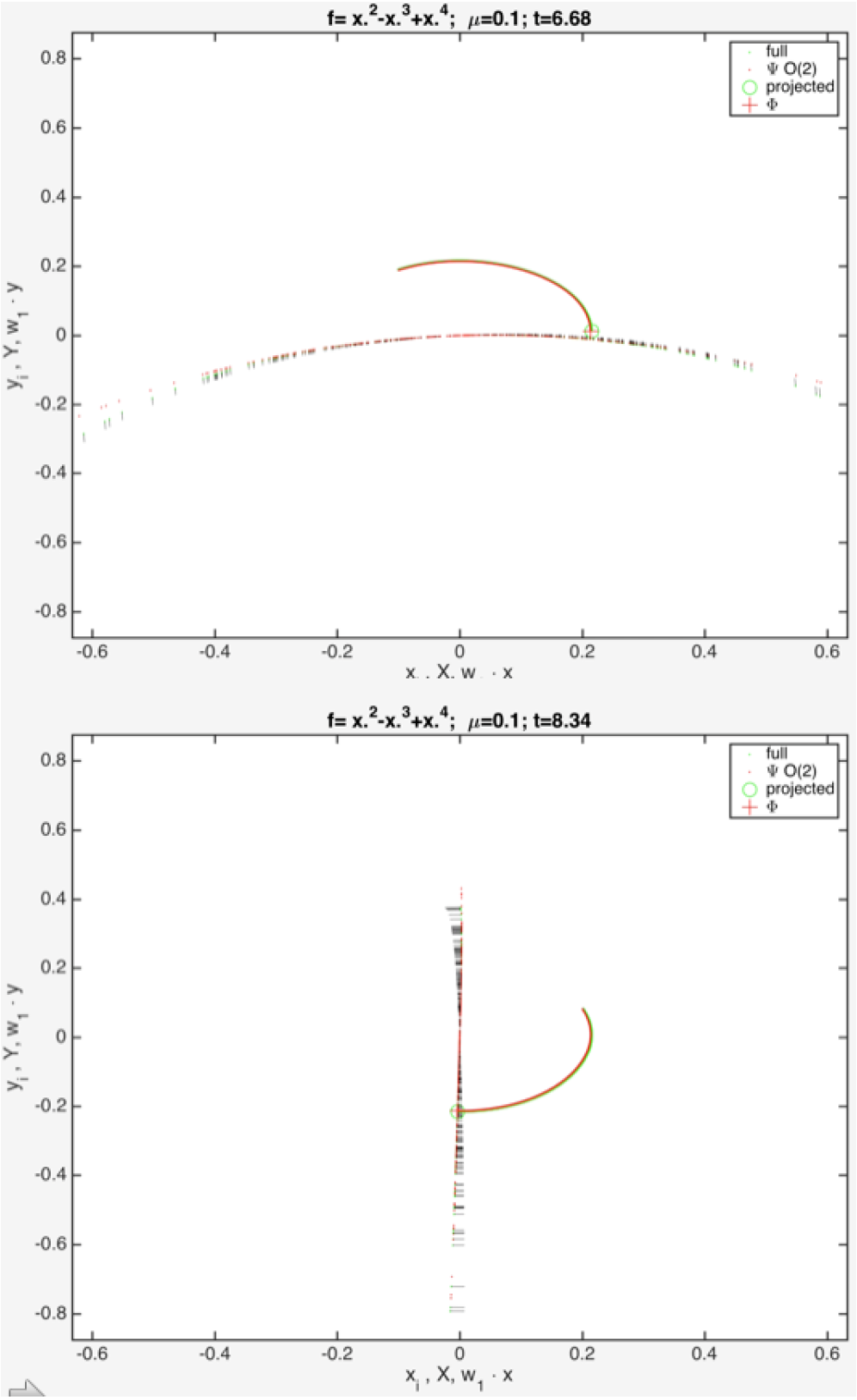

Figure 2.12: As in Fig. 2.11 with $f(x) = x^2 - x^3 + x^4$. Only second order terms of Ψ are not enough.

2.14 Numerical Ansatz for approximating Ψ when $f(x) = c_2x^2 + c_3x^3 + c_4x^4 + c_5x^5$ and M is normal and $\lambda_k \approx -d$ for $k \geq 2$.

Assuming that $O(2) * O(2)$ in (2.27) disappear in the limit and using the highly simplified guess from (2.28) and adding linear addition $O(2) + O(4)$ we get the approximations on the last movie. In the particular case described here this can intuitively be seen to be an appropriate simplification for $\Lambda \to \infty$ due to the nonlinearities only surviving on the x layer on Φ and on the y layer on Ψ.

The corrected Ψ is shown in green color in the movie: `https://drive.google.com/open?id=1pXFWluButTHG1jReFUm6Rv9J1ihzrNKe`. Snapshots of the simulation movie are shown in Fig. 2.13.

2.15 Complex-conjugate pair of eigenvalues, normal matrix

As shown in Fig. 2.5, the second-simplest case is to control two complex-conjugate eigenvalues, as they can be controlled by a single parameter, their real part, while leaving their imaginary part unchanged.

We follow the previous section in using M_a, a normal matrix, as our base connectivity structure. Now we choose a pair of complex-conjugate eigenvalues. The corresponding eigenvectors are also complex conjugate. Choosing as e the one corresponding to the eigenvalue with positive imaginary part, the 2D subspace is spanned both by e and $\bar{e}$, or by $e_R \equiv \Re e$ and $e_I \equiv \Im\, e$. Corollary 2 implies that the whole system bifurcates with 2 pairs of complex conjugate eigenvalues crossing the imaginary axis with frequencies $\frac{\sqrt{\omega^2+4} \pm \omega}{2}$.

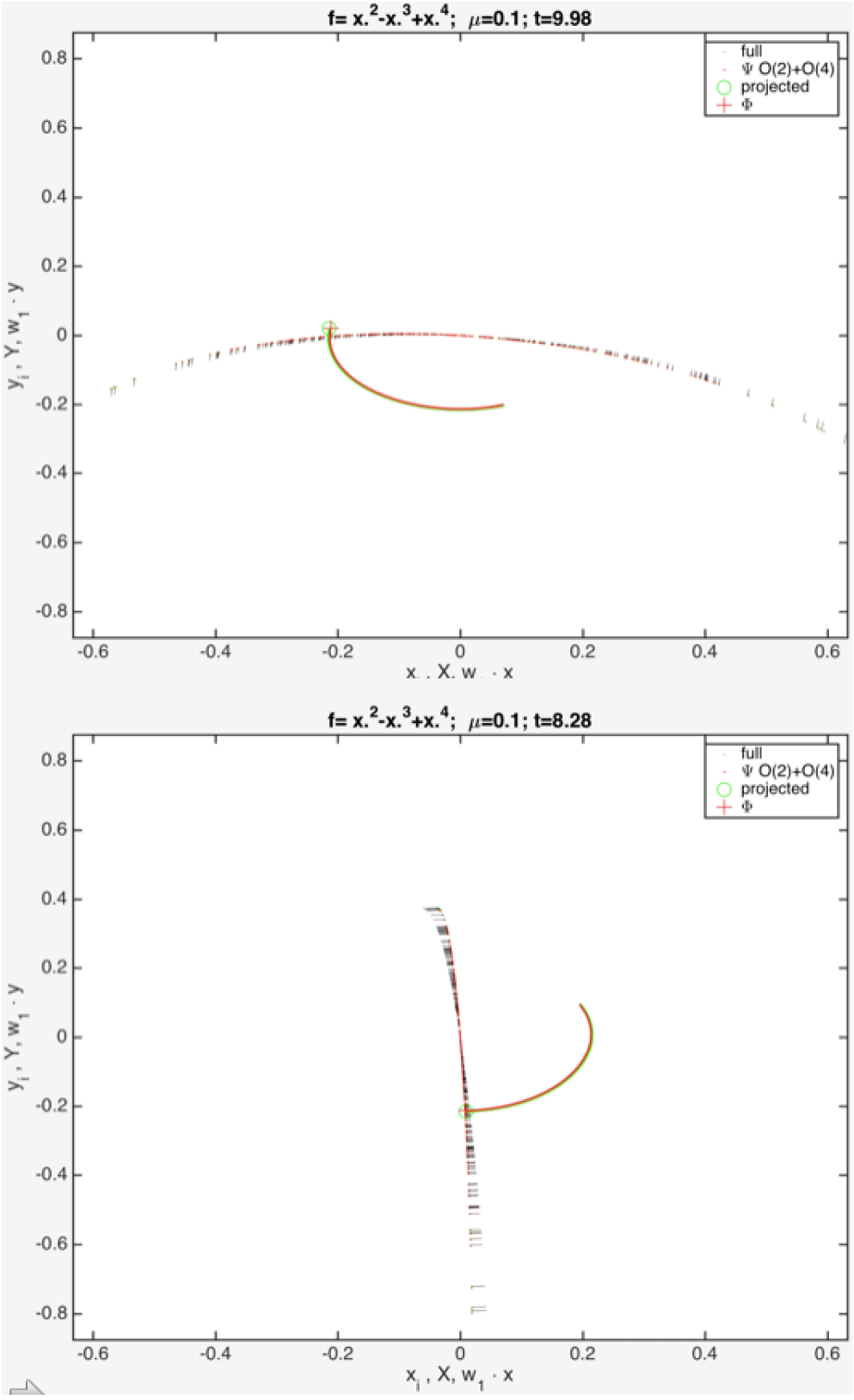

Figure 2.13: As in Fig. 2.12 but adding terms of order 4 in the approximation of Ψ.

Following the previous section, and remembering that now the left eigenvector is the complex conjugate of the right eigenvector, $e^\dagger = \bar{e}^t$ we define the coarse-grained variable X, now complex, as the normalized projection on e:

$$X\sqrt{\frac{N}{2}} = (e_R - e_I i)\cdot x$$

projection on critical mode, $X = X_R + X_I i$

Then the linear order approximation of the invariant manifold for the system:

$$\begin{aligned}\dot{x}_i &= y_i - x_i^\alpha + \sum_j M_{ij}x_j \\ \dot{y}_i &= -x_i\end{aligned}$$

gives us the linear order of Ψ

$$x \approx \sqrt{\frac{N}{2}}\left(X\left(e_R + ie_I\right) + \bar{X}\left(e_R - ie_I\right)\right)$$

The naive approximation of Ψ is given by :

$$\begin{aligned}x &= \sqrt{\frac{N}{2}}\left(\left(X_R + X_I i\right)\left(e_R + e_I i\right) + \left(X_R - X_I i\right)\left(e_R - e_I i\right)\right) = \sqrt{2N}\left(X_R e_R - X_I e_I\right) \\ y &= \sqrt{\frac{N}{2}}\left(\left(Y_R + Y_I i\right)\left(e_R + e_I i\right) + \left(Y_R - Y_I i\right)\left(e_R - e_I i\right)\right) = \sqrt{2N}\left(Y_R e_R - Y_I e_I\right)\end{aligned}$$

Then taking dot product with $\sqrt{\frac{N}{2}}e_R$ and $-\sqrt{\frac{N}{2}}e_L$, and ignoring projections other than in e_R and e_I the system:

$$\begin{aligned}\dot{x}_i &= y_i - x_i^\alpha + \sum_j M_{ij}x_j \\ \dot{y}_i &= -x_i\end{aligned}$$

gives us :

$$\begin{aligned}\dot{X}_R &= Y_R + \lambda_R X_R - \lambda_I X_I - \sum \sqrt{\frac{2}{N}} e_{R,i} \sqrt{2N}^\alpha \left(X_R e_{R,i} - X_{I,i} e_{I,i}\right)^\alpha \\ \dot{Y}_R &= -X_R \\ \dot{X}_I &= Y_I + \lambda_I X_R + \lambda_R X_I - \sum \sqrt{\frac{2}{N}} \left(-e_{I,i}\right) \sqrt{2N}^\alpha \left(X_R e_{R,i} - X_{I,i} e_{I,i}\right)^\alpha \\ \dot{Y}_I &= -X_I\end{aligned}$$

for α odd:

$$\sum \sqrt{\frac{2}{N}} e_{R,i} \sqrt{2N}^\alpha \left(X_R e_{R,i} - X_{I,i} e_{I,i}\right)^\alpha = \sum_{\varphi=0}^{\alpha} \binom{\alpha}{\varphi} \frac{1}{N} \sqrt{2N}^{\alpha+1} \sum_i e_{R,i}^{\alpha-\varphi} \left(-e_{I,i}\right)^\varphi =$$

$$X_R \sum_{\varphi=0}^{\frac{\alpha-1}{2}} \binom{\alpha}{2\phi} \left(\alpha - 2\phi + 1\right)!! \left(2\phi\right)!! X_R^{\alpha-2\phi-1} X_I^{2\phi} = \alpha!! X_R \left(X_R^2 + X_I^2\right)^{\frac{\alpha-1}{2}}$$

since $\binom{\alpha}{2\phi} \left(\alpha - 2\phi + 1\right)!! \left(2\phi\right)!! = \alpha!! \binom{\frac{\alpha-1}{2}}{\phi}$

similarly $\sum \sqrt{\frac{2}{N}} \left(-e_{I,i}\right) \sqrt{2N}^\alpha \left(X_R e_{R,i} - X_{I,i} e_{I,i}\right)^\alpha = \alpha!! X_I \left(X_R^2 + X_I^2\right)^{\frac{\alpha-1}{2}}$

So:

$$\begin{aligned} \dot{X} &= Y + \lambda X - \alpha!! \, \|X\|^{\alpha-1} X \\ \dot{Y} &= -X \end{aligned}$$

For $\alpha = 3$ this is a complex generalized van der Pol equation.

$$\begin{aligned} \dot{X} &= (\lambda - |X|^2)X + Y \\ \dot{Y} &= -X \end{aligned}$$

Notice the X equation is now a Hopf bifurcation normal form in a single complex variable, where $Imag(\lambda)$ is the rotational frequency in the X complex plane, and $Real(\lambda)$ is the control parameter, while the whole XY plane equation uses the same $Real(\lambda)$ as a control parameter for a Hopf bifurcation in the real XY plane. Thus this equation contains 2 distinct frequencies, $\omega = 1$ from the base equation, and $\omega = Imag(\lambda)$, the frequency of the eigenvector, from the complex X equation, and both cross the threshold of stability at the same time. Therefore, in this collective mode, a codimension-2 transition becomes generic, and the system in principle can bifurcate directly from a fixed point onto a torus. In this sense it is similar to a Takens-Bogdanoff normal form, only that it has two distinct and independent frequencies.

Thus the macroscopic equations are non-generic with respect to perturbations in the underlying microscopic dynamics in two ways: first, all even terms are destroyed, and second it can undergo a direct transition from a fixed point to a torus.

2.16 Finite number of modes

The naive approximation for a finite number of real modes crossing the real axis is also easy to calculate. In particular if we notice that:

$$\sum_{k_1+\ldots+k_N=n}\left(\frac{n!}{k_1!\cdots k_N!}\sqrt{N}^{(n-1)}\Gamma_\mu^{(k_1,\ldots,k_N)}\right)X_{\lambda_1}^{k_1}\cdots X_{\lambda_N}^{k_N}=\sum_{k_1+\ldots+k_N=n}n!!\binom{\frac{n-1}{2}}{\frac{k_1}{2}\cdots\frac{k_i-1}{2}\cdots\frac{k_N}{2}}X_{\lambda_1}^{k_1}\cdots X_{\lambda_N}^{k_N}=n!!X_{\mu_i}\sqrt{\sum_p X_\mu^2}^{(n-1)}=n!!\|X\|^{n-1}X_{\mu_i} \tag{2.33}$$

We see that in the antisymetric case the naive approximation takes a very specific form through the l^2 norm $\|X\|$ of $X=(X_\mu)_{\mu\, critical}$:

$$F_{\mu_i}\left(X_{\lambda_1},\ldots,X_{\lambda_N}\right)=\sum_{nodd}c_n n!!\|X\|^{n-1}X_{\mu_i} \tag{2.34}$$

$$\begin{aligned}\dot{X}_\mu &= \sum_{nodd}c_n n!!\|X\|^{n-1}X_\mu+Y_\mu+\lambda X_\mu \\ \dot{Y}_\mu &= -X_\mu\end{aligned} \tag{2.35}$$

2.17 Non-normal matrices

In general, matrices are non-normal. Therefore to study general matrices we need to learn how to understand how non-normality affects our strategy.

For normal matrices, eigenvectors are orthogonal and hence the matrix of left eigenvectors, the inverse of the matrix of right eigenvectors, can be simply obtained as the adjunct (complex conjugate transposed) of the right. However, when the matrix is not normal, the matrix of left

eigenvectors has to be obtained the hard way, by inverting the matrix of right eigenvectors; the most important thing that happens is that the left eigenvectors are no longer normalized to $|e^{\dagger}| = 1$.

We now study what happens when, instead of choosing our base connectivity matrix to be the antisymmetric M_a, which is normal, we choose the standard random matrix M_0, which is non-normal. The eigenvalue expansion of M_0 is $E_R D E_L$ where D is a diagonal matrix with the eigenvalues on the diagonal, E_R is the matrix of the right eigenvectors, and E_L, the matrix of left eigenvectors, satisfies $E_R E_L = I$.

While the matrix of right eigenvectors is, to lowest order, a matrix of i.i.d. Gaussian variables of standard deviation equal to $1/\sqrt{N}$, the matrix of left eigenvectors is not just substantially larger in magnitude, it is far from a Gaussian distribution. See Fig. 2.14.

Quantitatively this stems from a simple reason. The right eigenvectors of M_a, by normality, must be a unitary matrix and thus all its eigenvalues lie on the unit circle in the complex plane. However, the right eigenvectors of M_0 are not orthogonal to one another, but they are still normalized to unity, reducing drastically the determinant of E_R. This reduction can only be due to the eigenvalues of E_R lying inside the unit circle.

This effect is shown in Fig. 2.15.

The median determinant of an $N \times N$ Gaussian random matrix whose rows have been L2 normalized to 1 scales approximately like $\left(\frac{3}{5}\right)^N$. On the other hand, the median determinant of the eigenvectors of said matrix go to zero much faster, with the log-linear plot displaying significant convexity. Furthermore, the probability distribution of the log of said determinant is rather broad, as shown in Fig. 2.16.

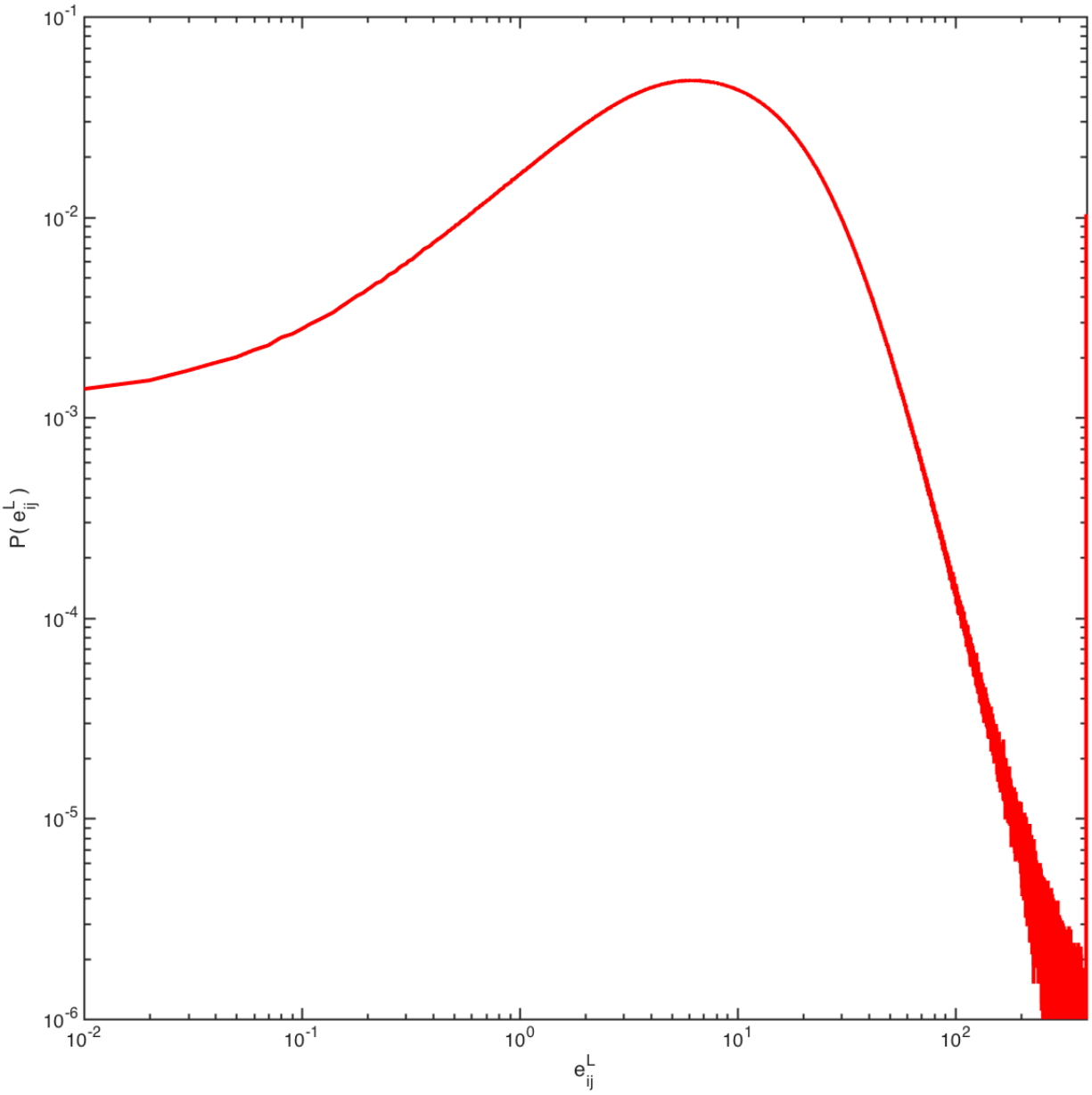

Figure 2.14

Histograms of the values of the elements of the matrix of left eigenvectors of M_0, a non-normal matrix of i.i.d. Gaussian variables. A histogram of the absolute values of the elements of the left eigenvalue matrix for the (nonsymmetric and non-normal) i.i.d. Gaussian matrix. The values have a broad, heavy-tailed distribution broadly consistent with a power law tail.

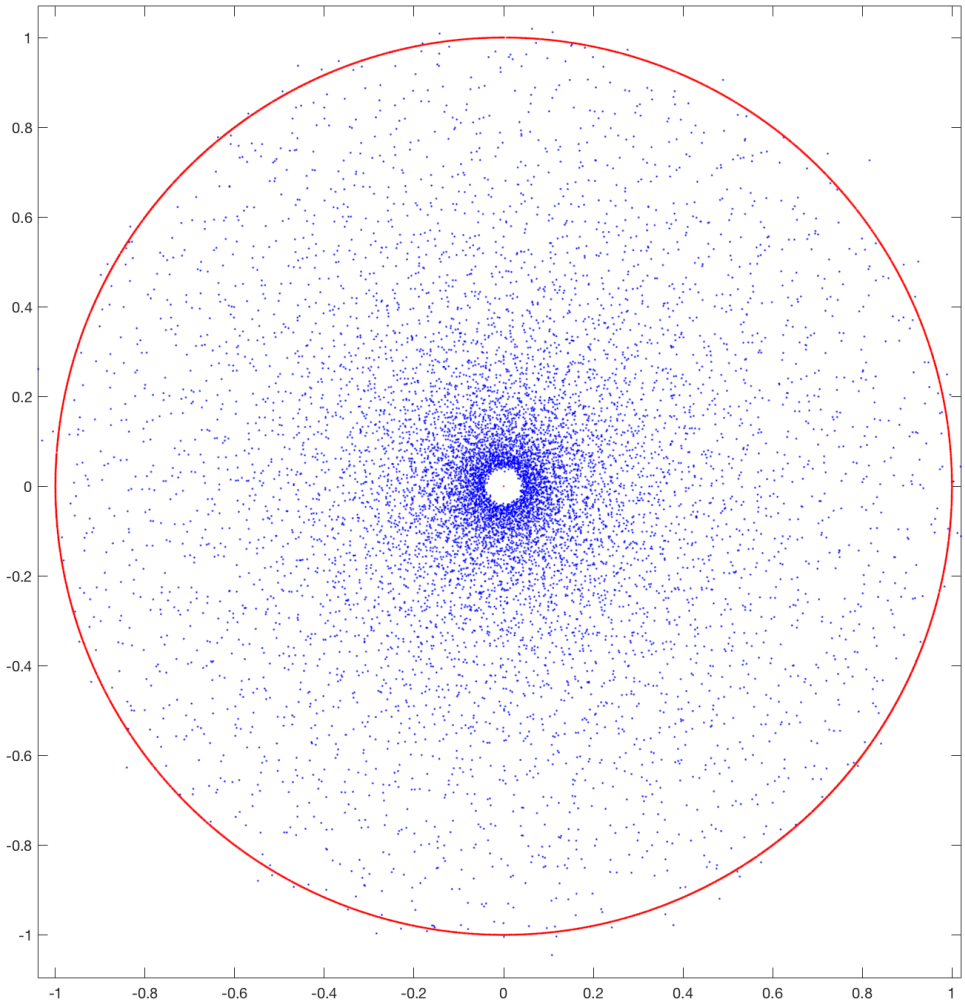

Figure 2.15

The eigenvalues of the matrix of right eigenvectors. Red, normal case (M_a), they lie on the unit circle. Blue, non-normal case (M_0), they form a funnel within the unit circle. This funnel is not uniform (i.e. no circle law) and the density increases for smaller radii; the smallest radius is proportional to $1/\sqrt{N}$. In this figure $N = 1000$ and we have accumulated 10 instances.

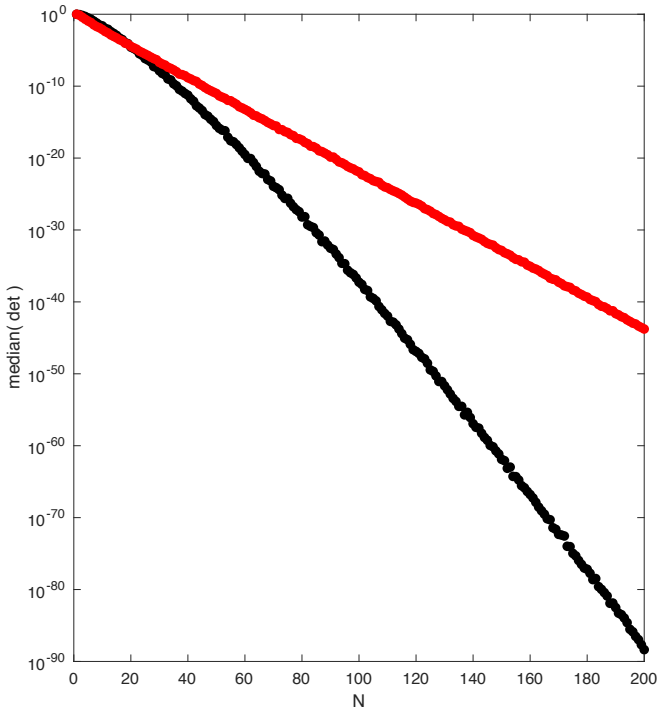

Figure 2.16

The determinant of the matrix of right eigenvectors (black) diminishes rapidly with dimension N. In fact it diminishes far faster than the determinant of a matrix of i.i.d. Gaussians whose rows have been normalized to 1 (red).

2.18 Conclusion

There are a number of points to be made at this juncture. First, that under certain circumstances our procedure converges properly and the diagram of Fig. 2.1 commutes: we can obtain in closed form the coarse-grained dynamics.

Second, our reduction procedure depends crucially on the structure of the eigenvectors. After more than 60 years of interest in eigenvalue statistical structure, and a tour-de-force theorem [Tao 2008] for the circular law, a lot is now understood about them. Still remarkably little is known about the structure of the eigenvectors of such matrices, which display much less universality than the eigenvalues; [Chalker 1998] was one of the first studies of eigenvectors of non-normal random matrices. Basic results link the PDF of entries in the eigenvector to the PDF of the matrix entries [Tao 2012], and a fair amount of effort has been spent in understanding localization of eigenvectors in nearly-one-dimensional systems; see [O'Rourke 2016] for a recent review.

Simple numerical exploration leads us to conjecture that a great deal about the geometrical structure of the network gets encoded into the statistical structure of the eigenvalues. To illustrate why, let us consider a simple example: a 2D toroidal (periodic boundary conditions) lattice of size $M \times M$, in which elements are connected by a random Gaussian term if they are ≤ 3 lattice units apart. There are 28 such near neighbors for each site. There are $N = M^2$ sites, and hence the interaction matrix is $N \times N = M^4$; this matrix is sparse because every row contains 29 nonzero elements (including the diagonal) no matter how large M is. Since the banded structure of the matrix exceeds $\sqrt{N} = M$ this construction narrowly escapes localization [O'Rourke 2016]. The spectrum of this matrix is still circular, following the strong universality results for the spectrum of sparse matrices; but the eigenvectors have a strongly interdependent statistical structure. The reason is simple: $29M^2$ random numbers are used in order to generate M^2 eigenvalues and M^2 eigenvalues with M^2 coefficients (minus

one for normalization). Therefore the eigenvectors are not merely correlated: they are not statistically independent from one another, and they become more and more codependent the larger the value of M. Our reduction operator is extremely sensitive to these dependencies, and we conjecture that the ambient space in which the columns are embedded gets encoded into these interdependencies.

Third, this procedure generates symmetries where there were no symmetries to begin with. In the current case, the global dynamics is always an odd vector field. This can lead to curious situations, in which the dynamics of the individual column is unstable (say due to a x^2 or x^4 term), but the reduced dynamics is a globally attractive limit cycle.

Finally, in classical statistical mechanics a notorious feature is that the system as a whole can develop singularities such as phase transitions where the underlying system was perfectly smooth. Like in statistical mechanics, the global dynamics is of a slightly smaller regularity class than the microscopic dynamics, as multiplication by the double-factorial of N makes the Taylor expansion less convergent. For example, if the microscopic dynamics f has a pole, then F is nowhere-convergent and the dynamics is not coarse-grainable through the method presented in this thesis. If, on the other hand, f is holomorphic, it may stay holomorphic because the double factorial is approximately the square root of the factorial for sufficiently large arguments. On the other hand certain holomorphic functions get mapped onto functions with poles, increasing their singularity class.

Part III

Center Manifold Dynamics in Cochlea

Chapter 3

A Nonhyperbolic Toy Model of Cochlear Dynamics

Cochlea displays complex and highly nonlinear behavior in response to wide-ranging auditory stimuli. While there have been many recent advancements in the modeling of cochlear dynamics, most of these models are just empirical, containing large amounts of biological detail, and thus don't shed much light on what mathematical structures underlie the essential features of the extended cochlea. We construct a dynamical system consisting of a series of strongly coupled critical oscillators to show that high-dimensional nonhyperbolic dynamics can account for high-order compressive nonlinearities, amplification of weak input, frequency selectivity, and traveling waves of activity. As a single Hopf bifurcation generically gives rise to features of cochlea at a local level, the nonhyperbolicity mechanism proposed in this thesis can be seen as a higher-dimensional analogue for the entire extended cochlea.

3.1 Introduction

The nature of signal processing in the cochlea has been a focus of interest in the study of sound perception. Gold was first to posit that the cochlea does not operate as a passive Fourier transformer but instead utilises an active regenerative system which amplifies incoming signals [Gold 1948a, Gold 1948b]. Experiments on living specimens have confirmed Gold's hypothesis [Ruggero 1992, Ruggero 2000] despite initial studies on cadavers showing that cochlea acts as a simple passive spatial frequency analyser [Békésy 1960]. Indeed, live, reasonably intact cochlea exhibits an active nonlinear process with three key characteristic properties: high gain amplification, sharp frequency tuning, and nonlinear compression of the dynamic range (Fig. 3.1) [Ruggero 1992, Ruggero 1997].

To understand the origin of the active process, one first needs to examine the physiological and anatomical properties of the cochlea (Fig. 3.2). As sound waves enter the inner ear, they set into vibration the cochlear partition, which results in traveling waves of activity that propagate unidirectionally from base to apex. The *basilar membrane* is the main compliance of the cochlear partition, whose stiffness increases, by two orders of magnitude, from apex to base. This stiffness gradient results in each point on the basilar membrane responding maximally to a single characteristic frequency with high frequencies at the base and exponentially decreasing frequencies towards the apex [Békésy 1960]. The cochlear partition also contains the organ of Corti, where the *hair cells*, the sound-sensitive cells, are located. The hair cells play an essential role in generating the features of the active process through *hair-bundle motility* in nonmammals [Hudspeth 2008, Hudspeth 2000, Martin 2008, Martin 1999, Martin 2001] a combination of hair-bundle motility [Chan 2005a, Chan 2005b, Kennedy 2005, Kennedy 2006] and *membrane-based electromotility* in mammals [Ashmore 2008, Dallos 2006, Fettiplace 2006].

It is now known [Hudspeth 2010] that at a local level, at a specific location on the basilar

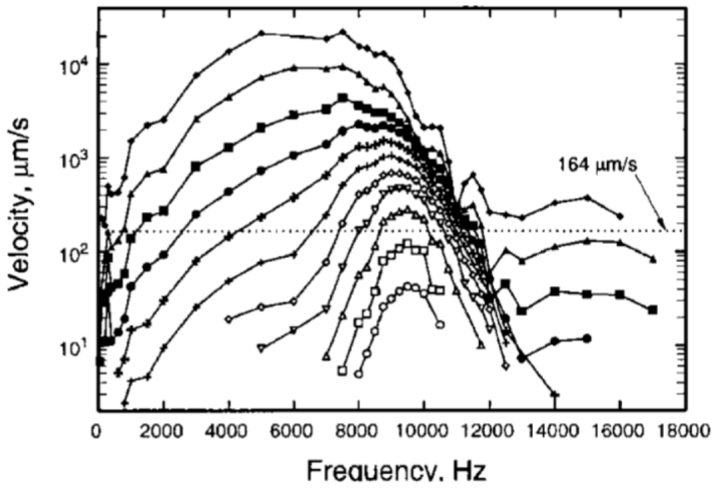

Figure 3.1: Cochlear Velocimetric Data. Reprinted from [Ruggero 2000] under a CC BY license, with permission from National Academy of Sciences, U.S.A. , original copyright (2000). Cochlear velocimetry data taken by laser interferometry at a spot in the basilar membrane of a living chinchilla. Basilar membrane speed vs frequency for varying intensities is plotted. Adjacent curves are separated by 10 dB.

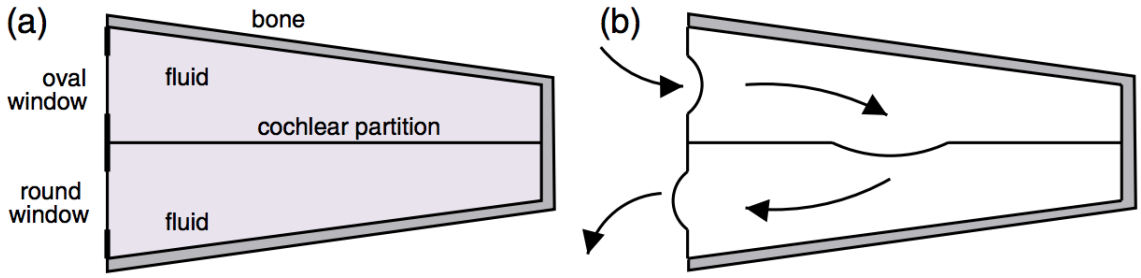

Figure 3.2: Cochlea Schematic. (a) The basilar membrane is the main compliance of the cochlear partition, whose stiffness increases, by two orders of magnitude, from apex(right) to base(left). (b) Sound waves entering the cochlea cause a traveling wave displacement across the basilar membrane peaking at a frequency dependent position with decreasing selective frequency from base(left) to apex(right).

membrane, the characteristic features of the active process generically arise from a *Hopf bifurcation* [Wiggins 2003, Kuznetsov 2013], a form of structural instability in dynamical systems theory which gives rise to critical oscillations. Several theoretical studies have extensively investigated this relationship between local cochlear dynamics and a single Hopf bifurcation [Choe 1998, Eguíluz 2000, Camalet 2000, Nadrowski 2004, Tinevez2007].

At the level of the extended cochlea, encompassing the full basilar membrane, models relying on multiple Hopf bifurcations, biophysical details of basilar membrane mechanics, and surrounding fluid hydrodyanmics have successfully reproduced a number of key features of cochlear dynamics [Kern 2003, Duke 2003, Magnasco 2003, Dierkes 2008]. However, in contrast to a single Hopf bifurcation in the local case, it is still unclear what underlying high-dimensional mathematical structures can generically give rise to the complex, nonlinear responses of the extended cochlea. In this thesis, we propose such a mathematical structure; we show that a high-dimensional nonhyperbolic system residing on a full-dimensional center manifold can exhibit the key nonlinear features of the active process as described above.

In dynamical systems theory, the classical approach to studying behavior in the neighborhood of an equilibrium point is to examine the eigenvalues of the Jacobian of the system at this point. If all eigenvalues have nonzero real part, then the equilibrium point is called *hyperbolic* and the dynamics around the point is topologically conjugate to the linearized system determined by the Jacobian [Grobman 1959, Hartman 1960a, Hartman 1960b]. On the other hand, if there exists at least one eigenvalue with zero real part, then the equilibrium point is called *nonhyperbolic* and the linearization does not determine the qualitative dynamics around the point.

Dynamics around nonhyperbolic fixed points are complex and give rise to a number of interesting features. First, since the dynamics are not enslaved by the exponent of the Jacobian, nonlinearities and input parameters play a crucial role in determining dynamical properties

such as relaxation timescales and correlations [Yan 2012, Hayton 2018a]. Nonhyperbolic points are also not *structurally stable*, meaning that small perturbations of the vector field can lead to substantial topological changes of the orbits around the point. Examples of these topological changes include the appearance of new invariant sets such as periodic orbits and tori, and if the dimension is high enough, chaotic dimensions can arise.

The standard technique in studying dynamics around a nonhyperbolic point is to investigate the reduced dynamics on an invariant subspace called a *center manifold*. The local existence of center manifolds has been rigorously proven [Kelley 1967, Carr 2012], and its dimension is equal to the number of eigenvalues on the imaginary axis. If there are no eigenvalues with positive real part (unstable modes), then the center manifold is attracting [Carr 2012], and instead of studying the full system, we can study the reduced dynamics on the center manifold. The *approximation theorem* for center manifolds provides us with the tool to calculate the center manifold and the reduced dynamics up to any degree of accuracy [Carr 2012].

In this thesis, we present a dynamical system poised at a nonhyperbolic point with all eigenvalues of the linearization being purely imaginary; the dynamics reside on a full dimensional center manifold. In general, the greater the number of eigenvalues on the imaginary axis, the more complex the dynamics could be [Wiggins 2003]. Thus, the rich and complex behavior we will be discussing is not surprising. We posit that the nervous system utilizes nonhyperbolic equilibrium points and the corresponding unique dynamical properties on center manifolds to flexibly respond to a wide range of input parameters and exhibit complex nonlinear behavior. Our aim in this thesis is not to provide a detailed anatomical and biophysical model of cochlea, but rather to construct a *toy model* which provides an existence proof that center manifold dynamics can account for and connect key characteristic properties of cochlea: high-order compressive nonlinearities, amplification of

weak input, frequency selectivity and traveling waves of activity. We do not suggest that a simple 1-D line topology is necessarily present in cochlea anatomy; although, if the cochlea does indeed utilize center manifolds in the processing of sound, it might be the case that the full high dimensional phase space of cortical dynamics could be reduced to simple, low dimensional structures on the center manifold. This approach of constructing a toy model to explain how a given mechanism can lead to a particular set of properties is common practice in theoretical physics and is the underlying philosophical approach of several well known theoretical neuroscience models, e.g. Wilson-Cowan equations, Hopfield networks, and Kuramoto models [Ermentrout 2012, Hoppensteadt 2012].

There are a number of studies regarding nonhyperbolic dynamics in neural systems, including entire hemisphere ECoG recordings [Solovey 2015], experimental studies in premotor and motor cortex [Churchland 2012], theoretical [Seung 1998] and experimental studies [Seung 2000] of *slow manifolds* (a specific case of center manifolds) in oculomotor control, slow manifolds in decision making [Machens 2005], Hopf bifurcation in the olfactory system [Freeman 2005], and theoretical work on regulated criticality [Bienenstock 1998].

Nonhyperbolic dynamics, also commonly referred to as *dynamical criticality*, is distinct from *statistical criticality* [Beggs 2012], which is related to the statistical mechanics of second-order phase transitions. It has been proposed that neural systems [Chialvo 2010], and more generally biological systems [Mora 2011], are statistically critical in the sense that they are poised near the critical point of a phase transitions [Silva 1998, Fraiman 2009]. Statistical criticality is characterized by power law behavior such as avalanches [Beggs 2003, Levina 2007, Gireesh 2008] and long-range spatiotemporal correlations [Eguíluz 2005, Kitzbichler 2009]. While both dynamical criticality and statistical criticality have had success in neuroscience, their relation is still far from clear [Magnasco 2009, Mora 2011, Kanders 2017a].

3.2 Mechanism for Higher-Order Compression

We first show that nonlinear compression arises naturally from a system of strongly coupled critical oscillators, on an order exponentially larger than one would obtain from a single critical oscillator alone. It's well known that the response of a single Hopf oscillator to exponentially distributed periodic input is given by the curves in Fig. 3.3. At the center of resonance, the response R scales as the cubic root of the forcing strength F, $R \propto F^{1/3}$. Away from resonance, the response scales linearly for small forcing and as a cubic root for large forcing.

Now we look at the more interesting case of a series of unidirectionally coupled Hopf oscillators (Fig. 3.4); the output of one oscillator acts as input to the next oscillator downstream. For sake of exposition, let us consider the case where all connections have strength of magnitude 1, coupling nonlinearities are discarded, and we force, with periodic input, only the last cell on the top row:

$$\begin{aligned} \dot{x}_i &= -y_i - |x_i|^2 x_i + x_{i+1} + F\delta_{i,N} e^{i\omega t} \\ \dot{y}_i &= x_i - |y_i|^2 y_i \end{aligned} \tag{3.1}$$

where $i \in \{1, 2, ..., N\}$, x_i and $y_i \in \mathbb{C}$. At resonance, when $\omega = 1$, the response $|x_{N-d}|$ at a distance d from the input scales as $|x_{N-d}| \propto F^{1/3^{d+1}}$ for all forcing strengths F. Away from resonance, the response scales linearly for small forcing and as $|x_{N-d}| \propto F^{1/3^{d+1}}$ for large forcing. This scaling behavior is illustrated in Fig. 3.5 where we plot the response of the last cell we force as well as the next two oscillators downstream.

By construction, the linear connectivity matrix describing the network in Fig. 3.4 is non-normal and has purely imaginary eigenvalues. Both features are not necessary to produce

the high order power law scaling seen in Fig. 3.5; however, at resonance, purely imaginary eigenvalues are necessary to give rise to nonlinear compression across all forcing strengths.

3.3 Main Toy Model

We have shown that a series of coupled critical oscillators can generate responses which are compressed to an arbitrarily large degree. We will now incorporate this mechanism into an extended model of cochlea that is selective to frequencies over an exponential range. Let us consider a network of $2N$ cells paired together to form N strongly coupled oscillators as shown in Fig. 3.6. The activity of the cells on the top row are given by $x_i \in \mathbb{C}$ and cells on the bottom by $y_i \in \mathbb{C}$. The ith oscillator in the network, consisting of cells x_i and y_i, has characteristic frequency ω_i and is coupled to the oscillator on its left via a unidirectional connection of strength ω_i from x_i to x_{i-1}. In agreement with frequency selectivity in the basilar membrane, the characteristic frequencies are exponentially distributed with $\omega_1 < \omega_2 < \omega_3 < ... < \omega_N$.

The cells evolve in time, under the influence of forcings $I_{x_i}(t)$ and $I_{y_i}(t)$, according to the equations:

$$\begin{aligned} \dot{x}_i &= -\omega_i y_i - |x_i|^2 x_i + \omega_{i+1} x_{i+1} + I_{x_i}(t) \\ \dot{y}_i &= \omega_i x_i - |y_i|^2 y_i + I_{y_i}(t) \end{aligned} \tag{3.2}$$

where $i \in \{1, 2, 3, ..., N\}$, x_i and $y_i \in \mathbb{C}$ (for formality let us define: $x_{N+1} = \omega_{N+1} = 0$). It should be noted that in these equations, nonlinearities are confined to the cubic order terms and do not couple distinct cells in the network.

Now let us concatenate the vectors $\vec{x}$ and $\vec{y}$ into a single vector $X \in \mathbb{C}^{2N}$ such that

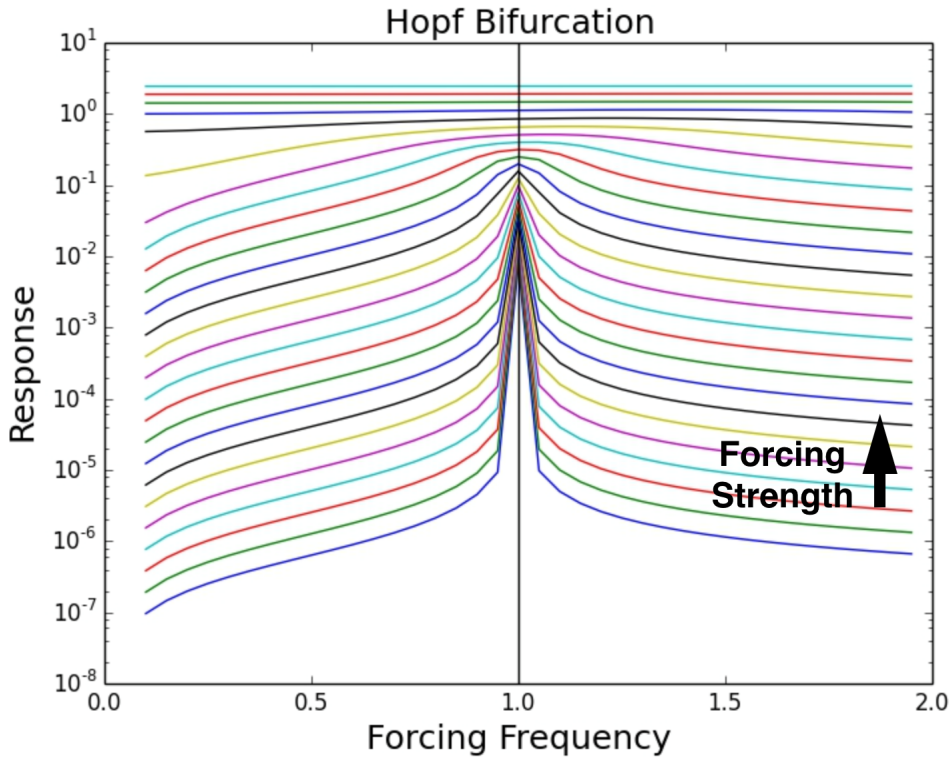

Figure 3.3: Response of a Single Critical Oscillator. The response of a single critical oscillator to a range of forcing frequencies and forcing strengths is shown. Each colored curve corresponds to a different forcing strength and the strength increases from bottom to top (direction of arrow). At resonance, when the forcing frequency is 1.0, the response increases as the cubic root of the forcing strength. Away from resonance the response is linear for small forcing and a cubic root for larger forcing.

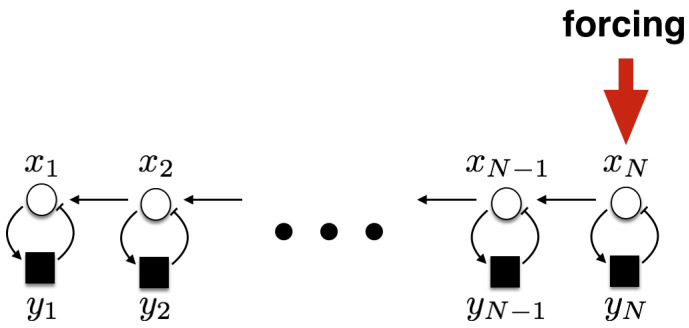

Figure 3.4: Strongly Coupled Critical Oscillators. Network of N critical oscillators with excitatory cells on top and inhibitory cells on the bottom. The oscillators are coupled together with connections along the excitatory layer. All connections have strength of magnitude equal to 1. Input to the network is denoted by the arrow.

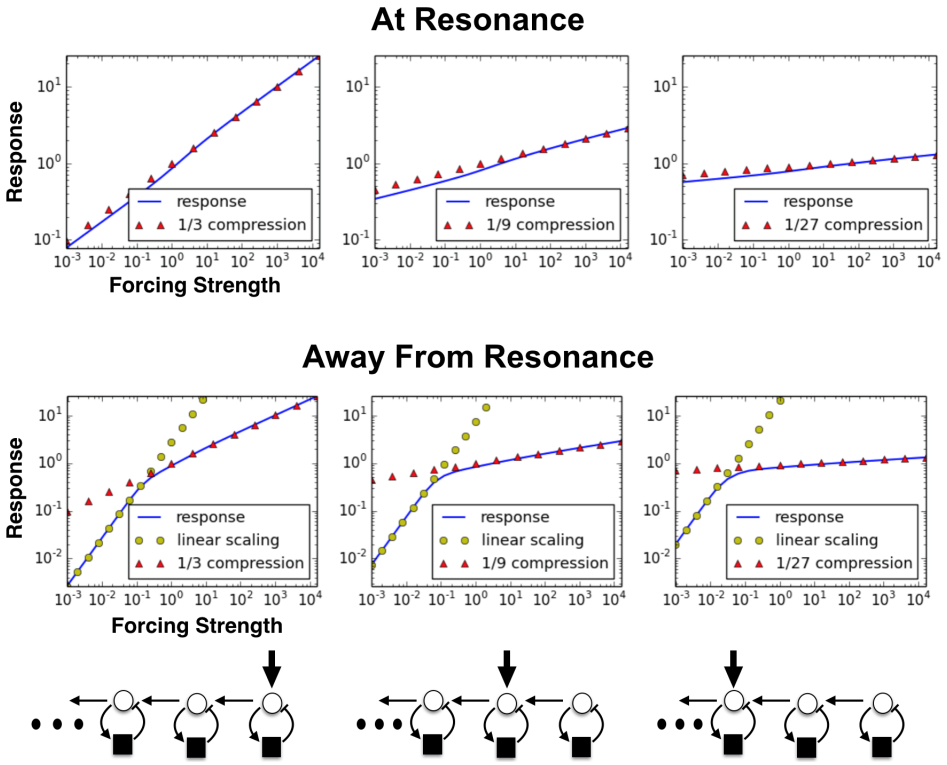

Figure 3.5: Scaling Behavior Along a Series of Coupled Identical Critical Oscillators. We force the last oscillator in a series of coupled identical critical oscillators with periodic input and plot the response as a function of forcing strength at the three different network locations (vertical arrow). The top and bottom rows in the figure correspond to the forcing frequency exactly at and away from resonance, respectively. At resonance, the response $|x_{N-d}|$ at a distance d from the input scales as $|x_{N-d}| \propto F^{1/3^{d+1}}$ for the entire range of forcing strengths. Away from resonance, the response scales linearly for small forcing and as $|x_{N-d}| \propto F^{1/3^{d+1}}$ for large forcing.

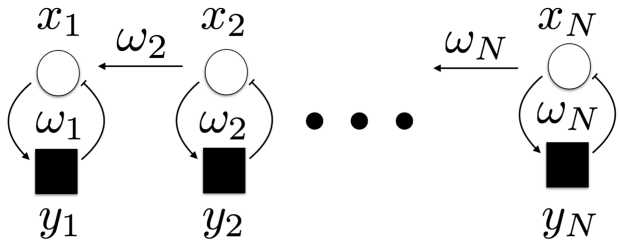

Figure 3.6: Network of Coupled Oscillators. A network of $2N$ cells, with top and bottom cell activities labeled as x_i and y_i, respectively, form N oscillators with exponentially distributed characteristic frequencies $\omega_1 < \omega_2 < \omega_3 < ... < \omega_N$. The oscillators are coupled to one another through unidirectional connections along the top.

$X_i = x_i$ and $X_{i+N} = y_i$ for $i = 1, ..., N$. In a similar way, we form $I(t) \in \mathbb{C}^{2N}$ from $I_{x_i}(t)$ and $I_{y_i}(t)$. We can then rewrite (3.2) as:

$$\dot{X} = AX - |X|^2 X + I(t) \tag{3.3}$$

where the $|X|^2$ and $|X|^2 X$ are element wise, and the matrix A describes the connectivity in Fig. 3.6. It is easy to check that A has a purely imaginary spectrum. Thus, the center manifold is full dimensional and we should expect to see nonlinear behavior even for the entire range of forcings.

We are specifically interested in the time-asymptotic response of the system to periodic input $I(t) = Fe^{i\omega t}$. The high dimensionality and nonhyperbolicity of the dynamics makes the ODE in (3.3) difficult to integrate since the step size necessary to numerically integrate the system decreases as the forcing strength is increased. Fortunately, we can bypass numerical integration methods by looking for asymptotic solutions $X(t) = Ze^{i\omega t}$, where $Z \in \mathbb{C}^{2N}$. Substituting these into (3.3), we find that:

$$0 = (A - i\omega)Z - |Z|^2 Z + F \tag{3.4}$$

and define $g(Z)$ to be equal to the right hand side of (3.4).

The solution of (3.4) can be found numerically by using the multivariable Newton-Raphson method in $\mathbb{C}^{4N}$:

$$\widetilde{Z} \to \widetilde{Z} - J(\widetilde{Z})^{-1}\widetilde{g}(Z) \tag{3.5}$$

where $\widetilde{Z} \coloneqq (z_1, z_2) = (Re(Z), Im(Z))$, $\widetilde{g}(Z) \coloneqq (g_1(Z), g_2(Z)) = (Re(g(Z)), Im(g(Z)))$, and J is the Jacobian of $\widetilde{g}$ with respect to $\widetilde{Z}$:

$$J_{ij}(z) = \frac{\partial g_i}{\partial z_j}$$

This Newton-Raphson algorithm can fail to converge for randomly chosen initial points. Furthermore, the algorithm's trajectory can get trapped in periodic orbits for step sizes not adequately small. To make simulations possible, we incorporate adaptive step sizes and initial points into the algorithm.

We define the response of the system as $|Z|$, the element-wise complex modulus of Z. We define the response of a single oscillator to be the l^2-norm of the oscillator $R_i = \sqrt{|Z|_i^2 + |Z|_{i+N}^2}$ for $i \in 1, ..., N$, which makes sense since the response of top and bottom cells are proportional element wise.

3.4 Results:Frequency Tuning, Compression, and Amplification

We consider the case of an $N = 60$ oscillator network with characteristic frequencies $\omega_i = 2^{(i-1)/10}$ where $i \in \mathbb{Z}$, $1 \leqq i \leqq N$. We force every cell in the network with uniform input of equal strength and plot the response of a single oscillator as a function of forcing frequency ω. We do this for a range of exponentially distributed forcings 2^{-45+k} where $k \in \mathbb{Z}, 0 \leqq k \leqq 63$. The results for oscillator $i = 31$ are shown in Fig. 3.7, where each curve corresponds to a different forcing strength and the strength increase in the direction of the arrow from bottom to top.

It is clear from Fig. 3.7 that the oscillator's response is selective for a particular forcing frequency. For weak forcing, there is a single peak in the response curves, which corresponds to an *effective characteristic frequency* different from the oscillator's characteristic frequency. This shift in frequency selectivity for weak forcing is a result of the oscillator integrating both direct input and input from other upstream oscillators with higher characteristic frequencies. For our specific model parameters, the effective characteristic frequency ω_{eff} is given by $2^{\frac{7}{10}}\omega_c$, where ω_c is the characteristic frequency of the oscillator. Note that ω_{eff} is exponentially distributed. As the forcing increases, the system reaches a regime in which the peaks of the response curves shift left towards the true characteristic frequency ω_c, in agreement with previous studies [Ruggero 2000] and which can be seen in Fig. 3.1. Finally, for high forcing the curves flatten out across all frequencies, lose selectivity and compress by a factor of 1/3.

The response curves for all oscillators in the system (except for the ones very close to the boundaries) have similar shape and properties each one with its own characteristic frequency ω_c and corresponding effective characteristic frequency $\omega_{eff} = 2^{\frac{7}{10}}\omega_c$. Results for two more example oscillators are shown in Fig. 3.8 and Fig. 3.9.

We now examine the three frequency domains demarcated by the vertical dashed lines $\omega = \omega_c$ and $\omega = \omega_{eff}$ in Fig. 3.7 (similar regimes for Fig. 3.8 , Fig. 3.9 and the rest of the oscillators). For $\omega < \omega_c$, the response scales linearly up until the point where the curves flatten out and compress by a factor of 1/3. For $\omega_c < \omega < \omega_{eff}$, we find a sharp transition to cubic root scaling for small forcing. This sharp transition is an artifact of the unidirectional coupling between oscillators; for forcing frequencies greater than the characteristic frequency, the oscillator integrates both direct input and input from oscillators upstream, while for forcing frequencies less than the characteristic frequency, the input from upstream oscillators is negligible compared to the direct input. For large forcing in this regime, ($\omega_c < \omega < \omega_{eff}$) we also find cubic compression. Between the two cubic scaling regimes, we observe the existence

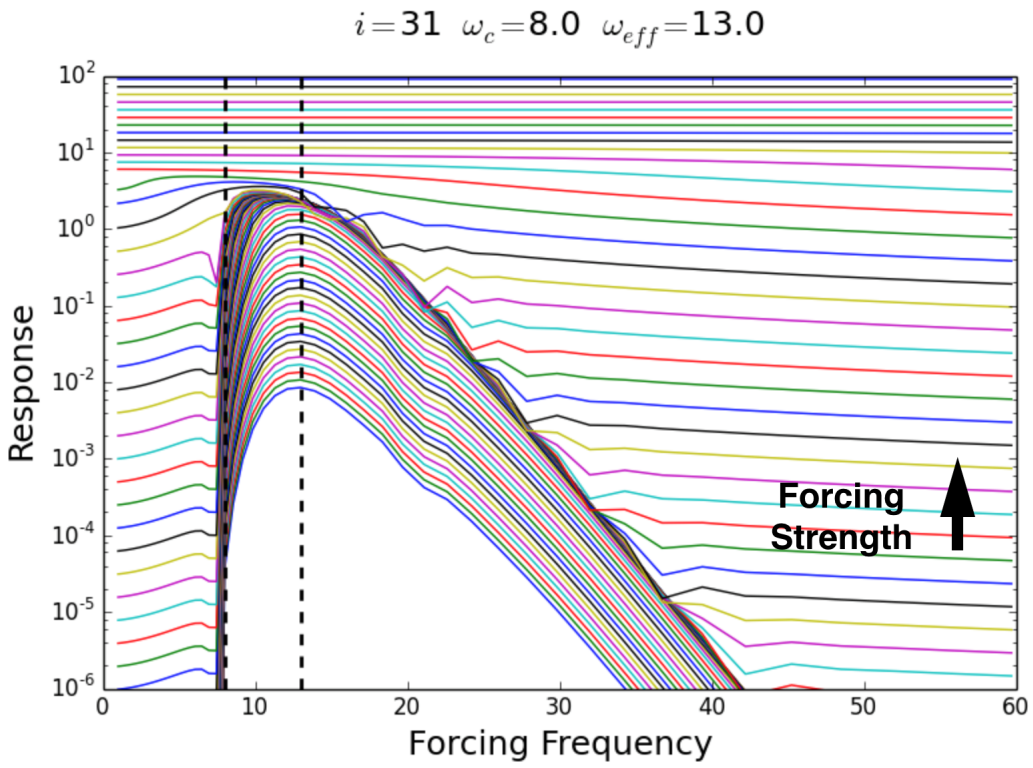

Figure 3.7: Response Curves of a Single Oscillator. We plot the response of a single oscillator in the coupled network (Fig. 3.6) in response to a range of forcing frequencies and 64 exponentially distributed input strengths (each colored curve corresponds to a different strength), $F = 2^{-45}$ to $F = 2^{18}$, which increase in the direction of the arrow from bottom to top. The two vertical dashed lines correspond to the true and effective characteristic frequencies.

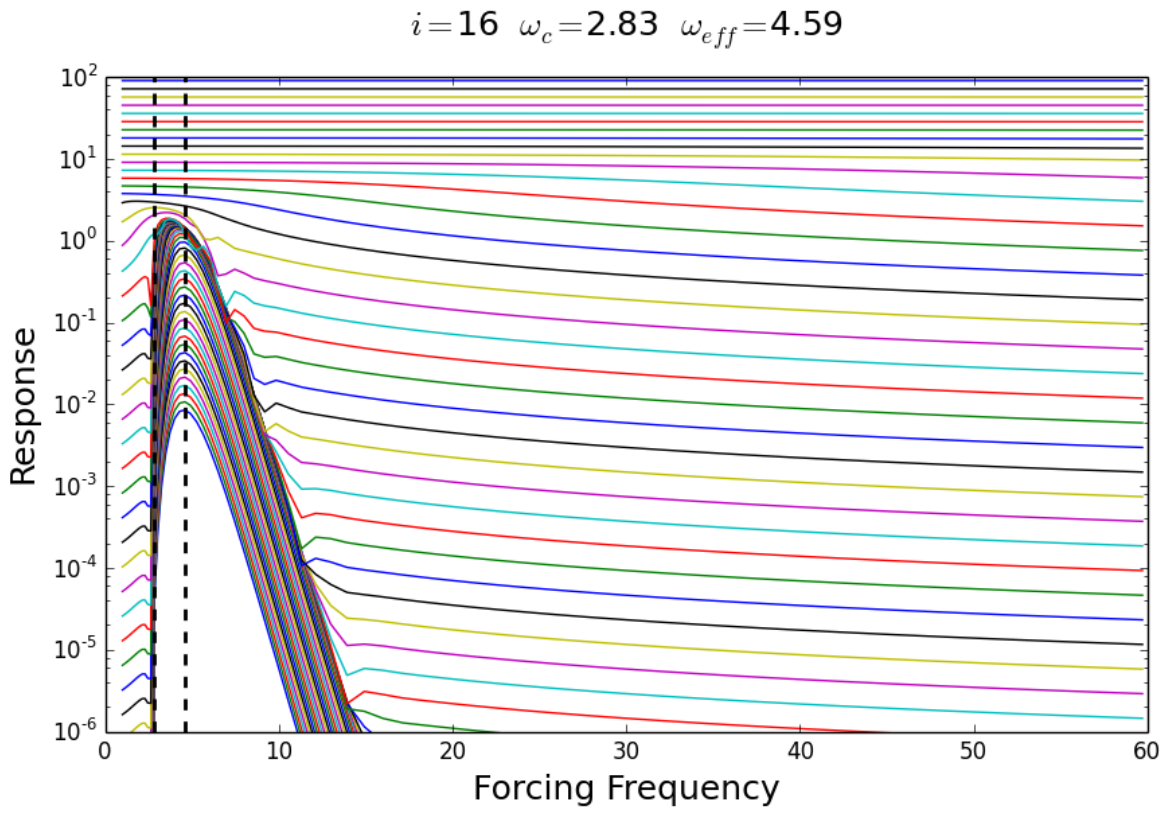

Figure 3.8: Response Curves of a Single Oscillator. As in Fig. 3.7 for oscillator $i = 16$

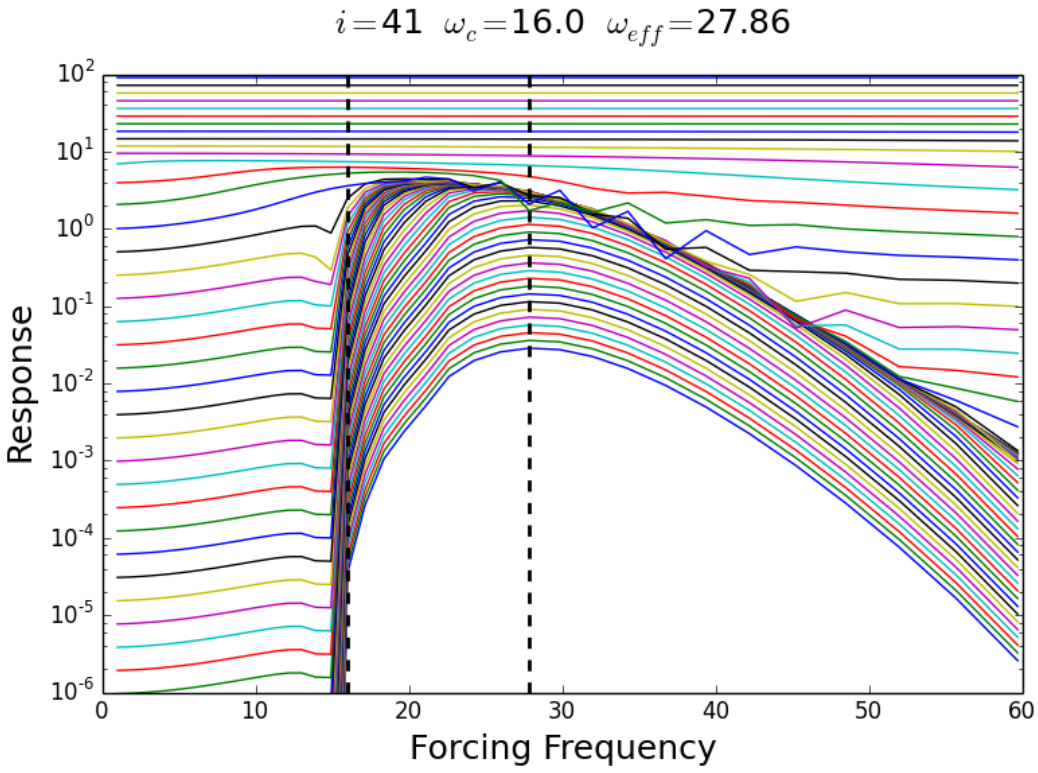

Figure 3.9: Response Curves of a Single Oscillator. As in Fig. 3.7 for oscillator $i = 41$

of higher-order compressive nonlinearities, with the response becoming nearly invariant as ω approaches ω_{eff}. This invariance for medium forcing persists for the frequency domain $\omega > \omega_{eff}$ but is now accompanied by a large forcing regime in which the response scales linearly up until the curves flatten and exhibit cubic compression. The scaling behavior in the different frequency domains is depicted in Fig. 3.10. Our results generally agree with Fig. 3.1 except for the sharp transition from linear to cubic scaling on the left flank of the response curves as the forcing frequency ω passes through ω_c.

3.5 Traveling Waves of Activity and Long Range Connections

In our toy model simulations, we observe traveling waves of activity, which propagate along the network of oscillators in the direction of decreasing characteristic frequency. Since the waves arise from the linear part of (3.3), we can study the waves by examining the eigenvectors of the connectivity matrix A. In Fig. 3.11, we plot the real (red dashed) and imaginary (blue) parts of the eigenvector corresponding to the eigenfrequency of median absolute value. The envelope or complex modulus of the eigenvector is also depicted. We omit the final N components of the eigenvector as they are a rescaled copy of the first N components.

It is clear that the real and complex parts of the eigenvector are out of phase by $\pi/2$. This phase difference is the source of traveling wave behaviour in our model. The envelope shape of the eigenvector is nearly symmetric and sharply peaks at a particular location, while the spatial frequency of the eigenvector is approximately uniform. These features are in disagreement with basilar membrane recordings, which predict a gradual increase in wave amplitude and spatial frequency in the direction of decreasing characteristic frequencies (basilar membrane base to apex).

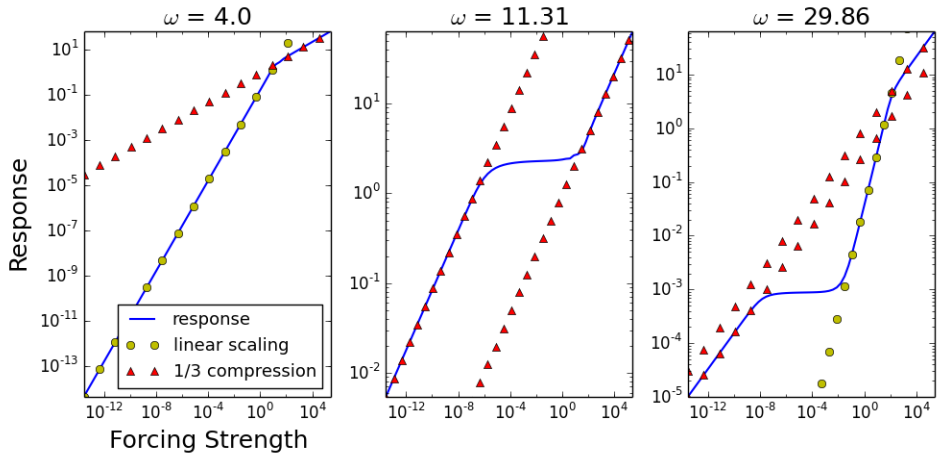

Figure 3.10: Scaling Regimes in the Response of a Single Oscillator. We plot the response of a single oscillator (Fig. 3.6) against the forcing strength for three different forcing frequencies ω. This oscillator has characteristic frequency $\omega_c = 8.00$ and effective frequency $\omega_{eff} = 12.13$. These define the boundaries of three different scaling regimes. In the plots, the red triangles represent 1/3 scaling, yellow dots represent linear scaling, and the blue curve is the oscillator response. In the first plot, $\omega = 4.0$, a linear oscillator response turns into 1/3 compression past a certain forcing strength. In the second regime, $\omega \approx 11.3$, the response first scales as the cubic root of the input, then approaches a region of near invariance, whereafter it settles back down to a cubic root. Finally, in the last regime, represented by $\omega \approx 29.9$, we find the following scaling pattern: 1/3, invariance, linear, 1/3.

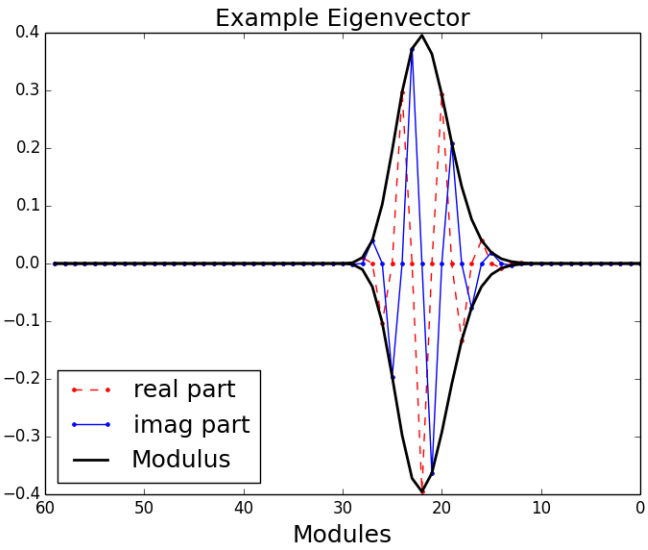

Figure 3.11: An Example Eigenvector of the Network Connectivity Matrix A. The real (red dashed) and imaginary (blue) parts of an eigenvector of the network connectivity matrix A is plotted above along with the eigenvector's complex modulus. As waves in the model are determined by the linear part of (3.3), wave behavior and shape can be studied in the context of eigenvectors.

The addition of long-range connections between oscillators helps to resolve this disagreement by improving both wave shape and spatial frequency variation. We incorporate this into our toy model by including linear, long-range, skew-symmetric connections that are proportional in strength to the characteristic frequencies and decay as an exponential with distance. We define the strength of the connections between two oscillators separated a distance d apart as $D\omega e^{-d}$ where ω is the characteristic frequency of the oscillator at the right side (higher frequency) of the connection and D is a scaling parameter. The skew-symmetric connectivity is depicted in Fig. 3.12. These connections sit on top of the original connections from Fig. 3.6.

We plot the response curves and eigenvectors of the system in Fig. 3.13. a is just the orignal response curves without any skew-symmetric connections. Fig. 3.13. b, corresponding to $D = 0.25$, exhibits a shift in the shape of the eigenvectors with the amplitude gradually increasing in the direction of decreasing characteristic frequencies. The spatial frequency of the eigenvector also increases in the direction of decreasing characteristic frequency. The case of relatively strong skew-symmetric connections, $D = 0.75$, is plotted in Fig. 3.13. c. The initial tail and spatial frequency variation are exaggerated in comparison to (a) and (b) and generally in agreement with basilar membrane studies, but this comes at a cost. As we increase D, the response curves lose their shape and no longer exhibit higher-order compression over a wide range of forcings; this is a direct result of the long range connections pushing the eigenvalues away from the imaginary axis and preventing the system from taking full advantage of the unique properties of center manifold dynamics. Therefore, to achieve response curves and waves that agree with experiments, a balance between the strength of the skew-symmetric and original network connections is needed.

Finally, we note that weak input is preferentially amplified in the model. We define the amplification of an oscillator in our network as R/F where R is the oscillator response and F

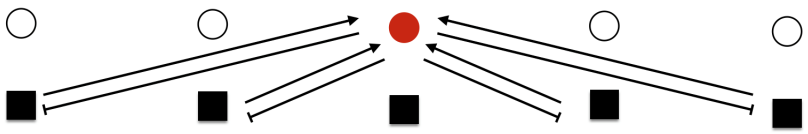

Figure 3.12: Long-Range, Skew Symmetric Connectivity. We illustrate the additional skew-symmetric connections to and from a single cell in the network. We omit showing the other connectivity (Fig. 3.12) to avoid clutter. Arrows denote excitation, while bars denote inhibition. This pattern is repeated for every cell in the network.

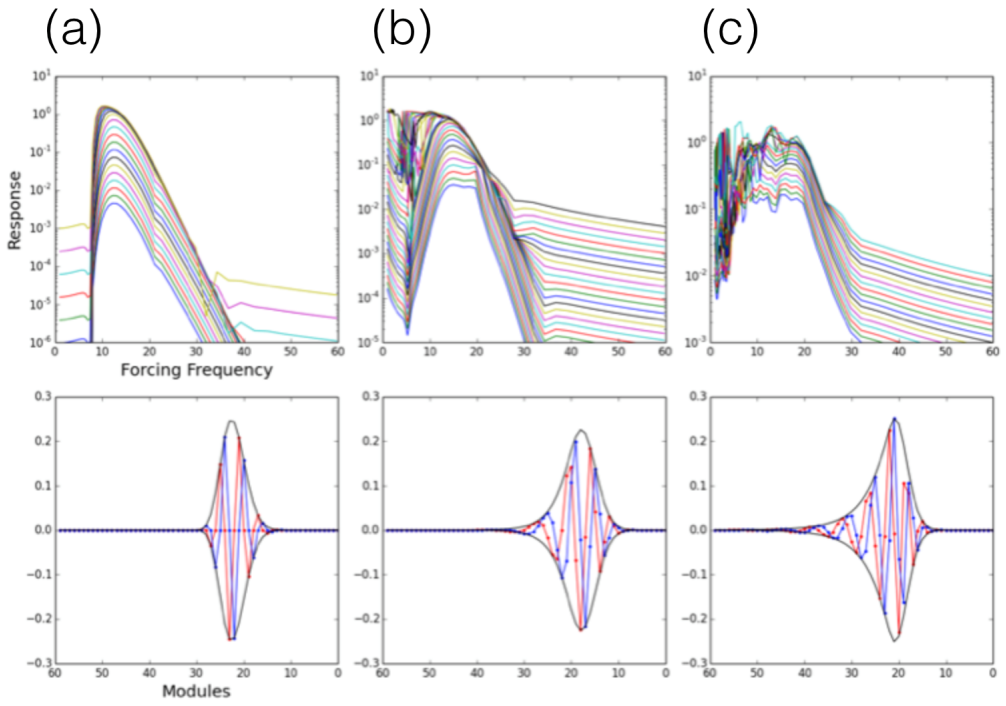

Figure 3.13: Coupled Critical Oscillators with Long-Range Connections. The response of a single oscillator in the network with long-range connections is plotted along with a representative eigenvector for three different scaling parameters D of the skew-symmetric connections. Columns (a), (b), (c) correspond to $D = 0$, 0.25, 0.75, respectively.

the input amplitude. For $F << 1$ and forcing frequencies above ω_c, $R \propto F^{1/3}$, which implies that the amplification is $F^{-2/3} >> 1$. To the left of ω_c, there is no amplification of weak input.

3.6 Conclusion

We have shown that high-dimensional nonhyperbolicity with dynamics residing on a full-dimensional center manifold can exhibit the key characteristic nonlinearities of the active process in cochlea: frequency selectivity, amplification of weak input, and higher-order nonlinear compression. The toy model presented in this thesis also gives rise to traveling waves of activity that propagate unidirectionally across the system. In order to better approximate the experimentally measured shape of traveling waves on the basilar membrane, we have included long-range, skew-symmetric connections between oscillators; however, these connections negatively impact the shape of the response curves by pushing the dynamics away from nonhyperbolicity. While we have been able to find a reasonable balance between the shape of traveling waves and response curves (Fig. 3.13(b)), we believe this conflict could be better solved by either finding an appropriate class of long range linear connections that preserve the high dimensionality of the center manifold or by including nonlinear couplings between the critical oscillators. Nonlinear couplings won't affect the linearization of the system, leaving the high-dimensional nonhyperbolicity of the original system unchanged.

As our model is just a toy model of center manifold dynamics, we do not suggest that our abstract critical oscillator network corresponds to actual anatomical and biophysical structures in the cochlea; although, if the cochlea does indeed utilize center manifolds in the processing of auditory stimuli, it might well be the case that the full high-dimensional phase space of cochlear dynamics could be reduced to a more simple structure on the center manifold. One possible simple structure is the toy model presented in this thesis.

Bibliography

[Adelmeyer 1999] Adelmeyer M. Topics in bifurcation theory and applications. World Scientific Publishing Company; 1999 Jan 22.

[Alonso 2014] Alonso LM, Proekt A, Schwartz TH, Pryor KO, Cecchi GA, Magnasco MO. Dynamical criticality during induction of anesthesia in human ECoG recordings. Frontiers in neural circuits. 2014 Mar 25;8:20.

[Andronov] Andronov AA, Vitt AA, Khaikin SE. Theory of Oscillators: Adiwes International Series in Physics. Elsevier; 2013 Oct 22.

[Amador 2013] Amador A, Perl YS, Mindlin GB, Margoliash D. Elemental gesture dynamics are encoded by song premotor cortical neurons. Nature. 2013 Mar;495(7439):59.

[Anderson 2010] Anderson GW, Guionnet A, Zeitouni O. An introduction to random matrices, volume 118 of Cambridge Studies in Advanced Mathematics.

[Arnold 1982] Arnold VI. Geometrical methods in the theory of ordinary differential equations. Springer-Verlag, New York

[Ashmore 2008] Ashmore J. Cochlear outer hair cell motility. Physiological reviews. 2008 Jan;88(1):173-210.

[Beggs 2003] Beggs JM, Plenz D. Neuronal avalanches in neocortical circuits. Journal of neuroscience. 2003 Dec 3;23(35):11167-77.

[Beggs 2012] Beggs JM, Timme N. Being critical of criticality in the brain. Frontiers in physiology. 2012 Jun 7;3:163.

[Békésy 1960] Von Békésy G, Wever EG. Experiments in hearing. New York: McGraw-Hill; 1960.

[Bienenstock 1998] Bienenstock E, Lehmann D. Regulated criticality in the brain?. Advances in complex systems. 1998 Dec;1(04):361-84.

[Brauer 1952] Brauer A. Limits for the characteristic roots of a matrix. IV: Applications to stochastic matrices. Duke Mathematical Journal. 1952 Mar;19(1):75-91.

[Brown 2016] Brown A. Smoothness of stable holonomies inside center-stable manifolds and the C^2 hypothesis in Pugh-Shub and Ledrappier-Young theory. arXiv preprint arXiv:1608.05886. 2016 Aug 21.

[Burns 2005] Burns K, Wilkinson A. A note on stable holonomy between centers. preprint. 2005 Jun 11.

[Camalet 2000] Camalet S, Duke T, Julicher F, Prost J. Auditory sensitivity provided by self-tuned critical oscillations of hair cells. Proceedings of the National Academy of Sciences. 2000 Mar 28;97(7):3183-8.

[Carr 2012] Carr J. Applications of centre manifold theory. Springer Science and Business Media; 2012 Dec 6.

[Casanova 2015] Casanova MF, Opris I, editors. Recent advances on the modular organization of the cortex. New York: Springer; 2015 Jun 22.

[Chalker 1998] Chalker JT, Mehlig B. Eigenvector statistics in non-Hermitian random matrix ensembles. Physical review letters. 1998 Oct 19;81(16):3367.

[Chan 2005a] Chan DK, Hudspeth AJ. Mechanical responses of the organ of corti to acoustic and electrical stimulation in vitro. Biophysical journal. 2005 Dec 1;89(6):4382-95.

[Chan 2005b] Chan DK, Hudspeth AJ. Ca^{2+} current-driven nonlinear amplification by the mammalian cochlea in vitro. Nature neuroscience. 2005 Feb;8(2):149.

[Chen 2014] Chen M, Yan Y, Gong X, Gilbert CD, Liang H, Li W. Incremental integration of global contours through interplay between visual cortical areas. Neuron. 2014 May 7;82(3):682-94.

[Chialvo 2010] Chialvo DR. Emergent complex neural dynamics. Nature physics. 2010 Oct;6(10):744.

[Choe 1998] Choe Y, Magnasco MO, Hudspeth AJ. A model for amplification of hair-bundle motion by cyclical binding of Ca2+ to mechanoelectrical-transduction channels. Proceedings of the National Academy of Sciences. 1998 Dec 22;95(26):15321-6.

[Churchland 2012] Churchland MM, Cunningham JP, Kaufman MT, Foster JD, Nuyujukian P, Ryu SI, Shenoy KV. Neural population dynamics during reaching. Nature. 2012 Jul;487(7405):51.

[Dallos 2006] Dallos P, Zheng J, Cheatham MA. Prestin and the cochlear amplifier. J Physiol 576: 3742, 2006.

[Dayan 2001] Dayan P, Abbott LF. Theoretical neuroscience. Cambridge, MA: MIT Press; 2001.

[Dierkes 2008] Dierkes K, Lindner B, Jlicher F. Enhancement of sensitivity gain and frequency tuning by coupling of active hair bundles. Proceedings of the National Academy of Sciences. 2008 Dec 2;105(48):18669-74.

[Dulac 1903] Dulac H. Recherches sur les points singuliers des quations diffrentielles. Gauthier-Villars; 1903.

[Duke 2003] Duke T, Julicher F. Active traveling wave in the cochlea. Physical review letters. 2003 Apr 16;90(15):158101.

[Eguíluz 2000] Eguíluz VM, Ospeck M, Choe Y, Hudspeth AJ, Magnasco MO. Essential nonlinearities in hearing. Physical Review Letters. 2000 May 29;84(22):5232.

[Eguíluz 2005] Eguíluz VM, Chialvo DR, Cecchi GA, Baliki M, Apkarian AV. Scale-free brain functional networks. Physical review letters. 2005 Jan 6;94(1):018102.

[Engelken 2016] Engelken R, Farkhooi F, Hansel D, van Vreeswijk C, Wolf F. A reanalysis of Two types of asynchronous activity in networks of excitatory and inhibitory spiking neurons. F1000Research. 2016;5.

[Ermentrout 2012] Ermentrout GB, Terman DH. Mathematical foundations of neuroscience. Springer Science and Business Media; 2010 Jul 1.

[Fechner 1966] Fechner G. 1966 Elements of Psychophysics. Howes, DH, Boring, EC, Adler, HE Holt, Rinehart and Winston, New York ((Translated from German) Originally published in 1860). 1860.

[Fettiplace 2006] Fettiplace R, Hackney CM. The sensory and motor roles of auditory hair cells. Nature Reviews Neuroscience. 2006 Jan;7(1):19.

[Fraiman 2009] Fraiman D, Balenzuela P, Foss J, Chialvo DR. Ising-like dynamics in large-scale functional brain networks. Physical Review E. 2009 Jun 23;79(6):061922.

[Freeman 2005] Freeman WJ, Holmes MD. Metastability, instability, and state transition in neocortex. Neural Networks. 2005 Aug 31;18(5):497-504.

[Freire 1988] Freire E, Gamero E, Ponce E, Franquelo LG. An algorithm for symbolic computation of center manifolds. InInternational Symposium on Symbolic and Algebraic Computation 1988 Jul 4 (pp. 218-230). Springer, Berlin, Heidelberg.

[Gardner 2001] Gardner T, Cecchi G, Magnasco M, Laje R, Mindlin GB. Simple motor gestures for birdsongs. Physical review letters. 2001 Oct 26;87(20):208101.

[Gawne 1996] Gawne TJ, Kjaer TW, Richmond BJ. Latency: another potential code for feature binding in striate cortex. Journal of neurophysiology. 1996 Aug 1;76(2):1356-60.

[Gireesh 2008] Gireesh ED, Plenz D. Neuronal avalanches organize as nested theta-and beta/gamma-oscillations during development of cortical layer 2/3. Proceedings of the National Academy of Sciences. 2008 May 27;105(21):7576-81.

[Gold 1948a] Gold T, Pumphrey RJ. Hearing. I. The cochlea as a frequency analyzer. Proceedings of the Royal Society of London B: Biological Sciences. 1948 Dec 14;135(881):462-91.

[Gold 1948b] Gold T. Hearing. II. The physical basis of the action of the cochlea. Proceedings of the Royal Society of London B: Biological Sciences. 1948 Dec 14;135(881):492-8.

[Grobman 1959] Grobman DM. Homeomorphism of systems of differential equations. Doklady Akademii Nauk SSSR. 1959 Jan 1;128(5):880-1.

[Guckenheimer 2013] Guckenheimer J, Holmes P. Nonlinear oscillations, dynamical systems, and bifurcations of vector fields. Springer Science and Business Media; 2013 Nov 21.

[Hansel 1997] Hansel D, Sompolinsky H. 13 Modeling Feature Selectivity in Local Cortical Circuits.

[Harish 2015] Harish O, Hansel D. Asynchronous rate chaos in spiking neuronal circuits. PLoS computational biology. 2015 Jul 31;11(7):e1004266.

[Hartman 1960a] Hartman P. A lemma in the theory of structural stability of differential equations. Proceedings of the American Mathematical Society. 1960;11(4):610-20.

[Hartman 1960b] Hartman P. On local homeomorphisms of Euclidean spaces. Bol. Soc. Mat. Mexicana. 1960 Oct;5(2):220-41.

[Hayton 2018a] Hayton K, Moirogiannis D, Magnasco M (2018) Adaptive scales of integration and response latencies in a critically-balanced model of the primary visual cortex. PLoS ONE 13(4): e0196566.

[Hayton 2018b] Hayton K, Moirogiannis D, Magnasco M. A Nonhyperbolic Toy Model of Cochlear Dynamics. arXiv preprint arXiv:1807.00764. 2018 Jul 2.

[Hopf 1942] Hopf E. Abzweigung einer periodischen Lsung von einer stationren Lsung eines Differentialsystems. Ber. Math.-Phys. Kl Schs. Akad. Wiss. Leipzig. 1942 Jan;94:1-22.

[Hoppensteadt 1997] Hoppensteadt FC, Izhikevich EM. Canonical models for mathematical neuroscience. InNeural Networks, 1997., International Conference on 1997 Jun 9 (Vol. 1, pp. 324-327). IEEE.

[Hoppensteadt 2001] Hoppensteadt FC, Izhikevich E. Canonical neural models. Brain Theory and Neural Networks, The MIT press, Cambridge, MA. 2001.

[Hoppensteadt 2012] Hoppensteadt FC, Izhikevich EM. Weakly connected neural networks. Springer Science and Business Media; 2012 Dec 6.

[Hudspeth 2000] Hudspeth AJ, Choe Y, Mehta AD, Martin P. Putting ion channels to work: mechanoelectrical transduction, adaptation, and amplification by hair cells. Proceedings of the National Academy of Sciences. 2000 Oct 24;97(22):11765-72.

[Hudspeth 2008] Hudspeth AJ. Making an effort to listen: mechanical amplification in the ear. Neuron. 2008 Aug 28;59(4):530-45.

[Hudspeth 2010] Hudspeth AJ, Julicher F, Martin P. A critique of the critical cochlea: Hopf?a bifurcation?is better than none. Journal of neurophysiology. 2010 Sep 1;104(3):1219-29.

[Ioos 1999] Ioos G, Adelmeyer M. Topics in Bifurcation Theory and Applications. Advanced Series in Nonlinear Dynamics. World Scientific, 2nd edition, 1999

[Izhikevich 2007a] Izhikevich EM. Dynamical systems in neuroscience. MIT press; 2007.

[Izhikevich 2007b] Izhikevich EM. Equilibrium. Scholarpedia. 2007 Oct 9;2(10):2014.

[Jones 2000] Jones EG. Microcolumns in the cerebral cortex. Proceedings of the National Academy of Sciences. 2000 May 9;97(10):5019-21.

[Kadmon 2015] Kadmon J, Sompolinsky H. Transition to chaos in random neuronal networks. Physical Review X. 2015 Nov 19;5(4):041030.

[Kanders 2017a] Kanders K, Lorimer T, Stoop R. Avalanche and edge-of-chaos criticality do not necessarily co-occur in neural networks. Chaos: An Interdisciplinary Journal of Nonlinear Science. 2017 Apr;27(4):047408.

[Kanders 2017b] Kanders K, Lorimer T, Gomez F, Stoop R. Frequency sensitivity in mammalian hearing from a fundamental nonlinear physics model of the inner ear. Scientific Reports. 2017 Aug 30;7(1):9931.

[Kapadia 1999] Kapadia MK, Westheimer G, Gilbert CD. Dynamics of spatial summation in primary visual cortex of alert monkeys. Proceedings of the National Academy of Sciences. 1999 Oct 12;96(21):12073-8.

[Katok 2005] Katok A, Hasselblatt B, editors. Handbook of Dynamical Systems: Volume 1B. Elsevier; 2005 Dec 17.

[Kauffman 1967] Kauffman SA, McCulloch WS. Random nets of formal genes. Quarterly Progress Report 34. 1967 Research Laboratory of Electronics, Massachusetts Institute of Technology

[Kauffman 1969] Kauffman SA. Metabolic stability and epigenesis in randomly constructed genetic nets. Journal of theoretical biology. 1969 Mar 1;22(3):437-67.

[Kelley 1967] Kelley A. The stable, center-stable, center, center-unstable, unstable manifolds. Journal of Differential Equations. 1967 Oct 1;3(4):546-70.

[Kennedy 2005] Kennedy HJ, Crawford AC, Fettiplace R. Force generation by mammalian hair bundles supports a role in cochlear amplification. Nature. 2005 Feb;433(7028):880.

[Kennedy 2006] Kennedy HJ, Evans MG, Crawford AC, Fettiplace R. Depolarization of cochlear outer hair cells evokes active hair bundle motion by two mechanisms. Journal of Neuroscience. 2006 Aug 1;26(10):2757-66.

[Kenet 2003] Kenet T, Bibitchkov D, Tsodyks M, Grinvald A, Arieli A. Spontaneously emerging cortical representations of visual attributes. Nature. 2003 Oct;425(6961):954.

[Kern 2003] Kern A, Stoop R. Essential role of couplings between hearing nonlinearities. Physical Review Letters. 2003 Sep 19;91(12):128101.

[Kitzbichler 2009] Kitzbichler MG, Smith ML, Christensen SR, Bullmore E. Broadband criticality of human brain network synchronization. PLoS computational biology. 2009 Mar 20;5(3):e1000314.

[Kuznetsov 2013] Kuznetsov YA. Elements of applied bifurcation theory. Springer Science and Business Media; 2013 Mar 9.

[Laughlin 1981] Laughlin S. A simple coding procedure enhances a neuron's information capacity. Zeitschrift fr Naturforschung c. 1981 Oct 1;36(9-10):910-2.

[Lalazar 2016] Lalazar H, Abbott LF, Vaadia E. Tuning curves for arm posture control in motor cortex are consistent with random connectivity. PLoS computational biology. 2016 May 25;12(5):e1004910.

[Landau 2016] Landau ID, Egger R, Dercksen VJ, Oberlaender M, Sompolinsky H. The impact of structural heterogeneity on excitation-inhibition balance in cortical networks. Neuron. 2016 Dec 7;92(5):1106-21.

[Levina 2007] Levina A, Herrmann JM, Geisel T. Dynamical synapses causing self-organized criticality in neural networks. Nature physics. 2007 Dec;3(12):857.

[Machens 2005] Machens CK, Romo R, Brody CD. Flexible control of mutual inhibition: a neural model of two-interval discrimination. Science. 2005 Feb 18;307(5712):1121-4.

[Magnasco 2003] Magnasco MO. A wave traveling over a Hopf instability shapes the cochlear tuning curve. Physical review letters. 2003 Feb 4;90(5):058101.

[Magnasco 2009] Magnasco MO, Piro O, Cecchi GA. Self-tuned critical anti-Hebbian networks. Physical review letters. 2009 Jun 22;102(25):258102.

[Martin 1999] Martin P, Hudspeth AJ. Active hair-bundle movements can amplify a hair cell's response to oscillatory mechanical stimuli. Proceedings of the National Academy of Sciences. 1999 Dec 7;96(25):14306-11.

[Martin 2001] Martin P, Hudspeth AJ. Compressive nonlinearity in the hair bundle's active response to mechanical stimulation. Proceedings of the National Academy of Sciences. 2001 Dec 4;98(25):14386-91.

[Martin 2008] Martin P. Active hair-bundle motility of the hair cells of vestibular and auditory organs. Inactive Processes and Otoacoustic Emissions in Hearing 2008 (pp. 93-143). Springer New York.

[Moirogiannis 2017] Moirogiannis D, Piro O, Magnasco MO. Renormalization of Collective Modes in Large-Scale Neural Dynamics. Journal of Statistical Physics. 2017 May 1;167(3-4):543-58.

[Mora 2011] Mora T, Bialek W. Are biological systems poised at criticality?. Journal of Statistical Physics. 2011 Jul 1;144(2):268-302.

[Nadrowski 2004] Nadrowski B, Martin P, Julicher F. Active hair-bundle motility harnesses noise to operate near an optimum of mechanosensitivity. Proceedings of the National Academy of Sciences. 2004 Aug 17;101(33):12195-200.

[Nauhaus 2009] Nauhaus I, Busse L, Carandini M, Ringach DL. Stimulus contrast modulates functional connectivity in visual cortex. Nature neuroscience. 2009 Jan 1;12(1):70-6.

[O'Rourke 2016] O'Rourke S, Vu V, Wang K. Eigenvectors of random matrices: a survey. Journal of Combinatorial Theory, Series A. 2016 Nov 1;144:361-442.

[Ostojic 2014] Ostojic S. Two types of asynchronous activity in networks of excitatory and inhibitory spiking neurons. Nature neuroscience. 2014 Apr;17(4):594.

[Poincarè 1893] Poincarè H. Les mthodes nouvelles de la mcanique cleste: Mthodes de MM. Newcomb, Glydn, Lindstedt et Bohlin. 1893. Gauthier-Villars it fils; 1893.

[Poincarè] Poincarè H. New methods of celestial mechanics. Springer Science and Business Media; 1992 Nov 15.

[Pugh 1997] Pugh C, Shub M, Wilkinson A. Hlder foliations. Duke Mathematical Journal. 1997;86(3):517-46.

[Rajan 2016] Rajan K, Harvey CD, Tank DW. Recurrent network models of sequence generation and memory. Neuron. 2016 Apr 6;90(1):128-42.

[Ruggero 1992] Ruggero MA. Responses to sound of the basilar membrane of the mammalian cochlea. Current opinion in neurobiology. 1992 Aug 31;2(4):449-56.

[Ruggero 1997] Ruggero MA, Rich NC, Recio A, Narayan SS, Robles L. Basilar-membrane responses to tones at the base of the chinchilla cochlea. The Journal of the Acoustical Society of America. 1997 Apr;101(4):2151-63.

[Ruggero 2000] Ruggero MA, Narayan SS, Temchin AN, Recio A. Mechanical bases of frequency tuning and neural excitation at the base of the cochlea: comparison of basilar-membrane vibrations and auditory-nerve-fiber responses in chinchilla. Proceedings of the National Academy of Sciences. 2000 Oct 24;97(22):11744-50.

[Sompolinsky 1998] Sompolinsky H, Crisanti A, Sommers HJ. Chaos in random neural networks. Physical review letters. 1988 Jul 18;61(3):259.

[Sompolinsky 2014] Sompolinsky, H.: Computational neuroscience: beyond the local circuit. Curr. Opin. Neurobiol. 25, 16 (2014)

[Sceniak 1999] Sceniak MP, Ringach DL, Hawken MJ, Shapley R. Contrast's effect on spatial summation by macaque V1 neurons. Nature neuroscience. 1999 Aug 1;2(8):733-9.

[Seung 1998] Seung HS. Continuous attractors and oculomotor control. Neural Networks. 1998 Nov 30;11(7):1253-8.

[Seung 2000] Seung HS, Lee DD, Reis BY, Tank DW. Stability of the memory of eye position in a recurrent network of conductance-based model neurons. Neuron. 2000 Apr 30;26(1):259-71.

[Shenoy 2013] Shenoy KV, Sahani M, Churchland MM. Cortical control of arm movements: a dynamical systems perspective. Annual review of neuroscience. 2013 Jul 10;36.

[Shnol 2007] Shnol EE. Stability of equilibria. Scholarpedia. 2007 Mar 15;2(3):2770.

[Silberberg 2002] Silberberg G, Gupta A, Markram H. Stereotypy in neocortical microcircuits. Trends in neurosciences. 2002 May 1;25(5):227-30.

[Silva 1998] da Silva L, Papa AR, de Souza AC. Criticality in a simple model for brain functioning. Physics Letters A. 1998 Jun 8;242(6):343-8.

[Solovey 2012] Solovey G, Miller KJ, Ojemann J, Magnasco MO, Cecchi GA. Self-regulated dynamical criticality in human ECoG. Frontiers in integrative neuroscience. 2012 Jul 19;6:44.

[Solovey 2015] Solovey G, Alonso LM, Yanagawa T, Fujii N, Magnasco MO, Cecchi GA, Proekt A. Loss of consciousness is associated with stabilization of cortical activity. Journal of Neuroscience. 2015 Jul 29;35(30):10866-77.

[Stern 2014] Stern M, Sompolinsky H, Abbott LF. Dynamics of random neural networks with bistable units. Physical Review E. 2014 Dec 16;90(6):062710.

[Tao 2008] Tao T, Vu V. Random matrices: the circular law. Communications in Contemporary Mathematics. 2008 Apr;10(02):261-307.

[Tao 2012] Tao T, Vu V. Random matrices: Universal properties of eigenvectors. Random Matrices: Theory and Applications. 2012 Jan;1(01):1150001.

[Tinevez2007] Tinevez JY, Julicher F, Martin P. Unifying the various incarnations of active hair-bundle motility by the vertebrate hair cell. Biophysical journal. 2007 Dec 1;93(11):4053-67.

[Tsodyks 1999] Tsodyks M, Kenet T, Grinvald A, Arieli A. Linking spontaneous activity of single cortical neurons and the underlying functional architecture. Science. 1999 Dec 3;286(5446):1943-6.

[Wiggins 2003] Wiggins S. Introduction to applied nonlinear dynamical systems and chaos. Springer Science and Business Media; 2003 Oct 1.

[Wiggins 2013] Wiggins S. Global bifurcations and chaos: analytical methods. Springer Science and Business Media; 2013 Nov 27.

[Yan 2012] Yan XH, Magnasco MO. Input-dependent wave attenuation in a critically-balanced model of cortex. PloS one. 2012 Jul 25;7(7):e41419.